Grant AFOSR-87-0233

ANNUAL REPORT

USE OF D_2 TO ELUCIDATE OMVPE GROWTH MECHANISMS

G.B. Stringfellow
Departments of Materials Science and Engineering
and Electrical Engineering
University of Utah
Salt Lake City, Utah 84112

August 4, 1988

Prepared for

Captain Kevin J. Malloy
Air Force Office of Scientific Research
Air Force Systems Command
USAF
Bolling AFB DC 20332

ADA 199841

SECURITY CLASSIFICATION OF THIS PAGE

REPORT DOCUMENTATION PAGE

Form Approved OMB No. 0704-0188

1a. REPORT SECURITY CLASSIFICATION UNCLASSIFIED	1b. RESTRICTIVE MARKINGS
2a. SECURITY CLASSIFICATION AUTHORITY	3. DISTRIBUTION/AVAILABILITY OF REPORT Approved for public release; distribution unlimited.
2b. DECLASSIFICATION/DOWNGRADING SCHEDULE	
4. PERFORMING ORGANIZATION REPORT NUMBER(S)	5. MONITORING ORGANIZATION REPORT NUMBER(S) AFOSR-TR- 88-0378
6a. NAME OF PERFORMING ORGANIZATION Gerald B. Stringfellow University of Utah 6b. OFFICE SYMBOL (If applicable)	7a. NAME OF MONITORING ORGANIZATION AFOSR
6c. ADDRESS (City, State, and ZIP Code) MSE - 304 EMRO Salt Lake City, Utah 84112	7b. ADDRESS (City, State, and ZIP Code) Bldg 410 Bolling AFB, DC 20332-6448
8a. NAME OF FUNDING/SPONSORING ORGANIZATION AIR FORCE OFFICE OF SCIENTIFIC RESEARCH 8b. OFFICE SYMBOL (If applicable)	9. PROCUREMENT INSTRUMENT IDENTIFICATION NUMBER Grant AFOSR-87-0233
8c. ADDRESS (City, State, and ZIP Code) AIR FORCE SYSTEMS COMMANC - USAF Bolling AFB DC 20332	10. SOURCE OF FUNDING NUMBERS PROGRAM ELEMENT NO. 61102F; PROJECT NO. 2306; TASK NO B1; WORK UNIT ACCESSION NO.

11. TITLE (Include Security Classification)

USE OF D_2 TO ELUCIDATE OMVPE GROWTH MECHANISMS

12. PERSONAL AUTHOR(S)
STRINGFELLOW, GERALD B.

13a. TYPE OF REPORT	13b. TIME COVERED	14. DATE OF REPORT (Year, Month, Day)	15. PAGE COUNT
ANNUAL	FROM 6/15/87 TO 6/14/88	1988, August 4th	9 plus 7 reprint

16. SUPPLEMENTARY NOTATION

17. COSATI CODES			18. SUBJECT TERMS (Continue on reverse if necessary and identify by block number)
FIELD	GROUP	SUB-GROUP	

19. ABSTRACT (Continue on reverse if necessary and identify by block number)

Research during the first year of this project has concentrated on determining the pyrolysis mechanisms for the precursor molecules trimethylgallium (TMGa), trimethylindium (TMIn), arsine (AsH_3), and phosphine (PH_3) commonly used for organometallic vapor phase eqpitaxial growth (OMVPE) of III/V semiconductors. The technique used is mass spectrometry with the pyrolysis occurring in various ambients including H_2, He, and D_2. The latter allows labellin of reaction products involving interactions with the ambient. TMGa and TMIn were discovered to pyrolyze by a new mechanism involving H (D) radicals. The hydrides decompose by heterogeneous release of H atoms. Together, the TMIII and group V hydride pyrolyze via a concerted reaction involving formation of an adduct. In addition, pyrolysis and OMVPE growth studies were conducted using the newly developed group V sources tertiarybutylarsine (TBAs) and tertiarybutylphosphine (TBP). These precursors pyrolyze by radical processes where a t-butyl radical is produced which subsequently attacks the parent molecule. Adding TMGa to the system has no effect on either TBAs or TBP pyrolysis. However, TBAs and TBP both enhance

UNCLASSIFIED

20. DISTRIBUTION/AVAILABILITY OF ABSTRACT	21. ABSTRACT SECURITY CLASSIFICATION
☒ UNCLASSIFIED/UNLIMITED ☐ SAME AS RPT ☐ DTIC USERS	
22a. NAME OF RESPONSIBLE INDIVIDUAL Lt Hoe	22b. TELEPHONE (Include Area Code) (202) 767-4931
	22c. OFFICE SYMBOL NE

DD Form 1473, JUN 86 — Previous editions are obsolete. — SECURITY CLASSIFICATION OF THIS PAGE

19. ABSTRACT (continued)

TMGa pyrolysis via heterogeneous attack of the TMGa by group V species such as AsH, AsH_2, and AsH_3 (or equivalent P species).

SUMMARY

Research during the first year of this project has concentrated on determining the pyrolysis mechanisms for the precursor molecules trimethylgallium(TMGa), trimethylindium (TMIn), arsine (AsH_3), and phosphine(PH_3) commonly used for organometallic vapor phase epitaxial growth (OMVPE) of III/V semiconductors. The technique used is mass spectrometry with the pryolysis occurring in various ambients including H_2, He, and D_2. The latter allows labelling of reaction products involving interactions with the ambient. TMGa and TMIn were discovered to pyrolyze by a new mechanism involving H (D) radicals. The hydrides decompose by heterogeneous release of H atoms. Together, the TMIII and group V hydride pyrolyze via a concerted reaction involving formation of an adduct. In addition, pyrolysis and OMVPE growth studies were conducted using the newly developed group V sources tertiarybutylarsine (TBAs) and tertiarybutylphosphine (TBP). These precursors pyrolyze by radical processes where a t-butyl radical is produced which subsequently attacks the parent molecule. Adding TMGa to the system has no affect on either TBAs or TBP pyrolysis. However, TBAs and TBP both enhance TMGa pyrolysis via heterogeneous attack of the TMGa by group V species such as AsH, AsH_2, and AsH_3 (or equivalent P species).

TABLE OF CONTENTS

I. INTRODUCTION

The first year of this research project has produced significant results. i) We have determined that TMIn and TMGa pyrolysis do not occur via simpe homolysis reactions, as supposed in the past. The ambient plays a significant role, with H (or D) radicals attacking the parent molecules. ii) When the group V hydrides are added to the system, the pyrolysis mechanisms for both precursor molecules change. The mechanism is believed to be a concerted reaction involving adduct formation. iii) The first results on pyrolysis mechanisms for the newly developed alternate group V sources tertiarybutylarsine(TBAs) and tertiarybutylphosphine(TBP) have been obtained. The mechanisms apparently involve largely radical cleavage with attack of the parent molecule by the t-butyl radical playing an important role. iv) Experimental results relating to the reaction mechanisms for TMGa+TBAs=GaAs and TMGa+TBP=GaP have been obtained.

The research has proceeded in accord with the objectives contained in the original proposal, with progress slightly ahead of schedule.

These results have formed the basis of 4 talks at National and International conferences and 7 completed papers. Several additional papers are in preparation.

Rather than repeating the information contained in the publications, this report will consist of a brief overview with the papers attached as an appendix.

II. RESULTS

A. SUMMARY OF RESEARCH RESULTS

1. TMGa and TMIn

Until now, the pyrolysis of TMGa and TMIn in an OMVPE reactor has been assumed to occur via simple homolytic fission where the molecule looses one radical at a time. However, for both precursor molecules, we have determined that the ambient has a significant effect. Pyrolysis is most rapid in H_2, slightly less rapid in D_2, and slowest in He. Since these gases are hydrodynamically equivalent, the effect is chemical. We have proposed a mechanism capable of quantitatively explaining the pyrolysis versus temperature behavior

as well as the product concentrations versus temperature. The overall reactions involve a series of steps. The initiation reaction is the production of CH_3 radicals. These react with the ambient to produce CH_3D (in D_2), CH_4 (in H_2), and CH_4+C_2H_6 in He. In D_2 (or H_2) a D (H) radical is also formed. This, in turn, attacks the parent molecule via formation of a hypervalent species. The pyrolysis temperature is higher in He since this pyrolysis mechanism is precluded, since no D (or H) radicals are formed.

2. AsH_3 and PH_3

Pyrolysis of the group V hydrides occurs via simple heterogeneous reactions. The pyrolysis temperatures are dependent on the surface but independent of the ambient. The only product in a D_2 ambient is H_2.

3. TBAs and TBP.

The t-butyl-metal bond is much weaker than a H-metal bond because the central carbon atom is bonded to three carbons in addition to the metal. Thus, the pyrolysis temperatures of the t-butyl-group V precursors are significantly lower than the hydrides. TBAs pyrolyzes at lower temperatures than TBP due to the lower t-butyl-As bond strength, as compared with the strength of the t-butyl-P bond. The volatile pyrolysis products are mainly isobutane (C_4H_{10}), isobutene (C_4H_8), and the hydride.

Initially, the pyrolysis reactions were interpreted to be simple unimolecular reactions in which the leaving t-butyl radical either left a H behind, forming C_4H_8 (the beta-elimination reaction), or took a H from the parent, forming C_4H_{10} (the oxidative coupling reaction). To test this hypothesis, butyl radicals from $(C_4H_9)NN(C_4H_9)$ were intentionally added to the system. The t-butyl radicals were found to attack the parent molecules. Furthermore, the addition of TBAs during TBP pyrolysis produced similar changes in the TBP pyrolysis behavior. These simple experiments clearly demonstrate that t-butyl radical reactions play a major role.

4. TMGa+AsH_3

The growth of GaAs using TMGa and AsH_3 is the standard OMVPE process. Pyrolysis of the two precursors together causes

major changes in both the pyrolysis temperatures and the product species. The pyrolysis temperatures of both are lowered and the major product is CH_4 (in a D_2 ambient). This strongly indicates gas phase and surface interactions between the two molecules, and/or, their pyrolysis products. One mechanism is the attack of AsH_3 by CH_3 radicals. This lowers the AsH_3 pyrolysis temperature, but the effect on TMGa pyrolysis is not clear. By removing CH_3 radicals from the system it might lower the pyrolysis temperature. However, as discussed above, the CH_3 radical play a major role by reacting with the ambient to produce reactive D (H) radicals. A simpler interpretation is a concerted pyrolysis reaction via formation of an adduct. The adduct concentration is believed to be very low. Nevertheless, collision of TMGa and AsH_3 followed by rapid CH_4 elimination explains the experimental results.

5. TMGa + TBAs

Unexpectedly, the growth reaction for GaAs using the source molecules TMGa and TBAs is considerably different than for TMGa and AsH_3, discussed above. Pyrolysis via adduct formation is expected to produce C_5H_{12} (C_4H_9+CH_3), which is detected in only minor concentrations. In addition, the pyrolysis temperature for TBAs is virtually unchanged by the presence of TMGa. The products are also nearly unchanged. On the other hand, the TMGa pyrolysis temperature is dramatically lowered by the presence of TBAs. The major reaction product also changes from CH_3D to CH_4. This is ascribed to heterogeneous reactions where TMGa is attacked by TBAs reaction products such as AsH, AsH_2, and AsH_3.

B. Summary of Resulting Talks and Papers

TALKS

1. "Reaction Mechanisms in the OMVPE Growth of GaAs and InP", OMVPE Workshop, Cape Cod, September 1987.
2. "GaAs Growth Using TBAs and TMGa", 4th International Conference on MOVPE, Hakone, Japan, May 1988.
3. "OMVPE Growth of GaAs Using TMGa and TBAs", Electronic Materials Conference, Boulder, June 1988.
4. "Reaction Mechanisms in OMVPE Growth of GaAs Determined Using D_2 Labelling Experiments", NATO Workshop on Mech-

anisms of Reactions of OM Compounds with Surfaces", St. Andrews, Scotland, June 1988. (joint session with European Workshop on MOVPE). (INVITED).

PAPERS

1. C.A. Larsen, N.I. Buchan, and G.B. Stringfellow, "Reaction Mechanisms in the OMVPE Growth of GaAs", Appl. Phys. Lett. **52** 480 (1988).
2. N.I. Buchan, C.A. Larsen, and G.B. Stringfellow, "Mass Spectrometric Studies of TMIn Pyrolysis", J. Crystal Growth (accepted for publication).
3. N.I. Buchan, C.A. Larsen, and G.B. Stringfellow, "A Mass Spectrometric Study of the Simulatneous Reaction Mechanism of TMIn and PH_3 to Grow InP", J. Crystal Growth (accepted for publication).
4. C.A. Larsen, N.I. Buchan, S.H. Li, and G.B. Stringfellow, "Decomposition Mechanisms of TBAs", J. Crystal Growth (accepted for publication).
5. C.A. Larsen, N.I. Buchan, S.H. Li, and G.B. Stringfellow, "Mechanisms of GaAs Growth Using TBAs and TMGa", J. Crystal Growth (accepted for publication).
6. C.A. Larsen, N.I. Buchan, S.H. Li, and G.B. Stringfellow, "GaAs Growth Using TBAs and TMGa", J. Crystal Growth (accepted for publication).
7. G.B. Stringfellow, "Reaction Mechanisms in OMVPE Growth of GaAs Determined Using D_2 Labelling Experiments", (to be published in the Proceedings of the NATO Workshop on OMVPE Reaction Mechanisms and also in Prog. Crystal Growth and Character.)

C. Students Supported and Graduated

1. N.I. Buchan -- PhD, EE, March 1988 -- Now at IBM, Yorktown Heights Thesis Title-"A Spectroscopic Study of Reaction Mechanisms"
2. C.A. Larsen -- PhD, MSE, August 1988 (expected)(will remain as Post Doctoral Fellow)
3. S.H. Li -- PhD, MSE, 1990 (expected)

III. RESEARCH PLANS

Near term the research on the pyrolysis of TBAs and TBP, with and without the group III precursor, will continue. This will concentrate on the intentional addition of radicals to the system and the removal of t-butyl radicals using radical scavengers. In addition,

deuterated TBP has been obtained which is being used to substantiate the proposed reaction mechanisms.

Next, the same precursor molecules will be studied at lower pressures, approaching the chemical beam epitaxy (CBE) regime, where all reactions will be heterogeneous. Considerable interest in the alternate group V sources for CBE exists since TBAs and TBP may not require precracking. The vaccum equipment has been ordered and received. Installation is anticipated within the next 9 months.

Finally, work on the group II and group VI precursors will follow. The literature has been studied thoroughly and arrangements have been made to obtain several of the most interesting precursors. This study will include some of the novel Te molecules such as ditertiarybutyltelluride (DTBTe), diisopropyltelluride (DIPTe), methylallyltelluride (MATe), and diethylditelluride (DEDTe) as they become available.

APPENDIX A: REPRINTS OF PAPERS RESULTING FROM AFOSR SUPPORT

Reaction mechanisms in the organometallic vapor phase epitaxial growth of GaAs

C. A. Larsen, N. I. Buchan, and G. B. Stringfellow
Departments of Materials Science and Engineering and Electrical Engineering, University of Utah, Salt Lake City, Utah 84112

(Received 14 September 1987; accepted for publication 4 December 1987)

The decomposition mechanisms of AsH_3, trimethylgallium (TMGa), and mixtures of the two have been studied in an atmospheric-pressure flow system with the use of D_2 to label the reaction products which are analyzed in a time-of-flight mass spectrometer. AsH_3 decomposes entirely heterogeneously to give H_2. TMGa decomposes by a series of gas-phase steps, involving methyl radicals and D atoms to produce CH_3D, CH_4, C_2H_6, and HD. TMGa decomposition is accelerated by the presence of AsH_3. When the two are mixed, as in the organometallic vapor phase epitaxial growth of GaAs, both compounds decompose in concert to produce only CH_4. A likely model is that of a Lewis acid-base adduct that forms and subsequently eliminates CH_4.

Organometallic vapor phase epitaxy (OMVPE) has become a leading technique for the growth of III/V semiconductors, but little is known of the chemical processes that take place. An understanding of the reaction mechanisms of the precursors leading to growth is essential for efficient development of the OMVPE process.

We have studied the growth reactions by replacing the H_2 normally used as the carrier in OMVPE with D_2 (Ref. 1) in an atmospheric-pressure flow-tube reactor. This allows isotopic labeling of the products that are identified by a mass spectrometer. Kinetic data are coupled with the labeling information to further elucidate the mechanisms. The results for AsH_3 and TMGa, both alone and in mixtures, will be presented in this letter. The technique leads to the conclusions that TMGa decomposes homogeneously, primarily by attack from atomic D, and that GaAs growth involves the interaction of TMGa and AsH_3 prior to pyrolysis.

The decomposition of AsH_3 was found to be a first-order reaction on glass, As, and GaAs surfaces.[2-4] Decomposition of a mixture of AsH_3 and AsD_3 yielded primarily HD, while a mixture of AsH_3 and D_2 gave no HD. The reaction rate in He and H_2 flows[3] was independent of the carrier gas, but was increased by GaAs wafers.

The pyrolysis of TMGa was first studied in a toluene flow system.[4] The first methyl group came off above 500 °C, but the second radical was liberated only above 550 °C. The third gallium-methyl bond did not break, but instead a solid $(GaCH_3)_x$ polymer was formed.

The reaction at atmospheric pressure was faster in H_2 than in N_2, as found by mass spectrometry.[5] The main product in H_2 was methane, with small amounts of ethane and higher hydrocarbons. In N_2 the major product was also CH_4, but more C_2H_6 was formed. It was concluded that the reaction in N_2 was via homolytic fission, but that in H_2 the mechanism was hydrogenolysis, in which a H_2 molecule bonds simultaneously with the central atom and one of the ligands.

In situ infrared (IR) absorption studies of the reaction in H_2 at 76 Torr (Ref. 6) gave clear evidence of free gas-phase methyl radicals. IR measurements of the gases removed from an atmospheric-pressure reactor by a sampling tube[7] showed that CH_4 was the main product, with 2 mol of CH_4 produced per mol of TMGa below 450 °C and 3 mol above 465 °C. These results conflict with those of Ref. 4. Leys and Veenvliet[8] also found CH_4 as the only product for a TMGa-H_2 mixture at atmospheric pressure.

Several studies have been done on the reaction mechanism of mixtures of TMGa and AsH_3. Addition of TMGa enhances the pyrolysis rate of AsH_3.[6-11] One model[6] suggests that this enhancement and CH_4 production are due to methyl radicals from TMGa abstracting hydrogen atoms from AsH_3 molecules in the gas phase. Another model is that of a homogeneous adduct. A new absorption band appeared in the IR spectrum of the TMGa-AsH_3 system when mixtures of the two were heated to 400–560 °C.[11] Frolov *et al.*[12] showed that AsH_3 alters the decomposition mechanism of TMGa and concluded that gas phase clusters form and eliminate methane molecules.

Heterogeneous mechanisms are supported by the work of Schlyer and Ring,[10] who used neat mixtures of TMGa and AsH_3 at temperatures of 203–259 °C. They proposed that the first step in the reaction was independent adsorption of the two reactants, followed by formation of a surface adduct of the form $(CH_3)_3Ga{:}AsH_3$. This reaction is a classic Langmuir–Hinshelwood (LH) mechanism. Reep and Ghandhi[13] found that the rate law for the surface catalyzed reaction is less than first order for both TMGa and AsH_3, lending support to the LH mechanism.

Our apparatus consists of a 4-mm-i.d. silica tube in a furnace with a hot zone 41.5 cm long. A controlled flow of D_2 or other gas is mixed with the reactants and let into the furnace. The flow rate for the experiments was 40 sccm. The gas mixture leaving the reactor is admitted to a CVC model 2000 time-of-flight mass spectrometer. For some of the experiments the surface area in the reactor was increased by packing with silica chips. GaAs surfaces were deposited *in situ* by decomposing TMGa-AsH_3 mixtures.

The results of studies of the decomposition of AsH_3 in N_2 and D_2 are given in Table I, which lists the temperatures for 50% pyrolysis (T_{50}) under different experimental conditions. The ambient has no effect on the reaction rate, confirming the results of Ref. 3. Coating the tube walls with

 0003-6951/88/060480-03$01.00

GaAs lowered the pyrolysis temperature by over 100 °C. Mixtures of AsH_3 in D_2 on silica and GaAs surfaces yielded only H_2. No deuterated arsines were detected.

Any H atoms liberated in the gas phase would collide with D_2 molecules to generate HD. Therefore, the reaction takes place entirely on the surface in all cases, via the mechanism in Ref. 2. The rate-determining step is removal of the first H atom; H_2 is produced by surface recombination. The first-order kinetics indicate that all subsequent steps are rapid and that the surface is not saturated with AsH_3.[10]

The decomposition of TMGa is more complicated. The results are given in Table I and also Fig. 1, which shows the percent pyrolysis versus temperature in various ambients. Curve a was calculated from the data in Ref. 5 for a N_2 carrier. D_2 accelerates the reaction as shown by curve b, and H_2 (also from Ref. 5) lowers the pyrolysis temperature even more. The difference between H_2 and D_2 indicates that the carrier is involved in the rate-determining steps. Increasing the surface area had a minimal effect on the rate, so the decomposition is predominantly homogeneous.

Figure 1 also shows the effect of adding AsH_3 to the reacting mixture. A 1:1 AsH_3:TMGa ratio results in curve c, and increasing the ratio to 10:1 increases the pyrolysis even more (curve d). The T_{50} values for curves a–d are included in Table I for comparison.

The products of the decomposition in D_2 are given in Fig. 2. The major product is CH_3D, with C_2H_6, CH_4, and HD also being produced. Other studies have reported CH_4 as the main product in H_2,[5–8] but the present work elucidates the source of the methanes: they come mainly from reactions between the methyl radicals[6] and ambient. There are two possible routes for CH_3D formation. One is recombination of methyl radicals and free deuterium atoms. At atmospheric pressure, however, the activated CH_3D complex resulting from a gas phase collision tends to eliminate a H atom before the energy can be transferred to a third body.[14] The result would be significant amounts of multiply deuterated methanes, which are not observed. The more likely route for CH_3D formation is a metathesis between gas phase methyl radicals and D_2 molecules, as given in step (2) below. This also produces D atoms that can further participate in the

TABLE I. Temperature for 50% pyrolysis

Species	AsH_3/TMGa/carrier	Surface (cm^{-1})	T_{50} (°C)
AsH_3	0.05/0/0.95 N_2	SiO_2 (60)	600
AsH_3	0.05/0/0.95 D_2	SiO_2 (60)	598
AsH_3	0.05/0/0.95 D_2	GaAs (60)	476
TMGa	in N_2[a]	Ga	550
TMGa	0/0.006/0.994 D_2	Ga (60)	487
TMGa	in H_2[a]	Ga	459
TMGa	0/0.006/0.994 D_2	Ga (600)	464
AsH_3	0.03/0.003/0.967 D_2	Ga (600)	476
TMGa	0.03/0.003/0.967 D_2	Ga (600)	420
AsH_3	0.003/0.003/0.994 D_2	GaAs (60)	443
TMGa	0.003/0.003/0.994 D_2	GaAs (60)	434
AsH_3	0.003/0.003/0.994 D_2	GaAs (600)	387
TMGa	0.003/0.003/0.994 D_2	GaAs (600)	360

[a] From Ref. 5.

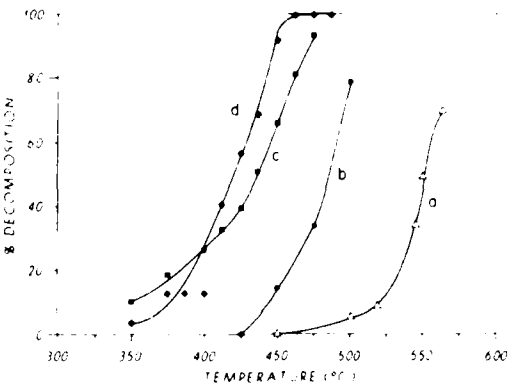

FIG. 1. Decomposition of TMGa: a, from Ref. 5 with the use of N_2; b,c,d, with AsH_3/TMGa/D_2 ratios of (b) 0/0.6/99.4, (c) 0.3/0.3/99.3, and (d) 3.3/0.3/96.3.

process. It is probable, based on kinetic modeling of the trimethylindium (TMIn)-D_2 system,[15] that these D atoms attack TMGa molecules as one of the decomposition steps. We propose the following mechanism for TMGa decomposition:

$$(CH_3)_3Ga \rightarrow 2CH_3 + CH_3Ga, \quad (1)$$

$$CH_3 + D_2 \rightarrow CH_3D + D, \quad (2)$$

$$D + (CH_3)_3Ga \rightarrow CH_3D + CH_3 + CH_3Ga, \quad (3)$$

$$n GaCH_3 \rightarrow (GaCH_3)_n\,(s), \quad (4)$$

$$2CH_3 \rightarrow C_2H_6. \quad (5)$$

Step (1) is an initiation step of homolytic fission of methyl groups from TMGa molecules. Steps (2) and (3) are the propagation steps of a chain reaction between the D atoms, the unreacted TMGa molecules, and the methyl groups. The chain cannot propagate in a N_2 carrier. Under low-pressure conditions or in cases where the residence time is short, the propagation steps may not be favorable. If the D_2 is replaced with H_2, its lower bond strength results in faster reactions. Step (4), the formation of a methylgallium polymer, accounts for the black deposits observed in the reactor and is consistent with the large dissociation energy of the last methyl-gallium bond.[3] The chain is terminated by the recombination step (5) to give C_2H_6. The minor amounts of CH_4 and

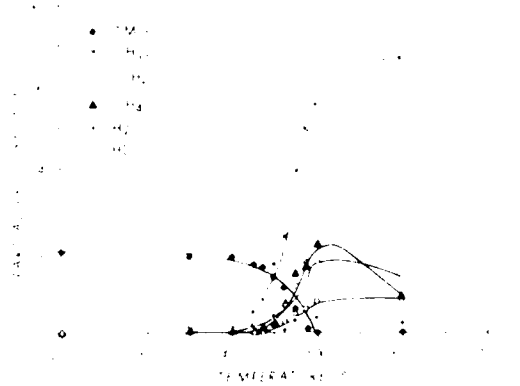

FIG. 2. Products of TMGa decomposition in D_2.

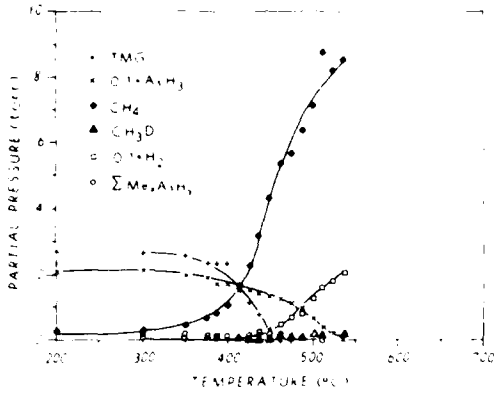

FIG. 3. Products of decomposition of a 10/1 AsH_3/TMGa mixture in D_2.

HD are probably due to degradation of the surface polymer by a complex tarring reaction.[16]

Mixtures of TMGa and AsH_3 decompose by a mechanism not available for either component alone. Figure 3 shows the products of the decomposition in D_2 with a V/III ratio of 10:1. The only hydrocarbon product is CH_4, except for some methylarsines at higher temperatures. All traces of CH_3D and C_2H_6 are absent. The H_2 comes from the excess AsH_3. The ratio of moles of TMGa to AsH_3 reacted is unity within experimental error. Furthermore, for mixtures with V/III ratios of 1:1, T_{50} for both reactants are identical. TMGa shifts the T_{50} for AsH_3 to a lower temperature than for a GaAs surface alone. Table I also shows that increasing the surface area further lowers the pyrolysis temperature, indicating that the reaction occurs heterogeneously.

The mechanism is concerted. The large surface effect shows that at low temperatures the reaction takes place heterogeneously. The reaction may proceed via the LH mechanism discussed above. Another possible route involves a Lewis acid-base adduct made of one TMGa and one AsH_3 molecule that forms in the gas phase, and subsequently eliminates CH_4 molecules. At low temperatures the elimination probably takes place heterogeneously. At higher temperatures the CH_4 production may be homogeneous, as predicted in Ref. 10. In actual OMVPE reactors with steep temperature profiles and complicated flow patterns, the reaction mechanism is probably between these two extremes. These results are qualitatively identical to those obtained for the trimethylindium-phosphine system.[17]

The technique of adding D_2 to the simulated OMVPE system has yielded important new results. AsH_3 decomposes by a purely heterogeneous mechanism. The pyrolysis of TMGa, on the other hand, proceeds via gas phase reactions. Methyl radicals produced by homolytic fission react with D_2 molecules to give CH_3D and D atoms. The D atoms may then participate in a chain reaction with the remaining TMGa. When TMGa and AsH_3 are mixed, the pyrolysis of both AsH_3 and TMGa occurs via a new mechanism in which the components react in concert to yield CH_4. The most likely pathway is via a Lewis acid-base adduct.

This work was supported by grants from NASA, Langley Research Center, contract No. NAG-1-608, and from the Air Force, contract No. AFSOR-87-0233.

[1]N. I. Buchan, C. A. Larsen, and G. B. Stringfellow, Appl. Phys. Lett. **51**, 1024 (1987).
[2]K. Tamaru, J. Phys. Chem. **59**, 777 (1955).
[3]I. A. Frolov, E. M. Kitaev, B. L. Druz', and E. B. Solokov, Russ. J. Phys. Chem. **51**, 651 (1977).
[4]M. G. Jacko and S. J. W. Price, Can. J. Chem. **41**, 1560 (1963).
[5]M. Yoshida, H. Watanabe, and F. Uesugi, J. Electrochem. Soc. **132**, 677 (1985).
[6]J. E. Butler, N. Bottka, R. S. Sillmon, and D. K. Gaskill, J. Cryst. Growth **77**, 163 (1986).
[7]S. P. DenBaars, B. Y. Maa, P. D. Dapkus, A. D. Danner, and H. C. Lee, J. Cryst. Growth **77**, 188 (1986).
[8]M. R. Leys and H. Veenvliet, J. Cryst. Growth **55**, 145 (1981).
[9]T. F. Keuch, E. Veuhoff, T. S. Kuan, V. Deline, and R. Potemski, J. Cryst. Growth **77**, 257 (1986).
[10]D. J. Schlyer and M. A. Ring, J. Organometal. Chem. **114**, 9 (1976).
[11]J. Nishizawa and T. Kurabayashi, J. Electrochem. Soc. **130**, 413 (198
[12]I. A. Frolov, P. B. Boldyrevskii, B. L. Druz', and E. B. Solokov, Inor. Mater. (Engl. transl.) **13**, 632 (1977).
[13]D. H. Reep and S. K. Ghandhi, J. Electrochem. Soc. **130**, 675 (1983).
[14]M. Brouard and M. J. Pilling, Chem. Phys. Lett. **129**, 439 (1986).
[15]N. I. Buchan, C. A. Larsen, and G. B. Stringfellow, J. Cryst. Growth (to be published).
[16]N. I. Buchan, C. A. Larsen, S. H. Li, and G. B. Stringfellow (unpublished results).
[17]C. A. Larsen, N. I. Buchan, and G. B. Stringfellow, J. Cryst. Growth **85**, 148 (1987).

GBS
5/23/85
JCG

MASS SPECTROMETRIC STUDIES OF TRIMETHYLINDIUM PYROLYSIS

N.I. Buchan, C.A. Larsen, and G.B. Stringfellow
Departments of Electrical Engineering
and Materials Science and Engineering
University of Utah, Salt Lake City, Utah 84112

Abstract

The homogeneous decomposition of trimethylindium (TMIn) in an atmospheric pressure flow tube apparatus was studied with a time-of-flight mass spectrometer in He, D_2, and H_2 carriers. Rate constants following the expressions

$$\log k_{gHe}(s^{-1}) = 17.9 - 54.0(\text{kcal/mol})/2.303\ RT,$$
$$\log k_{gD_2}(s^{-1}) = 13.4 - 39.8(\text{kcal/mol})/2.303\ RT,$$
$$\text{and } \log k_{gH_2}(s^{-1}) = 15.0 - 42.6(\text{kcal/mol})/2.303\ RT$$

were determined for the three carriers. The rate constant for pyrolysis in He is comparable to that found previously for pyrolysis in a radical scavenger; consequently, TMIn predominantly decomposes by homolytic fission in He, and not by radical attack of methyl groups on the TMIn. The pyrolysis of TMIn is enhanced in D_2 and H_2 carriers, where the principal products are CH_3D and C_2H_6, and CH_4 and C_2H_6, respectively. The ratio of the products (CH_3D or CH_4)/C_2H_6 in the H_2 and D_2 carriers monotonically decreases with increasing temperature. TMIn pyrolysis in a 1:1 D_2:H_2 carrier shows a very low production of HD due to isotopic randomization by H and D radicals. Both the enhanced pyrolysis in H_2 and D_2, and the gas phase mass balance of carbon at all temperatures, is attributed to radical attack by H or D on TMIn. With numerical modelling techniques a novel reaction mechanism involving a short-lived hypervalent DTMIn species was tested.

1. Introduction

Recently organometallic vapor phase epitaxy (OMVPE) has developed to the point that ultra-high purity III/V semiconductor materials such as GaInAs [1] and InP [2] have been grown. In addition, quantum structures are possible due to the achievement of atomically abrupt interfaces [3]. The organometallic compound in our study, TMIn, is important because it is nearly universally used as the OMVPE precursor for the growth of the In containing III/V semiconductors in atmospheric pressure reactors [4]. Further developments in OMVPE will be facilitated by an understanding of the fundamental mechanisms involved, both the fluid dynamics and the growth kinetics in the reactor. These results should prove useful in determining the viability of new group V-alkyl sources [5], photon assisted growth [6], and atomic layer epitaxy [7]. However, despite some preliminary work, fundamental research has lagged behind the practical development of OMVPE. The present work emphasizes the growth mechanisms that occur on the surface of the substrate and in the gas phase just above it in an atmospheric pressure reactor. In our technique the use of a D_2 ambient allows isotopic labelling of the reaction products which are analyzed with a time-of-flight mass spectrometer to indicate qualitatively the reaction mechanisms. The quantitative difference between the reaction products and rates found in D_2, and those found in H_2 show an isotope effect that can be modelled by chemical kinetic simulations to clarify the reaction mechanism.

We have previously reported results for the pyrolysis of PH_3 [8], the combined trimethylindium-phosphine (TMIn-PH_3) system in a D_2 carrier [9], and the combined trimethylgallium-arsine (TMGa-AsH_3) system [10]. In this work we report the results of a detailed study of the decomposition of TMIn in He, D_2, and H_2 carriers.

2. Summary of Research to Date

The pioneering work on the pyrolysis of TMIn was done by Jacko and Price with a typical flow system in a toluene carrier [11]. They concluded that TMIn pyrolyzed by homolytic fission, reaction R1a, and that the rate constant for breaking the second In-CH_3 bond, k_{1b}, was much higher than that for the first bond, k_{1a}. Thus, the first two CH_3 radicals are essentially produced simultaneously. Recently k_{1a} was recalculated to correct for the data being taken in the pressure fall-off region [12]. The Arrhenius parameters derived in refs. [11,12] are given in a later discussion.

$$In(CH_3)_3 \rightarrow In(CH_3)_2 + CH_3 \qquad (R1a)$$

$$In(CH_3)_2 \rightarrow In(CH_3) + CH_3 \qquad (R1b)$$

$$n\ In(CH_3) \rightarrow [In(CH_3)]_n\ (s) \qquad (R1c)$$

$$In(CH_3) \rightarrow In + CH_3 \qquad (R1d)$$

Jacko and Price also concluded that at temperatures < 480°C an involatile polymer results from the diffusion of monomethylindium (MMIn) molecules to the surface, reaction R1c. For temperatures > 480°C the breaking of the third In-CH_3 bond via reaction R1d

occurred in preference to reaction R1c. Support for reaction R1d was given in ref. [13] using infrared (IR) diode laser spectroscopy under low pressure OMVPE conditions. At temperatures > 480°C gas phase mass balance was achieved, i.e., the pre-reaction carbon content of the TMIn was equal to the total carbon content of the methyl radicals released during the reaction. An investigation using atomic absorption spectroscopy (AAS) [14] has cast doubt on reaction R1d because no gas phase In was observed during TMIn pyrolysis. Atmospheric pressure studies have shown enhanced pyrolysis of TMIn in H_2 (the TMIn-H_2 system) as opposed to N_2 as the carrier gas [15], and they also questioned the AAS results based on the experimental setup that was used. Since the existence of gas phase In is an unresolved issue we do not exclude reaction R1d.

For pyrolysis of TMIn in toluene, the principal reaction products were found to be C_2H_6 and CH_4 [11]. During low pressure OMVPE in the TMIn-H_2 system only methane was observed; hence, the abstraction by CH_3 of an H atom from either TMIn, reaction R1f, and/or H_2 , reaction R2b, were proposed [13].

$$CH_3 + In(CH_3)_3 \rightarrow In(CH_3)_2 + C_2H_6 \qquad (R1e)$$

$$\rightarrow In(CH_3)_2CH_2 + CH_4 \qquad (R1f)$$

$$CH_3 + D_2 \rightarrow CH_3D + D \qquad (R2a)$$

$$CH_3 + H_2 \rightarrow CH_4 + H \qquad (R2b)$$

$$CH_3 + CH_3 + M \rightarrow C_2H_6^* + M \rightarrow C_2H_6 + M \qquad (R3)$$

Because no ethane was observed, the methyl radical attack of TMIn, reaction R1e, and methyl radical recombination, reaction R3, were

considered unimportant at low TMIn pressures [13]. Radical attack of TMIn at low TMIn pressures, or in the presence of radical scavengers, is therefore considered unlikely. Reaction R3 involves a collision between two methyl radicals forming an activated $C_2H_6^*$. The relaxation of the $C_2H_6^*$ is dependent on a collision with a third body (M) and hence depends on the reactor pressure. At reactor pressures of one atmosphere, and the range of temperatures considered here, every collision results in the formation of C_2H_6, i.e., reaction R3 is at its high pressure limit [16]. In this paper we have used a novel approach to elucidate the reaction mechanism of TMIn. A D_2 carrier was used to approximate the reaction pathways in an H_2 carrier while isotopically labelling the reactions occurring during TMIn pyrolysis. A quantitative analysis of the non-condensed gas products of TMIn pyrolysis in the TMIn-He, TMIn-D_2, and TMIn-H_2 systems provides information leading to a determination of the likely reaction mechanisms in all three carriers.

3. Experimental Apparatus

3.1 Ersatz OMVPE Reactor

The typical atmospheric pressure flow tube apparatus used is the same as described in previous work [8-10]. The carrier gases D_2, H_2, and He were used. After the carrier gas is saturated with TMIn (Alfa lot#102486) in an isothermal bubbler held at 20°C, resulting in a 1.7 torr pressure of TMIn, it flows into the furnace through a 4 mm ID fused silica tube. The reaction products rapidly cool upon leaving the furnace and only those which have significant

room temperature vapor pressures flow to the adjustable leak inlet to the mass spectrometer. The majority of the reaction products flow on to scrubbing solutions where PH_3 and TMIn are completely decomposed, and the effluent hydrocarbons exhausted.

The 4 mm diameter fused silica reactor tube has a surface area of 50 cm^2. The surface area is increased to 600 cm^2 by packing with silica chips that are approximately 0.8 mm in diameter. The fused silica tubing and chips were cleaned with HF and dried before use. After commencing TMIn decomposition the reactor tube surface becomes coated with In. To simplify comparisons between experiments the average flow rates of the reactant gas mixtures were kept constant at 40 sccm.

3.2 *Furnace Profile*

The furnace profile is shown in fig. 1. The isothermal region in the tube has the same length at all temperatures, x_i = 41.5 cm, which allows the calculation of contact times and hence reaction rate constants. The steep temperature gradients allow the assumption that at moderate temperatures all reactions occur predominantly in the isothermal region, though at high temperatures, i.e., those at which the reactions are virtually complete in a small fraction of the tube length, the reactions occur predominantly in the region having a temperature gradient, which prevents an unambiguous interpretation of the results.

4. Results

4.1 Mass Spectra

The fragmentation pattern of TMIn at an electron-impact energy of 70 eV showed a large amount of methyl, ethyl, and metal containing ions similar to those previously reported [17]. Reduction of the electron impact energy to 20 eV reduced the fragmentation while maintaining an acceptable ionization cross-section, σ, for all the TMIn decomposition product species of interest. The mass spectra of the products of TMIn decomposition are split into two ranges, m/e = 0 to 45 appears in figs. 2a-c, and m/e = 100 to 180 in figs. 2d-f. The mass spectra of TMIn in He, D_2, and H_2 carriers as a function of reactor temperature are shown in figs. 2a and d, b and e, and c and f, respectively. Because the significant decomposition products all appear at m/e < 45, figs. 2a-c show the variation of the reaction products with carrier gas. At m/e > 100, fig. 2d-f, only the TMIn fragmentation pattern is evident. It shows enhanced TMIn decomposition in D_2 and H_2 carriers compared to that found in a He carrier. The fragmentation pattern of TMIn depends on the gas mixture, as is shown by the contributions at m/e = 15, 16, and/or 17 at room temperature in figs. 2a-c. Contributions at m/e = 18, 19, and 20 are due to H_20 resident in the mass spectrometer and a D_2O impurity in the CP grade D_2. The random error associated with the signal from the H_20 and D_20 impurity reduces our detection limit of the multiply deuterated species CH_2D_2 to approximately 0.15 torr. At elevated reactor temperatures the decomposition of TMIn in the

D_2 carrier, fig. 2b, produces CH_3D and C_2H_6. To quantitatively establish the amount of CH_3D produced at a given reactor temperature we subtracted the fragmentation pattern contributions of TMIn, normalized to the m/e = 145 intensity, that superpose those of the CH_3D. The decomposition of TMIn in He, fig. 2a, and H_2, fig. 2c, carriers at elevated temperatures was treated similarly to remove fragmentation effects. The results of these analyses are shown in Sect. 4.3.

4.2 Reaction Rates

To establish that the decomposition of TMIn in D_2 is homogeneous as opposed to heterogeneous, i.e., occurring in the gas phase rather than on the reactor walls, the percent TMIn decomposition at In-coated surface areas of 50 cm^2 and 600 cm^2 is shown in fig. 3. In light of the large change in reactor surface area a heterogeneous reaction is not consistent with the slight change in TMIn decomposition. We conclude that the rate constant for breaking the first In-CH_3 bond in a D_2 carrier is predominantly homogeneous in a 50 cm^2(In) reactor tube, similar to the conclusion reached for the TMIn-toluene system in [11].

All subsequent experiments were performed in a 50 cm^2 reactor tube coated with In. The effect on the decomposition of TMIn of using three different carriers, He, D_2, and H_2, is shown in fig. 4. The partial pressure of TMIn was determined by measuring the principal mass spectral peak of TMIn (m/e = 145) which is proportional to the partial pressure of TMIn. To establish the order

of TMIn decomposition in a D_2 carrier (the TMIn-D_2 system), reaction orders of zero and one were assumed, and the TMIn decomposition was plotted versus residence time in fig. 5. A zeroth order reaction shows a distinctly non-linear plot, but the good linear fit achieved assuming a first order reaction indicates a reaction order close to one. Hence, the decomposition of TMIn in all three carriers was treated as a first order reaction and shown in an Arrhenius plot in fig. 6. Only the data for TMIn decomposition between 5 and 95% were included, to minimize the effect of experimental uncertainty on the plot. Included in fig. 6 is the curve established in ref. [12] for the TMIn-toluene system. We established the overall rate constants for TMIn decomposition, k_g, which follow the expressions

$$\log k_{gHe}(s^{-1}) = 17.9 - 54.0(\text{kcal/mol})/2.303\ RT$$
$$\log k_{gD_2}(s^{-1}) = 13.4 - 39.8(\text{kcal/mol})/2.303\ RT$$
$$\log k_{gH_2}(s^{-1}) = 15.0 - 42.6(\text{kcal/mol})/2.303\ RT$$

in He, D_2, and H_2, respectively.

4.3 Reaction Products

The partial pressures of all species in the gas phase were calculated as a function of temperature by summing the ion currents for each species in the mass spectra, fig. 2, and dividing by the empirically determined ionization cross-sections of the molecules at 20 eV. The principal pyrolysis product in the TMIn-He system is C_2H_6 with a small amount of CH_4 as shown in fig. 7. A slight carbon

deposit was observed in the reaction tube as was reported earlier [15]. The pyrolysis of TMIn in the TMIn-D_2 and TMIn-H_2 systems evolved the products CH_3D and C_2H_6 as shown in fig. 8, and CH_4 and C_2H_6 in fig. 9, respectively. No carbon deposit was observed in these systems, and no HD was observed in the TMIn-D_2 system. The ratio of methane to ethane ((CH_4 or CH_3D)/C_2H_6) is plotted versus temperature for these systems in fig. 10. In the TMIn-D_2 and TMIn-H_2 systems a gas phase mass balance of carbon containing species was observed at all temperatures. For the products of the TMIn-He system a mass balance was not observed, due in part to a calibration error as well as the carbon deposit on the reaction tube. However, it is important to note that in all three carriers at one atmosphere there was no sudden change in the mass balance above 480°C as was reported in refs. [11,13] under low pressure OMVPE conditions.

4.4 Formation of HD in the TMIn-D_2-H_2 system

A key result for defining the reaction mechanism was obtained by studying the pyrolysis of TMIn in an ambient containing both H_2 and D_2. To unambiguously determine the effect of TMIn in a 1:1 D_2:H_2 carrier we first studied the HD formation with only D_2 and H_2 present, reaction R4.

$$H_2 + D_2 \rightarrow 2HD\,. \qquad \text{(R4)}$$

The HD formation in a 1:1 mixture of D_2:H_2 in the presence of an SiO_2(50 cm^2) surface is shown in fig. 11. The HD formation in a 1:1 mixture of D_2-H_2 including a 1.7 torr partial pressure of TMIn (the

TMIn-D_2-H_2 system) is also shown. The 6 torr background level of HD is due to an impurity in the CP grade D_2 used. The products for the TMIn-D_2-H_2 mixture, principally undeuterated methane, and the k_g are very similar to those in the TMIn-H_2 system. However, the HD formed in the TMIn-D_2 system at temperatures below 400°C was less than the detectable limit of 0.05 torr (to enhance the detectability limit of HD a D_2 source was used that contained a background level of only 1.5 torr HD). The production of HD, precisely at the temperatures at which TMIn pyrolyzes in the TMIn-D_2-H_2 system, contrasts with the absence of HD in the reaction products for the TMIn-D_2 system.

5. Discussion

5.1 Radical Attack of TMIn

The results presented in Sect. 4 give a new insight into the reaction mechanisms for TMIn decomposition. The similarity of the k_g for pyrolysis of TMIn in toluene (a radical trapping ambient) to that of TMIn in He indicates that the trapping of CH_3 radicals has little effect on TMIn pyrolysis. Thus, reactions R1e and R1f appear to be less important than the homolytic fission of TMIn, reaction R1a. Additional weight is given this argument by the small amount of CH_4 formed in the products of the TMIn-He system, fig. 7; even if this product were attributed to reaction R1f it would suggest that only a minority of TMIn is decomposed in this way. Further support is generated by comparing the reaction rates of methyl radical abstraction of hydrogen from metal-alkyls to the reaction rate of

methyl radicals with D_2 (or H_2). Assuming the value of the Arrhenius parameters for hydrogen abstraction from TMIn are comparable to those listed in table 1, the Arrhenius parameters for reaction R1f and reaction R2a (or R2b) [18-21] (table 2) are approximately the same. Hence, because the concentration of the D_2 (or H_2) is two and a half orders of magnitude higher than that of TMIn, the reaction rates of reactions R2a (or R2b) are much higher than that for reaction R1f. Therefore, we conclude that reactions R1e and R1f are not important in the TMIn-He system at reactor pressures of one atmosphere, and in the TMIn-H_2 and TMIn-D_2 systems, where a competitive reaction removes methyl radicals, reactions R1e and R1f are even more insignificant. However, as will be discussed in Sect. 6.2.3, modelling of the results shows that methyl radicals play a role in radical recombination with D (or H) on hypervalent DTMIn (or HTMIn) species.

The reactions presented so far do not explain the higher values of $k_{g_{H_2}}$ and $k_{g_{D_2}}$ as compared to $k_{g_{He}}$ and kg in the TMIn-toluene system [11]. D (or H) radical attack on TMIn is a likely explanation. A possible analog reaction for similar group IV molecules exists (H + tetramethylsilane shown in table 1), but the HD formed in the TMIn-D_2 system at temperatures below 400°C was less than 0.05 torr, as compared to the 0.68 torr of TMIn that is decomposed at 350°C in a D_2 ambient in excess of that in an He ambient. Therefore, the abstraction of H from TMIn by D radicals is not considered important in our system. However, we do believe radical attack by D (or H) radicals on TMIn forms a hypervalent, short-lived DTMIn (or HTMIn) species, as discussed in Sect. 6.2.3.

5.2 Radical Attack on MMIn

In contrast to the gas phase mass balance of carbon observed in our experiments, the formation of polymers and a lack of carbon mass balance were reported for low reactor pressures and in radical scavenging carriers, as discussed in Sect. 2. These contrasting results suggest that radical attack of MMIn occurs at one atmosphere reactor pressure, but perhaps not at reduced pressures. In a He carrier the radical attack of MMIn by CH_3 is possible, as indicated by reactions R5a and R5b. Reaction R5a has an energetically favorable ΔH of reaction of -47.3 kcal/mol based on the bond energies of In-CH_3 (40.7 kcal/mol [11]) and H_3C-CH_3 (88 kcal/mol [25]).

$$CH_3 + MMIn \rightarrow C_2H_6 + In \qquad (R5a)$$

$$\rightarrow CH_4 + In\text{-}CH_2 \qquad (R5b)$$

$$D + MMIn \rightarrow CH_3D + In \qquad (R6)$$

In a D_2 or H_2 carrier MMIn could be attacked by a D or H radical, as shown in reaction R6. This is also an energetically favorable reaction having a ΔH of reaction of -65.3 kcal/mol based on the bond energies of H-CH_3 (104 kcal/mol [26]) and In-CH_3. Reaction R5a might also occur in H_2 and D_2 since it is consistent with the observed products in those systems.

5.3 Other D Radical Reactions

In addition to D radical attack of metal-alkyls, other D radical reactions must be considered to explain our results. These include D radical recombination which is dependent on a third body (M) collision, reaction R7, and the formation of a surface adsorbed D(s) due to the diffusion of D radicals to surface sites, reaction R8. D (or H) radical attack on H_2 (or D_2) forms HD via reaction R9 (or R10), but H or D attack on HD is ignored because of the low HD partial pressures observed in our experiments. The recombination of CH_3 and D radicals to form the activated complex CH_3D^* [27], reaction R11a, is followed by reaction R11b, forming a C-D in preference to the C-H bond before breaking apart. At a reactor pressure of one atmosphere and at 600K the third body dependent relaxation of the CH_3D^*, reaction R11c, is far from its high pressure limit, and has a reaction rate constant that is at least 20 times slower than that for reaction R11b [28]. Reaction R11a does not occur significantly in our TMIn-carrier systems because it leads to reaction R11b which would then couple with reaction R2a to form $CH_{4-x}D_x$ $x>1$ species that are not observed.

$$D + D + M \rightarrow D_2 + M \qquad \text{(R7)}$$

$$D + (s) \rightarrow D(s) \qquad \text{(R8)}$$

$$D + H_2 \rightarrow HD + H \qquad \text{(R9)}$$

$$H + D_2 \rightarrow HD + D \qquad \text{(R10)}$$

$$CH_3 + D \leftrightarrow CH_3D^* \qquad \text{(R11a)}$$

$$CH_3D^* \rightarrow CH_2D + H \qquad \text{(R11b)}$$

$$CH_3D^* + M \rightarrow CH_3D + M \qquad \text{(R11c)}$$

6. Reaction Mechanism

6.1 Numerical Modelling

Four salient features of our results can be used for developing models for the reaction mechanism in the TMIn-D_2 and TMIn-H_2 systems. 1) The experimental TMIn pyrolysis curves in the H_2 and D_2 ambients, fig. 4, show an isotope effect and both differ from results obtained in the TMIn-He system. 2) The ratio of the principal products (CH_3D or CH_4)/C_2H_6 for TMIn decomposition in H_2 and D_2 ambients, fig. 10, also demonstrate an isotope effect and differ significantly from results obtained in an inert ambient (the TMIn-He system). 3) The low HD partial pressure formed in the TMIn-D_2-H_2 system, fig. 11, cannot be explained by H abstraction from TMIn by D radicals. 4) The gas phase carbon must be conserved, i.e., any MMIn that is formed must be decomposed. Due to the large number of reactions discussed above, and the number of additional reactions we later consider, the modelling of TMIn decomposition was beyond the scope of a simple qualitative analysis. Instead we used Euler's method to extrapolate the partial pressures of homogeneous species, i.e., we calculated the partial pressure of a species at time t + dt by evaluating the derivative of the partial pressure at time t, multiplying by dt, and adding the result to the partial pressure at time t. As an example, eqs. 1 and 2 are the time derivatives of the CH_3D and C_2H_6 partial pressures resulting from the bimolecular reactions R2a and R3, respectively. The Arrhenius parameters used in our modelling efforts are listed in table 2.

$$\frac{dCH_3D}{dt}\ (mol/l\cdot s) = 10^{8.85}e^{-11.9(kcal/mol)/RT}\ [CH_3][D_2] \qquad (1)$$

$$\frac{dC_2H_6}{dt}\ (mol/l\cdot s) = 10^{10.54}\ [CH_3]^2 \qquad (2)$$

Our strategy was to first model the TMIn decomposition in H_2 and D_2 ambients assuming simple homolytic fission, and then to make the model more complex one step at a time until the major features of the experimental data were explained. In an effort to develop chemical insight the models were kept as simple as possible.

Because the diffusion velocities of the gas species can be estimated to be an order of magnitude less than the average flow velocity, the conditions in the flow tube were simulated by specifying initial non-zero partial pressures for only the TMIn and the D_2 (or H_2) carrier. It is clear that Euler's method generates the data with which to calculate the temperature dependence of the amount of TMIn decomposition, (CH_3D or CH_4)/C_2H_6 ratio, and the final MMIn concentration. It is more complicated to calculate the exact concentration of HD formed in the TMIn-D_2-H_2 system for which reactions R7-R10 must be included.

In the TMIn-D_2-H_2 system the reaction products and overall reaction rate are approximately those of the TMIn-H_2 system. Hence, H radicals are produced by reaction R2b in the TMIn-D_2-H_2 system at a greater rate than are D radicals by reaction R2a. Therefore, it is estimated that reaction R10 depends on half an atmosphere of D_2 and dominates reaction R9, which has similar Arrhenius parameters. In a 1:1 mixture of H and D radicals the reactions R7 and R8 would produce an approximate stoichiometric ratio of D_2:HD:H_2 equal to

1:2:1. Therefore, as an upper limit, reactions R7 and R8 were estimated to produce HD half of the time, otherwise reforming H_2 and D_2. The diffusion time of H and D radicals to the In coated walls, reaction R8, was estimated to be 0.02 seconds based on an estimated diffusion coefficient of 2 cm^2/sec and the 2 mm radius of the tube. The reaction was only modelled at temperatures below 437°C, because at higher temperatures the reactions occur in the steep thermal gradient at the input to the furnace and are not amenable to simple modelling.

6.2 Modelling Results

6.2.1 Model 1

In model 1 we assumed methyl radicals were generated by a modified version of reaction R1a in which 3 methyl radicals are produced simultaneously by homolytic fission. To be consistent with our experimental results the Arrhenius parameters for reaction R1a used in modelling were those of k_{gHe} generated for the TMIn-He system, and not the values for refs. [11,12] listed in table 2. In the TMIn-D_2 and TMIn-H_2 systems the methyl radicals reacted with their respective ambients by reactions R2a (or R2b); in either ambient the methyl radicals recombined by reaction R3 to form C_2H_6. The numerically calculated TMIn decomposition in each ambient is displayed as a broken curve in fig. 4; because no provision was made for enhanced pyrolysis of TMIn in the TMIn-D_2 or TMIn-H_2 systems, the decomposition curves fit the TMIn-He data. The calculated (CH_3D or CH_4)/C_2H_6 ratios in both D_2 and H_2

ambients corresponding to the model are shown in fig. 10. The HD formation is shown in fig.11 as a broken curve.

The calculated (CH_3D or CH_4)/C_2H_6 ratios are higher than the experimental data at low temperatures and lower than the experimental data at high temperatures. However, the calculated ratios qualitatively mimic the trend of the experimental data. These trends are related to the dependence of reactions R3 and R2a and b on [CH_3]. Because the homolytic fission of TMIn is rapid at high temperatures, the generation rate of methyl radicals is orders of magnitude higher at high temperatures. Consequently, due to the dependence of the reaction rate of reaction R3 on [CH_3]^2 shown in eq. 2, it becomes competitive with those of reactions R2a and R2b, which have a linear dependence on [CH_3] shown in eq. 1.

The calculated HD production in the TMIn-D_2-H_2 system is shown in fig. 11. As reactions R2a and R2b produce D and H radicals, reactions R7 and R8 remove the radicals from the reaction. However, due to the low reaction rates of reactions R7 and R8 they only have an influence at high D concentrations. Consequently HD is produced so quickly by reactions R9 and R10 that the 1:1 D_2:H_2 mixture forms its random, isotopically mixed ratio of D_2:HD:H_2 = 1:2:1 in a fraction of the reactor tube length.

6.2.2 Model 2

To improve the model our next objective was to increase the (CH_3D or CH_4)/C_2H_6 ratio at high temperatures and decrease the formation of HD by reducing the concentration of H and D radicals. In

model 2 reaction R1a was assumed to form two methyl radicals and an MMIn simultaneously. As in model 1, reactions R2a (or R2b) and R3 were used. MMIn was decomposed via reaction R1d, and the novel reaction R6 was added. Reaction R6 is approximately collision controlled, i.e., the reaction rate depends solely on the collision frequency, with an estimated rate constant of 5×10^9 l/mol·s. Model 2 produced results that are compared to the experimental data in figs. 4, 10, and 11.

As in model 1, the enhanced decomposition of the TMIn-H_2 and TMIn-D_2 systems is not accounted for. However, the (CH_3D or CH_4)/C_2H_6 ratio is raised because one CH_3 per TMIn is guaranteed to react via reaction R6, as opposed to being homolytically released and subsequently forming some C_2H_6 by reaction R3 (homolytic fission of MMIn, reaction R1d, is not competitive below 480°C). Reaction R6 reduced the D concentration by reacting the D with the MMIn, though this effect is barely noticeable in the HD formation resulting from reactions R9 and R10.

6.2.3 Model 3

Clearly, a more complex model is necessary to explain both the enhanced decomposition in the TMIn-D_2 and TMIn-H_2 systems and the low concentration of HD formed by reactions R9 and R10, which implies maintaining a very low [D] throughout the reaction. The most appealing method of reducing [D] is the formation of a hypervalent DTMIn species by reaction R12. Subsequent collision of this species with CH_3 or D radicals was assumed, in our model, to

cause annihilation of a CH_3 radical by recombination with D via reaction R13, and the annihilation of an additional D radical by reforming D_2 via reaction R14. For simplicity, the formation of a (CH_3)TMIn species was not included in this model. Decomposition of the DTMIn species, reaction R15, was assumed to form no MMIn.

$$D + TMIn \rightarrow DTMIn \qquad (R12)$$

$$CH_3 + DTMIn \rightarrow CH_3D + TMIn \qquad (R13)$$

$$D + DTMIn \rightarrow D_2 + TMIn \qquad (R14)$$

$$DTMIn \rightarrow CH_3D + 2\,CH_3 + In \qquad (R15)$$

The formation of hypervalent organometallic molecules is not without precedent. Reactions analogous to R12 and R14 were proposed for H abstraction by D radicals on SiH_4 by Glasgow et al [23]. In their experiments no D-containing species were formed despite the disappearance of photolytically created D radicals. Hence, they invoked the existence of a moderately stable, though short lived, SiH_4D species upon which D radical recombination occurred. This mechanism was supported by a molecular model that was used to calculate ΔG of reaction for the formation of the SiH_4D molecule from a D radical and SiH_4. Depending on the assumed molecular configuration, a ΔG between -36.9 and -83.0 kcal/mol was calculated for the reaction. Although the results were later explained by adsorption on the reactor walls via reaction R8, the very exothermic energy of reaction for the SiH_4D species supports the viability of the formation of DTMIn via reaction R12.

Model 3 used the same reactions R1a, R2a or b, R3, R1d, and R6 as did model 2. The rate constants for CH_3 and D radical attack in reactions R6 and R12-R14 were given approximate collision controlled Arrhenius parameters. The calculated pyrolysis of the TMIn-D_2 system was matched to the experimental pyrolysis by adjusting the rate constant for the decomposition of the DTMIn species, reaction R15. Based on the same rate constants for reactions R6 and R12-R15 in the TMIn-H_2 system as were used in the TMIn-D_2 system, the numerically calculated decomposition curve accurately matched the experimental data. The enhanced pyrolysis in the TMIn-H_2 system over that in the TMIn-D_2 system is caused by the higher rate constant for reaction R2b than for reaction R2a which in turn causes a higher concentration of H than of D radicals. The calculated (CH_3D or CH_4)/C_2H_6 ratios agree with the experimental data better than the results of models 1 and 2, following the experimental trends both qualitatively and quantitatively. Most significantly, the low HD formation correlates with the experimental data very well, indicating that the H and D radicals produced by reactions R2a and b are quenched rapidly.

The effect of including reactions R11a-c in model 3 was analyzed in recent modelling results. In a D_2 ambient, and throughout the temperature regime of our experiment, less than 4.6% of the methane was multiply deuterated ($\approx$ 0.15 torr at 400°C), the amount of deuterated ethane produced by the recombination of these multiply deuterated ethanes in the model is comparably small. The small amount of multiply deuterated methane (predominantly CH_2D_2) produced in the model is at our experimentally detectable threshold

of 0.15 torr (see section 4.1). Hence, the amounts of CH_2D_2 produced experimentally and in the modelling effort are comparably low, and reactions R11a-c are not considered important in this reaction mechanism.

The evolution of the product partial pressures versus time for the TMIn-H_2 system at 350°C is shown in fig. 12. The monotonically decreasing concentration of TMIn is accompanied by an HTMIn concentration that is significantly and consistently lower than that of the TMIn (the concentration of HTMIn is low enough that Butler [13] might not have detected it). The MMIn, though it increases through the early stages of pyrolysis, is effectively decomposed by the H radicals via reaction R6 as shown by the decreasing MMIn concentration after 1.5 seconds. However, contrary to our experimental results, the calculated MMIn concentration at other temperatures in the TMIn-H_2 system, and at all temperatures in the TMIn-D_2 system, is higher than that shown in fig. 12. Throughout the reaction the concentrations of CH_4 and C_2H_6 increase monotonically and maintain a nearly constant ratio. The virtually total decomposition of TMIn occurs within 2.2 seconds. Subsequently, the reaction lacks a source of CH_3 and H radicals and the symbiotic annihilation of HTMIn, CH_3, and H by reactions R13 and R14 is observed. The concentrations of CH_3 and H at all times show that the formation of $CH_{4-x}D_x$ ($x>1$) in the TMIn-D_2 system, initiated by reactions R11a and b, will occur only to a minor extent because of the competitive reactions R6 and R12-R14. This result agrees with the experimentally determined absence of detectable amounts of multiply deuterated methanes in the TMIn-D_2 system.

In developing model 3 several speculative assumptions were made: invoking a hypervalent species, DTMIn, and assuming the DTMIn and MMIn species react with CH_3 and D radicals. In addition, the pre-exponential Arrhenius parameter for the decomposition of the DTMIn species, listed in table 2, is far below that expected for a unimolecular gas phase decomposition process [29]. Therefore, we are forced to conclude that the reaction mechanism analyzed in model 3 still represents a simplification of the actual reaction mechanisms. Furthermore, a numerical model that includes speculative reactions and reaction rate constants cannot unequivocally be described as unique; it can only be described as one of several possible models. However, the excellent qualitative description of the experimental data by our model indicates that radical attack on TMIn by D and H radicals is likely to be the dominant reaction mechanism. Radical attack by H on group III organometallic species should be considered in the analysis of reaction mechanisms important for atmospheric pressure OMVPE growth systems.

7. Summary

The rate constant for the pyrolysis of TMIn in He is comparable to that found previously in ref. [11] in a toluene carrier, a radical scavenger; consequently, TMIn is presumed to decompose predominantly by homolytic fission in He, and not by radical attack of methyl groups on the TMIn. The decomposition of TMIn in a D_2 carrier is predominantly homogeneous. It is enhanced in a D_2 carrier

and even more so in an H_2 carrier, indicating that the reaction pathway in these carriers is different from that in He and toluene ambients. The principal products in a D_2 carrier are CH_3D and C_2H_6; the methane to ethane ratio, (CH_3D/C_2H_6), decreases monotonically as the temperature is raised. The reaction products in an H_2 carrier are analogous, CH_4 and C_2H_6; their methane to ethane ratio is higher than that found in D_2, but has a similar dependence on temperature. In our results the carbon content of the decomposed TMIn in D_2 and H_2 ambient is equal to the carbon content of the products. This gas phase mass balance at all temperatures differs from the results reported for low pressure systems and for radical scavenging carriers; in these cases the balance was only achieved above 480°C. This difference is attributed to the radical attack of D or H atoms on MMIn and TMIn at atmospheric pressure. The concentration of HD formed during the pyrolysis of TMIn in a 1:1 D_2:H_2 carrier is very low, indicating that an approximately collision controlled reaction with gas species removes the D radicals.

Using numerical modelling techniques, the most likely reaction mechanism of TMIn in a D_2 ambient was determined to involve the radical attack of D on TMIn forming a short-lived hypervalent DTMIn species. Decomposition of this species is responsible for the enhanced pyrolysis of TMIn in a D_2 ambient. Reaction of this species with D or CH_3 radicals quenches the radical concentrations and forms the reaction product CH_3D. The relatively stable MMIn molecules are decomposed in a reaction with D radicals in atmospheric pressure reactors, also forming CH_3D. The CH_3D and C_2H_6 reaction products in D_2 ambient also result in part from methyl

radical attack on the ambient and methyl radical recombination, respectively. The reaction mechanism is the same in an H_2 ambient.

Acknowledgements

This work was supported by grants from NASA, Langley Research Center, contract number NAG-1-608, and from the Air Force, contract number AFSOR-87-0233.

Table 1: Hydrogen Abstraction from Metal-alkyls

Reaction	log A(l/mol·s)	Ea (kcal/mol)	logk(l/mol·s) @ 32°C	ref
$CH_3 + B(CH_3)_3$	8.8	9.9	1.7	[18]
$CH_3 + Ge(CH_3)_4$	8.8	9.9	1.7	[18]
$CH_3 + Si(CH_3)_4$	8.8	10.4	1.4	[22]
		10.3		[23]
$H + Si(CH_3)_4$			< 7.0	[24]

Table 2: Arrhenius parameters for known and postulated reactions

	Reaction	log(A)	Ea(kcal/mol)	log k	ref
(R1a)	$TMIn \rightarrow MMIn + 2CH_3$	17.9 [a]	53.9		
		15.7 [a]	47.2		[11]
		16.1 [a]	48.0		[12]
(R1d)	$MMIn \rightarrow In + CH_3$	10.91 [a]	38.7		[11]
(R2a)	$CH_3 + 2 \rightarrow CH_3D + D$	8.85 [b]	11.9		[18]
(R2b)	$CH_3 + H_2 \rightarrow CH_4 + H$	8.93 [b]	10.9		[18]
(R3)	$CH_3 + CH_3 \rightarrow C_2H_6$	10.54 [b]	0.0		[30]
(R6)	$D + MMIn \rightarrow In + CH_3D$	9.7 [b]	0.0		
(R12)	$D + TMIn \rightarrow DTMIn$	10.0 [b]	0.0		
(R13)	$CH_3 + DTMIn \rightarrow CH_3D + TMIn$	9.7 [b]	0.0		
(R14)	$D + DTMIn \rightarrow D_2 + TMIn$	9.7 [b]	0.0		
(R15)	$DTMIn \rightarrow CH_3D + 2CH_3 + In$	9.3 [a]	20.0		
(R7)	$D + D + M \rightarrow D_2 + M$				
	$H + H + M \rightarrow H_2 + M$	9.6 [c]	0.0		[30]
(R8)	$D + (s) \rightarrow D(s)$			1.7 [a]	
(R9)	$D + H_2 \rightarrow HD + H$				
(R10)	$H + D_2 \rightarrow HD + D$	10.7 [b]	9.4		[31]
(R11a,b)	$CH_3 + D \rightarrow CH_2D + H$ (@600K)			11.45 [b]	[28]
(R11a,c)	$CH_3 + D + M \rightarrow CH_3D + M$ (@600K,1 atm D_2)			10.15 [b]	[28]
	$CH_3 + H \rightarrow CH_3 + H$ (@600K)			11.45 [b]	[28]
	$CH_3 + H + M \rightarrow CH_4 + M$ (@600K,1 atm H_2)			10.55 [b]	[28]

a (s^{-1}), b (l/mol·s), c ($l^2/mol^2 \cdot s$)

References

[1] C.P. Kuo, J.S. Yuan, R.M. Cohen and G.B. Stringfellow, Appl. Phys. Lett. 44 (1984) 50.

[2] L.D. Zhu, K.T. Chan and J.M. Ballantyne, Appl. Phys. Lett. 47 (1985) 47; C.H. Chen, M. Kitamura, R.M. Cohen and G.B. Stringfellow, Appl. Phys. Lett. 49 (1986) 963.

[3] T.H. Wang, K.L. Fry, A. Persson, E.H. Reihlen, and G.B. Stringfellow, Appl. Phys. Lett. (accepted).

[4] C.C. Hsu, R.M. Cohen and G.B. Stringfellow, J. Cryst. Growth 63 (1983) 8.

[5] C.H. Chen, C.A. Larsen and G.B. Stringfellow, J. Cryst. Growth 77 (1986) 11.

[6] P. Balk, H. Heinecke, N. Putz, C. Plass and H. Luth, J. Vac. Sci. Technol. A4 (1986) 711.

[7] C.H. Goodman and M.V. Pessa, J. Appl. Phys. 60 (1986) R65.

[8] C.A. Larsen, N.I. Buchan and G.B. Stringfellow, J. Cryst. Growth 85 (1987) 148.

[9] N.I. Buchan, C.A. Larsen and G.B. Stringfellow, Appl. Phys. Lett. 51 (1987) 1024.

[10] C.A. Larsen, N.I. Buchan and G.B. Stringfellow, Appl. Phys. Lett. (accepted); G.B. Stringfellow, N.I. Buchan and C.A. Larsen Mat. Res. Soc. Symp. Proc. Vol. 94 p. 245.

[11] M.J. Jacko and S.J.W. Price, Can. J. Chem. 42 (1964) 1198.

[12] G.P. Smith and R. Patrick, Int. J. Chem. Kinet. 15 (1983) 167.

[13] J.E. Butler, N. Bottka, R.S. Sillmon and D.K. Gaskill, J. Cryst. Growth 77 (1986) 163.

[14] J. Haigh and S. O'Brien, J. Cryst. Growth 67 (1984) 75.

[15] C.A. Larsen and G.B. Stringfellow, J. Crystal Growth 75 (1986) 247.

[16] A.M. Dean, J. Phys. Chem. 89 (1985) 4600.

[17] F. Glockling and R.G. Strafford, J. Chem. Soc. (A) (1971) 1761.

[18] J.A. Kerr and M.J. Parsonage, Evaluated Kinetic Data on Gas Phase Hydrogen Transfer Reactions of Methyl Radicals, (Butterworths, London, 1976).

[19] R.M. Marshall and G. Shahkar, J. Chem. Soc., Faraday Trans. 1, 77 (1981) 2271.

[20] H. Furue and P.D. Pacey, J. Phys. Chem. 90 (1986) 397.

[21] A.E. Rodriguez and P.D. Pacey, J. Phys. Chem. 90 (1986) 6298.

[22] R. E. Berkley, I. Safarik, H.E. Gunning and O.P. Strausz, J. Phys. Chem. 77 (1973) 1734.

[23] L.C. Glasgow, G. Olbrich and P. Potzinger, Chem. Phys. Lett. 14 (1972) 466.

[24] E.R. Austin and F.W. Lampe, J. Phys. Chem. 81 (1977) 1546.

[25] J.A. Kerr, Chem. Rev. 66 (1966) 465.

[26] D.M. Golden and S.W. Benson, Chem. Rev. 69 (1969) 125.

[27] M. Brouard and M.J. Pilling, Chem. Phys. Lett. 129 (1986) 439.

[28] M.J. Pilling, private communication.

[29] S.W. Benson, private communication.

[30] J.A. Kerr and S.J.Moss, Handbook of Bimolecular and Termolecular Gas Reactions, Vol.2, (CRC Press, Boca Raton, 1981).

[31] A.A. Westenberg and N. deHass, J. Chem. Phys. 47 (1967) 1393.

Figure Captions

Figure 1: Furnace temperature profile at set points of 300, 400, 500, and 600°C.

Figure 2: Mass spectra @ 20 eV for TMIn decomposition in He (a and d), D_2(b and e), and H_2 (c and f) ambients.

Figure 3: Percent TMIn decomposition versus temperature in D_2 ambient with In surface areas of 50 and 600 cm^2.

Figure 4: Percent TMIn decomposition versus temperature. Experimental results: (Δ) in He, (■) in D_2, (□) in H_2, and ( ) in toluene, ref. [12]. Numerical calculations: (– – –) models 1 and 2, (——) model 3.

Figure 5: $-\ln(p/p_o)$ and $100\ (p_o-p)/p_o$ versus residence time for decomposition of TMIn in D_2 ambient at 337°C with an In surface area of 600 cm^2.

Figure 6: Arrhenius plot of the first order TMIn rate constant: (Δ) in He, (■) in D_2, (□) in H_2, and (▬) in toluene ambient [12]; rate constants in text.

Figure 7: TMIn decomposition in He ambient: Principal product partial pressures versus temperature.

Figure 8: TMIn decomposition in D_2 ambient: Principal product partial pressures versus temperature.

Figure 9: TMIn decomposition in H_2 ambient: Principal product partial pressures versus temperature.

Figure 10: Principal product ratios (CH_3D or CH_4)/C_2H_6 for pyrolysis of TMIn in D_2 and H_2 ambients. Experimental results: (■) in D_2, and (□) in H_2. Numerical calculations: (——) in D_2, and (– – –) in H_2 for models 1, 2, and 3.

Figure 11: Partial pressure of HD versus temperature in a 1:1 D_2:H_2 mixture in a 50 cm^2 reactor tube. Experimental results: (△) with an In surface, (▲) with TMIn and an In surface. Numerical calculations with TMIn and an In surface: (– – –) model 1, (• • •) model 2, and (——) model 3.

Figure 12: Product partial pressures versus time for the theoretically modelled (model 3) decomposition of TMIn in H_2 ambient.

A Mass Spectroscopic Study of the Simultaneous Reaction Mechanism of TMIn and PH_3 to Grow InP

N. I. Buchan, C.A. Larsen, and G.B. Stringfellow
Departments of Electrical Engineering and Materials Science and Enginneering
University of Utah
SLC, UT 84112

ABSTRACT

The reaction mechanisms for the organometallic vapor phase epitaxial (OMVPE) growth of InP using the reactants trimethylindium (TMIn) and PH_3 were studied using mass spectrometry. The reaction was carried out in a D_2 ambient to allow isotopic labelling of the reaction products. The salient features of the data allow a determination of the reaction mechanisms. TMIn has a dramatic effect on PH_3 decomposition, causing PH_3 to decompose 225°C below the temperature at which it decomposes without TMIn present. Likewise, PH_3 causes TMIn to decompose 50°C below the temperature at which it decomposes without PH_3. At the temperatures where the pyrolysis reactions begin, equal amounts of TMIn and PH_3 were decomposed, indicating a simultaneous reaction mechanism. The sole reaction product is CH_4 at low temperatures and at all temperatures with high values of V/III ratio, indicating that the H to make CH_4 comes from the PH_3 rather than reactions with the ambient. The reactions are clearly different than those for the precursors alone, where the reaction products are CH_3D and C_2H_6 for TMIn, and H_2 for PH_3 pyrolysis. The low temperature reaction rate is a strong function of surface area, indicating that the reaction is heterogeneous. At V/III ratios of 4.2 or above and at low temperatures the results indicate that InP grows via a simultaneous heterogeneous reaction between TMIn and PH_3.

1. Introduction

Organometallic vapor phase epitaxy (OMVPE) has advanced to the point that it fulfills all the requirements of an epitaxial growth technique for fabrication of the complex materials and structures, such as superlattices, necessary for many advanced devices. OMVPE, even in atmospheric pressure reactors, has now achieved the distinction of producing atomically abrupt interfaces in both the GaAs/AlGaAs [1], and InP/GaInAs [2] systems. The growth of extremely high purity material is now routine. For example, OMVPE has produced the highest purity InP grown by any technique, with mobilities exceeding 130,000 cm^2/Vs at 77K [3-5]. The OMVPE technique is also extremely versatile, having the capability to produce essentially all the III-V alloys composed of Al, Ga, and In with As, P, and Sb, and is inherently suitable for commercial ventures requiring high production rates and low equipment costs [6]. Thus, OMVPE has become the most promising commercial epitaxial growth technique for III/V semiconductors.

An understanding of the fundamental aspects of the OMVPE growth process has lagged the practical advances. The role of thermodynamics in determining solid composition [7], and to a lesser extent the stoichiometry and associated defect and dopant incorporation [8] have been investigated. The study of the hydrodynamics in closed ampoules has been extended to the more demanding study in open flow reactors via both numerical modelling [9] and closed form solutions [10]. The level of understanding is least developed in the study of the homogeneous and heterogeneous reactions occurring in the reactor, specifically those at or near the solid-vapor interface. An understanding of the reaction mechanisms is necessary to improve existing technology, for example to reduce the carbon incorporation inherent to OMVPE [8]. Advances in the OMVPE technique include the use of alternate group III and V sources [11], photon assisted growth [12], and atomic layer epitaxy [13]; these also require an understanding of reaction mechanisms to guide their development.

The earliest approach to understanding OMVPE reaction mechanisms was to analyze the growth rate as a function of external parameters such as the reactant flow rates and ratios, and substrate temperature and orientation [7,14,15]. This approach allowed classification of the growth processes into mass transport, thermodynamic, and kinetically limited regimes [7,14]. However, these results do not provide useful information about the decomposition steps involved in the growth process. Further attempts have used spectroscopic techniques in ersatz OMVPE reactors accomodated to fundamental research [16-20]. The variation of external parameters, including the majority component ambient, were used to study the gas phase reaction products and hence the reaction mechanisms [18].

We have taken a novel approach, one not previously applied to the growth of semiconductors, by employing a D_2 ambient. The D_2 ambient allows isotopic labelling of the reaction products which are analyzed with a time-of-flight mass spectrometer to indicate qualitatively the reaction mechanisms [21-23]. The quantitative differences between the reaction products and rates found in D_2 and those found in H_2 ambients show isotope effects. These are modelled using chemical kinetic simulations to clarify the reaction mechanisms. The objective of our studies has been to first investigate the reaction mechanisms involved in the thermal decomposition of the organometallic and hydride precursors separately, and then in combined mixtures. Previously we have reported the pyrolysis mechanisms of PH_3 [22] and TMIn [23], which are nearly universally used as the OMVPE precursors for the growth of InP in atmospheric pressure reactors [7,24], in D_2, H_2, and He ambients. We have also studied the reaction mechanisms of TMGa and AsH_3 and combined mixtures of TMGa and AsH_3 in a D_2 ambient [25]. In this work we focus on the reactions occurring during OMVPE growth of InP from mixtures of TMIn and PH_3, giving a complete description of our studies described in a preliminary, brief communication [21].

2. Summary of Previous Results for TMIn and PH_3 Pyrolysis

2.1 TMIn Decomposition

The decomposition of TMIn in a D_2 ambient was found to be homogeneous and of first order in the presence of an In surface [23]. Numerical modelling led to the conclusion that decomposition occurs via a chain reaction involving the steps R1-R6 :

$$In(CH_3)_3 \rightarrow MMIn + 2\,CH_3 \qquad (R1)$$

$$CH_3 + D_2 \rightarrow CH_3D + D \qquad (R2)$$

$$D + TMIn \rightarrow DTMIn \rightarrow CH_3D + 2\,CH_3 + In \qquad (R3)$$

$$CH_3 + CH_3 + M \rightarrow C_2H_6^* + M \rightarrow C_2H_6 + M \qquad (R4)$$

$$CH_3 + DTMIn \rightarrow TMIn + CH_3D \qquad (R5)$$

$$D + MMIn \rightarrow CH_3D + In\ . \qquad (R6)$$

Reaction R1 is the initiating step in the decomposition of TMIn in a D_2 ambient; the same reaction occurs for TMIn decomposition in a toluene ambient (a radical scavenger) as discussed by Jacko and Price [26]. They concluded that TMIn decomposed by homolytic fission, and found that the rate constant for breaking the second In-CH_3 bond was much higher than that for the first bond. Hence, the TMIn loses two methyl radicals in rapid succession to form monomethylindium (MMIn). The methyl radicals resulting from TMIn decomposition attack the D_2 ambient to form CH_3D and the D radical, as in reaction R2. Reaction R3 is the dominant reaction causing TMIn decomposition in D_2. The D radicals attack the TMIn to form a hypervalent DTMIn species that decomposes to release two methyl radicals and CH_3D. Reaction R4 is a termination step in which the methyl radicals combine to form C_2H_6. Reactions R5 and R6 are also terminating steps which quench the methyl and D radical concentrations by radical attack on the DTMIn and MMIn species.

2.2 PH_3 Decomposition

Two temperature regimes distinguish heterogeneous and homogeneous PH_3 decomposition. At temperatures below 850°C the decomposition of PH_3 is heterogeneous and at concentrations of PH_3 as high as15% in a D_2 ambient the reaction is of first order on SiO_2 and InP surfaces [22], in agreement with other investigations [27,28]. An activation energy of 36.0 kcal/mol was determined for the decomposition occurring on the InP surface [22]. The sole reaction product observed in the effluent was H_2 with no HD detected above the background level (the involatile P_4 collects on the room temperature walls downstream from the reactor tube and is not observed). Therefore, the reaction does not release H radicals from the surface which would have caused the formation of HD via homogeneous reactions with the D_2 ambient. Instead, PH_3 dissociatively adsorbs via reactions R7a, b, and c and H_2 and P_2 desorb from the surface via reactions R8 and R9 as observed in UHV investigations of PH_3 adsorption on a Si surface [29,30].

$$PH_3 + (s) \leftrightarrow PH_3(s) \qquad \text{(R7a)}$$

$$PH_3(s) + (s) \rightarrow PH_2(s) + H(s) \qquad \text{(R7b)}$$

$$PH_2(s) + 2(s) \rightarrow P(s) + 2\,H(s) \qquad \text{(R7c)}$$

$$H(s) + H(s) \rightarrow H_2 + 2\,(s) \qquad \text{(R8)}$$

$$P(s) + P(s) \rightarrow P_2 + 2\,(s) \qquad \text{(R9)}$$

At temperatures above 850°C the decomposition of PH_3 occurs homogeneously via unimolecular decomposition, R10, to form a moderately stable PH_2 radical [31-33] and an H radical. The homogeneous decomposition of PH_3 is most likely assisted by a chain reaction involving H radical attack on PH_3 via reaction R11[34].

$$PH_2\text{-}H \rightarrow PH_2 + H. \qquad \text{(R10)}$$

$$H + PH_3 \rightarrow H_2 + PH_2 \qquad \text{(R11)}$$

2.3 Reaction Mechanisms for the Combined TMIn-PH_3 System

Prior to our experiments using deuterium to trace the reactions, little work was done to elucidate the reaction mechanism of TMIn and PH_3 (the TMIn-PH_3 system) during OMVPE growth of InP. However, several mechanisms have been proposed for the TMGa-AsH_3 system used for GaAs growth. The most widely accepted mechanism for OMVPE growth of GaAs is a Langmuir-Hinshelwood (L-H) type mechanism. The partially decomposed reactants, monomethylgallium (MMGa) and AsH_x adsorbed on the surface, react heterogeneously forming CH_4 which is desorbed from the surface. This mechanism has been proposed to explain the GaAs growth rate from TMGa and AsH_3 [14]. A recent review of the OMVPE technique [35] proposed a similar mechanism also combining homogeneous and heterogeneous reactions. The pyrolysis of TMGa and AsH_3 together was suggested to commence with the elimination of two CH_4 molecules from TMGa (via a bimolecular reaction with H_2) and the novel homogeneous elimination of H_2 from AsH_3. The AsH and $Ga(CH_3)$ species resulting from the homogeneous reac. ns were postulated to subsequently react, either homogeneously or heterogeneously, forming GaAs, with the elimination of the last CH_4 molecule.

More recent investigations using infrared spectroscopy suggest that the reaction mechanism for GaAs growth from TMGa and AsH_3 at higher temperatures must incorporate both homogeneous and heterogeneous steps [17,20]. Methyl radical attack was considered important because the temperature at which AsH_3 decomposes in the TMGa-AsH_3 system is lowered relative to the temperature at which it decomposes alone (in the presence of a GaAs substrate in both cases). The effect of AsH_3 on TMGa decomposition was not investigated. Attack by radicals derived from TMGa (CH_3 radicals according to ref. [20]) is proposed. The infrared spectra of Nishizawa and Kurabayashi [17] indicate the formation of a new intermediate gas phase species. Following the homogeneous reactions, heterogeneous steps were assumed to occur via a L-H type mechanism [20].

Another possible reaction mechanism involves the decomposition of III-V adducts. The adduct, formed by association of the group III organometallic molecule and the group V source molecule, may either dissociate to reform its constituents, which then decompose independently, or it may decompose by eliminating alkanes either homogeneously or heterogeneously. For the growth of InP, TMIn:PEt_3 and TMIn:PMe_3 are examples of adducts which dissociate [36], whereas TMIn:VH_3 adducts such as TMIn:AsH_3 [37] and TMIn:PH_3 [38] decompose. In early work of Didchenko et al [38], the TMIn:PH_3 adduct formed by the reaction of condensation of TMIn and PH_3 at low temperatures was found to decompose upon heating to room temperature, to form an involatile polymer (-MeInPH-)$_n$, eliminating two CH_4 molecules in the process. However, it was proposed recently that what was presumed to be the decomposition of a TMIn:PH_3 adduct may actually have been a reaction initiated by trace impurities in the alkyl or hydride sources, or moisture in the reactor [39]. The successful OMVPE growth of InP using the combination of TMIn and PH_3 with no evidence of deposition on the walls makes the room temperature decomposition of a TMIn:PH_3 adduct to form a nonvolatile polymer unlikely

3. Experimental Apparatus

The atmospheric pressure flow tube apparatus is the same as that described previously [21-23]. The carrier gas, D_2 in all cases, is saturated with TMIn in an isothermal bubbler held at 20°C, forming a 1.7 Torr partial pressure of TMIn. The flow rates of both the deuterium and the electronic grade PH_3 are controlled using electronic mass flow controllers. The mixture then flows through a 4 mm ID silica tube inside a furnace with a hot zone 41.5 cm long. The total flow rate is held at 40 sccm. The reaction products rapidly cool upon leaving the furnace and only those which have significant room temperature vapor pressures flow to the adjustable leak inlet to the CVC 2000 time-of-flight mass spectrometer which has a resolution of one-quarter mass unit. Though the TMIn concentration is well established by saturating a high flow of the carrier, the PH_3

flow was low enough that the PH_3 flow controller was near its lower limit of adjustability (and was displayed on a coarse incremental scale). Hence, the error associated with the actual PH_3 flow is large and the listed V/III ratios and PH_3 concentrations reflect the flow set points but do not account for the error estimated to be ±25% at V/III values of 4.2 and 2.1.

The ionization energy used in these experiments was 70 eV. Calibration experiments were performed to determine the cracking patterns and ionization cross-sections for the major species. All the results presented are corrected for the relative ionization cross-sections to allow a meaningful comparison of intensities. The 4 mm fused silica reactor tube has a surface area of 50 cm^2. The surface area was increased to1200 cm^2 by packing with silica chips. The fused silica tubing and chips were cleaned with HF and dried before use. In some experiments the reactor tube and chips were coated *in situ* with InP by thermally decomposing a mixture of TMIn and PH_3.

4. Experimental Results

4.1 Reaction Products

The mass spectra taken at an ionization energy of 70 eV for the TMIn-PH_3-D_2 system at a PH_3/TMIn ratio (V/III ratio) of 4.2 in the presence of an InP (50 cm^2) surface, at reactor temperatures between room temperature and 475°C, are shown in fig. 1. Additional spectra, not shown here, were taken at V/III = 47 and 2.1 in the presence of InP (50 cm^2), and at V/III = 4.2 in the presence of InP (1200 cm^2). At room temperature the mass spectral peaks H_2^+ and HD^+ represent the H_2 and HD in the CP grade D_2 used, and the peak labelled OH^+ (m/e=17) results from H_2O resident in the mass spectrometer. The contributions at m/e = 15 and 16 are part of the fragmentation spectrum of TMIn. The contributions at m/e = 31-34 correspond to the PH_3 fragment peaks (P^+, PH^+, PH_2^+, and PH_3^+), and the contributions at m/e=115 and 145 correspond to TMIn fragment peaks. In the spectrum taken at 450°C a spectral contribution centered at m/e=46 is attributed to methylphosphine [40]. Because the methylphosphine peaks

only appeared at a temperature at which TMIn was completely reacted and the CH_4 intensity was a maximum, they are not artifacts of ion-molecule reactions between PH_3 and TMIn or CH_4 in the ionization region of the mass spectrometer.

The mass spectra were corrected for differences in the species ionization cross-sections to provide the product partial pressures as a function of temperature. The product partial pressures at V/III = 4.2 on InP (50 cm^2), 4.2 on InP (1200 cm^2), and 2.1 on InP (50 cm^2) are shown in figs. 2, 3, and 4 respectively. A significant feature in the reaction products at V/III=4.2 is the appearance of CH_4, with neither CH_3D or C_2H_6 as was found for the decomposition of the TMIn-D_2 system[23], nor H_2 as was found for the decomposition of the PH_3-D_2 system[22]. Of additional interest is the dramatic lowering of the temperatures at which both PH_3 and TMIn decompose in a combined mixture. PH_3 decomposition initiates at 175°C, 225 degrees below the temperature at which PH_3 decomposes alone. The best measure of TMIn decomposition is the temperature at which decomposition is 50% complete. TMIn is 50% decomposed at 287°C, 50 degrees below the temperature at which it decomposes without PH_3 in D_2 [22].

4.2 Decomposition of PH_3 with TMIn

The effect of V/III ratio on PH_3 pyrolysis gives important clues to the role of TMIn in the reaction mechanism. The percent decomposition of P-containing species (including methylphosphines and deuterated phosphines), determined at values of V/III ratio of ∞, 47, 4.2, and 2.1 in the presence of InP (50 cm^2), is shown in fig. 5. At all V/III ratios, except 2.1, the majority P-containing species throughout the decomposition was PH_3; hence, the decomposition of P-containing species is discussed below in terms of the decomposition of PH_3 per se. The decomposition of PH_3 at V/III = ∞, is shown by curve a. A small concentration of TMIn has hardly any effect, as seen by the data at V/III = 47, which corresponds closely to curve a.

The decomposition of PH_3 at V/III = 4.2, curve b in fig 5, shows that at higher concentrations TMIn causes a dramatic lowering of the temperature at which PH_3 decomposes. Decomposition is initiated at the remarkably low temperature of 175°C and plateaus with 25% decomposed at 325°C. The temperature at which the plateau begins clearly coincides with the temperature at which TMIn decomposition is complete in fig. 2. Since the V/III ratio is 4.2, approximately equal parts of TMIn and PH_3 have decomposed at this temperature. This strongly suggests a simultaneous reaction mechanism for TMIn and PH_3 pyrolysis. Further decomposition of PH_3 continues only at T > 400°C. This is approximately the temperature at which PH_3 decomposition begins without TMIn on an InP surface. Thus, the decomposition of the PH_3 in excess of the initial TMIn concentration occurs via the same reaction mechanism as for PH_3 without TMIn on an InP surface. The PH_3 decomposition at V/III = 2.1, curve d in fig. 5, is inititiated at a similar temperature as for curve b, but above approximately 350°C the decomposition of P-containing species plateaus until 425°C. The PH_3 decomposition resulting from a change in the surface area of InP from 50 cm^2 to 1200 cm^2 at a V/III ratio of 4.2 is shown by curve c. The pyrolysis is initiated at approximately the same temperature as curve b and plateaus at a slightly higher amount of PH_3 decomposition. The plateaus for curves c and d do not exactly reflect the listed V/III ratios (that are based on flow controller set points) because the actual V/III ratios are slightly different (see Section 3). The behavior of curve c is qualitatively consistent with a heterogeneous reaction mechanism for PH_3 decomposition below 400°C.

4.3 Rate Constant Analysis

The Arrhenius plot of the reaction rate constant for PH_3 decomposition, assuming first order kinetics for the pyrolysis of both the deuterated and undeuterated phosphine species [22], is shown in fig. 6. The data are for V/III = ∞ and 4.2 with InP (50 cm^2) and V/III = 4.2 with InP (1200 cm^2). Methylphosphines are not included as part of the PH_3 signal in this analysis because an

additional reaction is required for their formation; hence, the inclusion of methylphosphines would produce Arrhenius parameters not relevant to the kinetics of the reaction for PH_3 decomposition. The curves a and b in fig. 6 correspond to the data indicated by curves a and b in fig. 5. The activation energy obtained from curve a is 36.0 kcal/mole. The breakpoint at 400°C in curve b coincides with the end of the plateau region for this mixture, curve b of fig. 5. The reaction mechanism obviously changes at this temperature.

The slope of curve b above 400°C is similar to that of curve a, confirming that the pyrolysis mechanism of the PH_3 remaining after the stoichiometric amount (in this case 25%) has reacted with TMIn is a similar heterogeneous process to that for PH_3 alone. The higher reaction rate indicated by the data in curve b above 400°C indicates that the growing surface has more active sites upon which PH_3 can decompose than a surface that is not growing (as is the case of curve a). At temperatures below 400°C the decomposition of PH_3 has a much lower activation energy, reflecting the change in the pyrolysis mechanism caused by the presence of TMIn. The data for the decomposition of PH_3 at V/III = 4.2 with an increased InP surface area (1200 cm^2) has a slope similar to that of curve b at temperatures below 400°C; therefore, the reaction mechanism is independent of surface area. However, the rate constant for PH_3 decomposition at temperatures below 400°C is dependent on the TMIn concentration, so simple first order analysis must be restricted to the low temperature regime (T<230°C) where the TMIn concentration is nearly constant . At these temperatures the ratio of the reaction rates at high and low surface areas is approximately 24. This is equal to the 24 fold difference in surface area; therefore, the decomposition of PH_3, assisted by the presence of TMIn, is definitely heterogeneous below 300°C.

The Arrhenius plot of the rate constant for TMIn decomposition at V/III = 4.2, assuming TMIn decomposition is of first order, in the presence of InP (50 cm^2) and InP (1200 cm^2), is shown in fig 7. At a V/III ratio of 4.2 and at temperatures below 400°C the partial pressure of PH_3 is nearly

constant. Thus, the rate constant for TMIn pyrolysis is properly calculated assuming a first order reaction throughout the entire temperature range. The activation energy is apparently independent of surface area , with a value of approximately 18.1 kcal/mol. The ratio of the rate constants for the two surface areas is 30, approximately equal to the ratio of surface areas. Both TMIn and PH_3 decompose heterogeneously in the TMIn-PH_3 system below 400°C.

5. Discussion of Results

TMIn has a dramatic effect on PH_3 decomposition. With no TMIn present the decomposition of PH_3 begins at 400°C. Adding TMIn (at V/III = 4.2 with an InP surface of 50 cm^2) decreases the temperature for the onset of PH_3 decomposition by 225°C. The addition of PH_3 has a similar effect on TMIn decomposition, lowering the TMIn decomposition curve by 50°C. The enhanced decomposition of both the group III and group V precursors in the TMIn-PH_3-D_2 system is analogous to our results for the TMGa-AsH_3-D_2 system [25], and agrees with previous results which showed that TMGa increased the decomposition of AsH_3 [17,20]. Another salient feature of the decomposition of the TMIn-PH_3-D_2 system is the simultaneous decomposition of TMIn and PH_3: equal amounts of P and In are depleted from the vapor via the heterogeneous reaction below 400°C. Also remarkable is the reaction product, solely CH_4 in a D_2 ambient, for the combined decomposition of PH_3 and TMIn at V/III ratios of 4.2 or above. Of course, H_2 is also produced by the independent pyrolysis of the excess PH_3.

At temperatures > 400°C TMIn by itself decomposes rapidly before it can diffuse to a surface to participate in a heterogeneous reaction, and it is unlikely that the presence of PH_3 stabilizes the thermal decomposition of TMIn. Hence, the reaction mechanism must become homogeneous at these high temperatures. In this temperature regime and at V/III ratio of 4.2 and above, CH_4 is still the only reaction product observed. However, at lower V/III ratios the decomposition of some TMIn occurs independently of the PH_3 to produce CH_3D and C_2H_6.

A purely L-H reaction mechanism adequately explains the results obtained by others for the TMGa-AsH_3 system. This model, as formulated by Reep and Ghandhi [14] and applied here to the TMIn-PH_3-D_2 system, would involve the independent adsorption of PH_3 and TMIn and their subsequent partial decomposition to form $InCH_3$ and PH which react to form InP. Three CH_4 molecules would be produced in the reaction. This mechanism explains the CH_4 product, and the heterogeneous nature of the TMIn and PH_3 decomposition below 400°C, but fails to explain the simultaneous decomposition of TMIn and PH_3, and the enhancement of the decomposition of both PH_3 and TMIn. A modification of the Reep and Ghandhi model which postulates the independent adsorption of PH_3 and TMIn, and their association on the surface to form a surface adduct prior to pyrolysis, with the subsequent elimination of 3 CH_4 molecules, explains the salient features of our experimental results. This would be similar to the very low temperature reactions described by Schlyer and Ring [41]. However, at higher temperatures the homogeneous decomposition of TMIn occurs in a fraction of the tube length before diffusion of the reactants to the walls occurs. Therefore, a L-H reaction mechanism involving TMIn is excluded above 400°C.

The homogeneous decomposition of TMIn forms CH_3 radicals; hence, radical attack is considered as a possible pyrolysis reaction mechanism above 400°C. The results require a simultaneous reaction in which the decomposition of both PH_3 and TMIn is enhanced in the TMIn-PH_3-D_2 system. Enhancement of the decomposition of PH_3 via CH_3 radical attack , reaction R12, requires an initiation reaction, the homolytic fission of TMIn via reaction R1, to create CH_3 radicals. The enhancement of the decomposition of TMIn requires a chain reaction in which the PH_2 radical attacks a TMIn molecule via reaction R13, forming a $H_2PIn(CH_3)_3$ molecule which decomposes via reaction R14.

$$CH_3 + PH_3 \rightarrow CH_4 + PH_2 \qquad (R12)$$

$$PH_2 + TMIn \rightarrow H_2PIn(CH_3)_3 \qquad (R13)$$

$$H_2PIn(CH_3)_3 \rightarrow In + PH_2CH_3 + 2\,CH_3 \qquad (R14)$$

$$PH_2 + CH_3 \rightarrow PH_2CH_3 \qquad (R15)$$

Reactions R13 and R14 for PH_2 radical attack on TMIn are speculative, but are directly analogous to reaction R3 in the TMIn-D_2 system for D radical attack on TMIn. A possible terminating step in the chain reaction would be reaction R15.

Methyl radical attack on PH_3 and D_2, reactions R12 and R2 respectively, are competitive, and CH_3D is not an experimentally observed product at high V/III ratios. Consequently, to explain the experimental results, reaction R12 would have to occur with a much higher reaction rate than reaction R2. The concentration of PH_3 at the V/III ratio of 4.2 is only 1.1% of the D_2 concentration. In order for the reaction rates of reaction R12 and R2 to be equal, and assuming that rate constants for reactions R12 and R2 have the same preexponential, the activation energy for reaction R12 would have to be significantly lower than that for reaction R2 (approximately 6 kcal/mol). At low PH_3 concentrations (such as V/III = 2.1) the reaction rate for reaction R12 would become competitive and eventually dominate reaction R2. This would explain the formation of CH_3D at a V/III ratio of 2.1.

This reaction mechanism explains the enhanced decomposition of both TMIn and PH_3, the dominant CH_4 reaction product, and even the formation of methylphosphine. However, it would be fortuitous if this mechanism explained the simultaneous decomposition of TMIn and PH_3 observed experimentally at the V/III ratio of 4.2. Consequently it probably is not the dominant route for simultaneous decomposition of TMIn and PH_3.

The simplest possible reaction mechanism which explains the results involves the formation of an adduct of TMIn and PH_3. A low concentration of a metastable adduct might be formed via reaction R16, where it exists in equilibrium with the individual precursor molecules.

$$(CH_3)_3In + PH_3 \leftrightarrow (CH_3)_3In{:}PH_3 \qquad (R16)$$

$$(CH_3)_3In{:}PH_3 + (s) \leftrightarrow (CH_3)_3In{:}PH_3(s) \qquad (R17)$$

$$(CH_3)_3In{:}PH_3 \rightarrow (CH_3)_2InPH_2 + CH_4 \qquad (R18)$$

At low temperatures, <400°C, the adduct could be formed either homogeneously, with subsequent condensation on the InP surface, R17, or heterogeneously via the L-H mechanism described above. Formation of the adduct would enhance both TMIn and PH_3 pyrolysis at low temperatures on the InP surface. At higher temperatures the reaction would proceed homogeneously via reaction R18, to eliminate CH_4 and form a $(CH_3)_2InPH_2$ molecule. The elimination of alkanes from adducts involving similar Ga- and In-alkyls is common [42] and both homogeneous and heterogeneous direct interaction of the OMVPE precursors to eliminate CH_4 is suspected in an analogous group III-group V system (the TMGa-AsH_3 system) [43]. The decomposition of the $(CH_3)_2In$-PH_2 molecule would then proceed to eliminate additional CH_4 molecules either homogeneously or heterogeneously. In this mechanism the methylphosphines are explained by surface recombination of PH_2 and CH_3 radicals. The independent decomposition of TMIn to form CH_3D and C_2H_6 at the V/III ratio of 2.1 is interpreted to indicate that the TMIn decomposes before association with PH_3 at these low V/III ratios. Therefore, the formation and subsequent decomposition of an adduct would explain the experimentally observed simultaneous decomposition of TMIn and PH_3 over the entire temperature range.

6. Conclusions

The pyrolysis of TMIn and PH_3 together during the OMVPE growth of InP has been studied in a deuterium ambient to label the product molecules which are later analyzed mass spectrometrically. At normal growth temperatures TMIn alone pyrolyzes homogeneously forming CH_3D and PH_3 alone pyrolyzes heterogeneously producing H_2. For TMIn and PH_3 together, the pyrolysis reactions are completely different. The pyrolysis temperatures of both PH_3 and TMIn are significantly reduced, by 225°C for PH_3 and 50°C for TMIn. The sole reaction product is CH_4 at high values of the V/III ratio. In addition, the pyrolysis reactions are coupled, as evidenced by the equal depletion of TMIn and PH_3 from the vapor. Finally, the reaction is proven to be

heterogeneous at temperatures below 400°C. At higher temperatures, more typical of the OMVPE growth process, the pyrolysis reaction apparently remains simultaneous, since the products are the same, but is homogeneous. From these results, it is difficult to determine unambiguously which of the two possible reaction mechanisms occur in the TMIn-PH_3-D_2 system: the homogeneous radical attack mechanism valid when TMIn decomposes homogeneously, or the homogeneous (at high temperatures) and heterogeneous (at low temperatures) decomposition via formation of an adduct. However, the radical attack mechanism does not guarantee decomposition of equal amounts of TMIn and PH_3. The simplicity of decomposition via an adduct, either homogeneously or on the surface, throughout the entire temperature range is appealing due to its simplicity, and appears the most likely reaction mechanism for OMVPE growth of InP from TMIn and PH_3.

Acknowledgements

This work was supported by grants from NASA, Langley Research Center, contract number NAG-1-608, and from the Air Force, contract number AFSOR-87-0233.

References

[1] A. Ishabashi, Y. Mori, M. Itabashi, and N. Watanabe, J. Appl. Phys. 58 (1985) 2691.

[2] T.Y. Wang, K.L. Fry, A. Persson, E.H. Riehlen, and G.B. Stringfellow, App. Phys. Lett. (to be published).

[3] M.A. DiForte-Poisson, C. Brylinski, and J.P. Duchemin, Appl. Phys. Lett.46 (1985) 476.

[4] C.H. Chen, M. Kitamura, R.M. Cohen, and G.B. Stringfellow, Appl. Phys.Lett. 49 (1986) 963.

[5] L.D. Chu, K.T. Chan, and J.M. Ballantyne, Appl. Phys. Lett. 47 (1985) 47.

[6] G.B. Stringfellow, in Semiconductors and Semimetals, Vol. 22, Part A, ed. W. Tsang (Academic Press, Inc., Orlando, 1985).

[7] G.B. Stringfellow, J. Crystal Growth. 70 (1984) 133.

[8] G.B. Stringfellow, J. Crystal Growth, 75 (1986) 91.

[9] C. Houtman, D.B. Graves, and K. Jensen, J. Electrochem. Soc. 133 (1986) 961

[10] J. van de Ven, G.J.M. Rutten, M.J. Raaymakers, and. L.J. Giling, J. Cryst. Growth 76 (1986) 352.

[11] C.H. Chen, C.A. Larsen and G.B. Stringfellow, J. Cryst. Growth 77 (1986) 11.

[12] P. Balk, H. Heinecke, N. Putz, C. Plass and H. Luth, J. Vac. Sci. and Technol. A4 (1986) 711.

[13] C.H. Goodman and M.V. Pessa, J. Appl. Phys. 60 (1986) R65.

[14] D.H. Reep and S.K. Ghandhi, J. Electrochem. Soc. 130 (1983) 675.

[15] D.H. Reep and S.K. Ghandhi, J. Electrochem. Soc. 131 (1984) 2697.

[16] M.R. Leys and H. Veenliet, J. Cryst. Growth 55 (1981) 145.

[17] J. Nishizawa and T. Kurabayashi, J. Electrochem. Soc. 130 (1983) 413.

[18] M. Yoshida, H. Watanabe and F. Uesugi, J. Electrochem. Soc 132 (1985) 677.

[19] S.P. Denbaars, B.Y. Maa, P.D. Dapkus, A.D. Danner and H.C. Lee, J. Cryst. Growth 77 (1986) 188.

[20] J.E. Butler, N. Bottka, R.S. Sillmon and D.K. Gaskill, J. Cryst. Growth 77 (1986) 163.

[21] N.I. Buchan, C.A. Larsen and G.B. Stringfellow, Appl. Phys. Lett. 51 (1987) 1024.

[22] C.A. Larsen, N.I Buchan and G B. Stringfellow, J. Cryst. Growth 85 (1987) 148.

[23] N.I. Buchan, C.A. Larsen and G.B. Stringfellow, J. Cryst. Growth (to be published).

[24] C.C. Hsu, R.M. Cohen and G.B. Stringfellow, J. Cryst. Growth 63 (1983) 8.

[25] C.A. Larsen, N.I. Buchan and G.B. Stringfellow, Appl. Phys. Lett. (to be published).

[26] M.G. Jacko and S.J.W. Price, Can. J. Chem. 41(1963) 1560.

[27] C.N. Hinshelwood and B. Topley, J. Chem. Soc. 125 (1924) 393.

[28] G.G. Devyatykh, V.M. Kedyarkin and A.D. Zorin, Russ. J. Inorg. Chem. 14 (1969) 1055.

[29] M.L. Yu and B.S. Meyerson, J. Vac. Sci. Technol. A 2 (1984) 446.

[30] M.L. Yu, D.K. Vitkavage and B.S. Meyerson, J. Appl. Phys. 59 (1986) 4032.

[31] J.P. Ferris and R. Benson, J. Am. Chem. Soc. 103 (1981) 1922.

[32] D. A. Ramsay, Nature 178 (1956) 374.

[33] D.M. Wiles and C.A. Winkler, J. Phys. Chem. 61 (1957) 620.

[34] J.H. Lee, J.V. Michael, W.A. Payne, D.A. Whytock, and L.J. Stief, J. Chem. Phys. 65 (1976) 3280.

[35] P.M. Frijlink, Heterojunctions and Semiconductor Superlattices, Eds. G. Allan, G. Bastard, N. Boccara, M. Lannoo, and M. Voos, (Springer, Berlin, 1986).

[36] R. Karlicek, J.A. Long and V.M. Donnelly, J. Cryst. Growth 68 (1984) 123.

[37] C.H. Cheng and K.A. Jones, J. Electron. Mater. 13 (1984) 703.

[38] R. Didchenko, J.D. Alix and R.H. Toeniskoetter, J. Inorg. Nucl. Chem. 14 (1960) 35.

[39] R.H. Moss, J. Cryst. Growth 68 (1984) 78.

[40] Y. Wada and R.W. Kiser, J. Phys. Chem. 68 (1964) 2290.

[41] D.J. Schleyer and M.A. Ring, J. Organometallic Chem. 114 (1976) 9.

[42] D.G. Tuck, "Comprehensive Organometallic Chemistry, Ed. G. Wilkinson, F.G.A. Stone and E.W. Abel, (Pergamon Press, New York, 1982), 711.

[43] G. Arens, H. Heinecke, N. Pütz, H. Lüth and P. Balk, J. Cryst. Growth 76 (1986) 305.

Figure Captions

Fig. 1 Mass Spectra, for a 70eV ionization energy, of the TMIn-PH_3-D_2 gas mixture for V/III = 4.2 with an InP surface area of 50 cm^2. Reactor temperatures are 20, 275, 325, 450, and 475°C.

Fig. 2 PH_3 and TMIn decomposition in the TMIn-PH_3-D_2 gas mixture: Principal product partial pressures are plotted versus temperature at V/III = 4.2 with an InP surface area of 50 cm^2.

Fig. 3 PH_3 and TMIn decomposition in the TMIn-PH_3-D_2 gas mixture: Principal product partial pressures are plotted versus temperature at V/III = 4.2 with an InP surface area of 1200 cm^2.

Fig. 4 PH_3 and TMIn decomposition in the TMIn-PH_3-D_2 gas mixture: Principal product partial pressures are plotted versus temperature at V/III = 2.1 with an InP surface area of 50 cm^2.

Fig. 5 Percent PH_3 decomposition versus temperature as a function of TMIn concentration (all decomposition occurring with an InP surface of 50 cm^2 unless otherwise noted): a) V/III = ∞, 47, b) V/III = 4.2, c) V/III = 4.2 (with an InP surface area of 1200 cm^2), and d) V/III = 2.1.

Fig. 6 Arrhenius plot of the first order PH_3 rate constant for the TMIn-PH_3-D_2 gas mixture: (▲) V/III = ∞,(■) V/III = 4.2, (Δ) V/III = 4.2 with a high InP surface area of 1200 cm^2.

Fig. 7 Arrhenius plot of the first order TMIn rate constant for the TMIn-PH_3-D_2 gas mixture: (■) V/III = 4.2 with an InP surface area of 50 cm^2, (Δ) V/III = 4.2 with an InP surface area of 1200 cm^2.

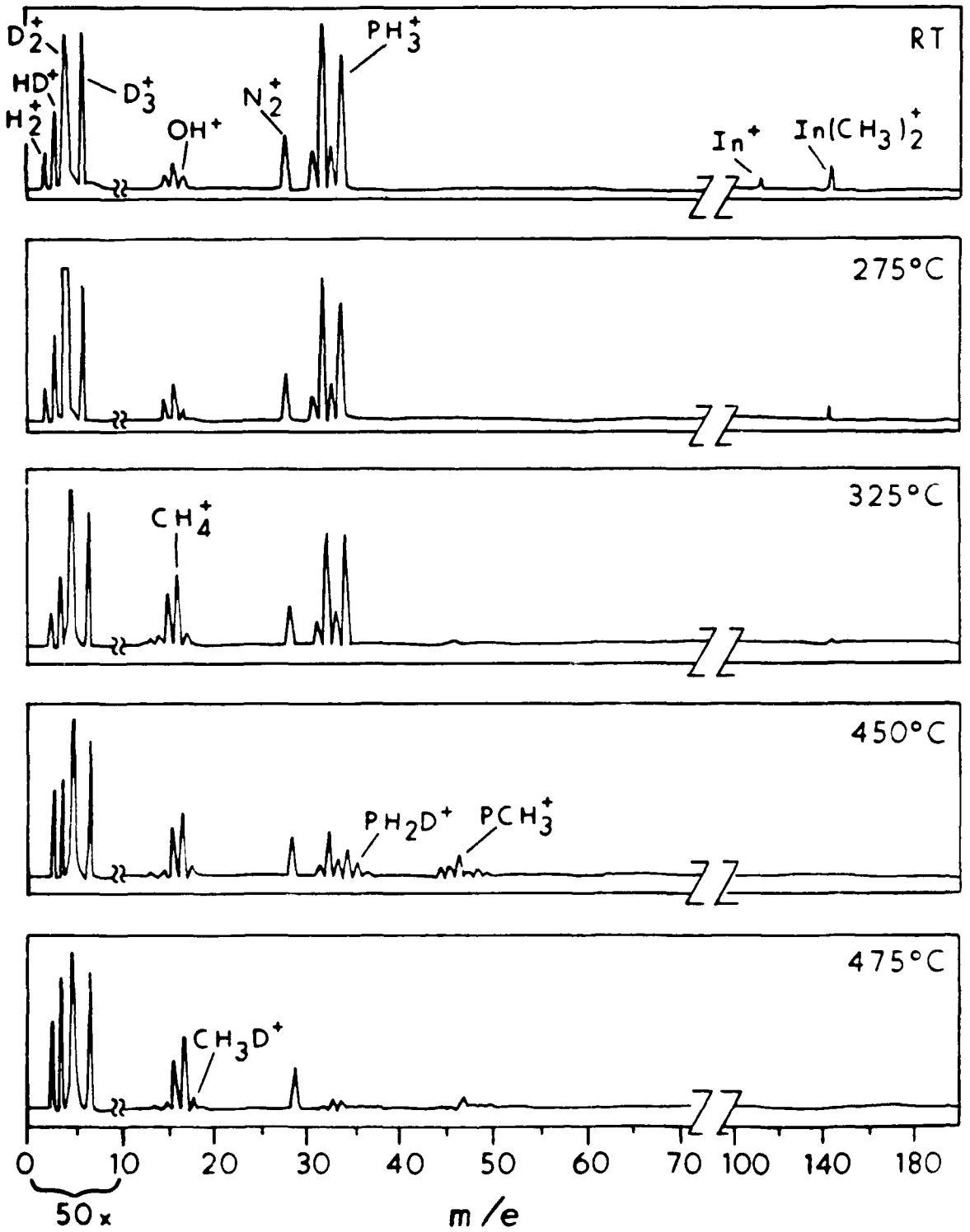
D_2^+
HD^+
H_2^+
D_3^+
OH^+
N_2^+
PH_3^+
RT
In^+
$In(CH_3)_2^+$
275°C
325°C
CH_4^+
450°C
PH_2D^+
PCH_3^+
475°C
CH_3D^+
0
10
20
30
40
50
60
70
100
140
180
50x
m/e

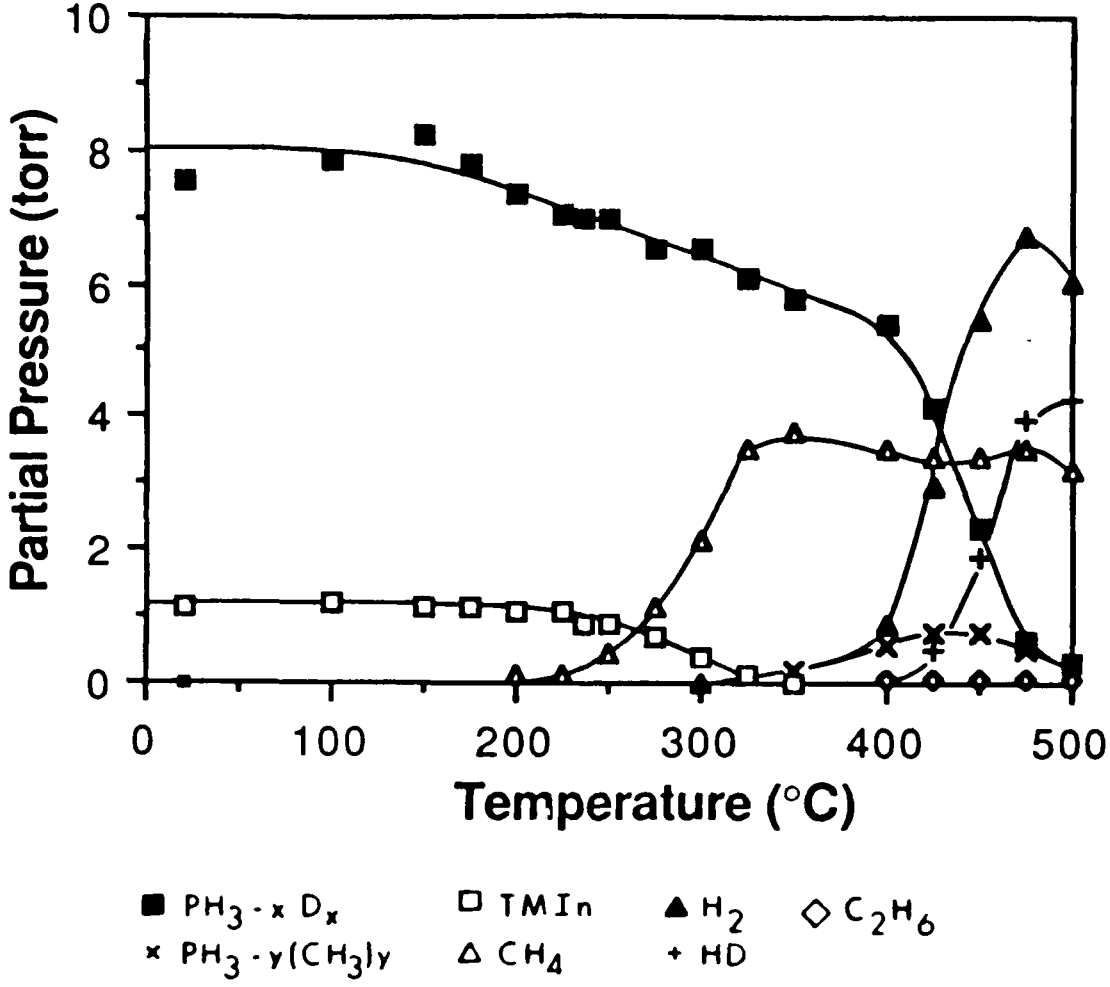
Partial Pressure (torr)
10
8
6
4
2
0
0
100
200
300
400
500
Temperature (°C)
■ $PH_3 - x\ D_x$
□ TMIn
▲ H_2
◇ C_2H_6
× $PH_3 - y(CH_3)y$
△ CH_4
+ HD

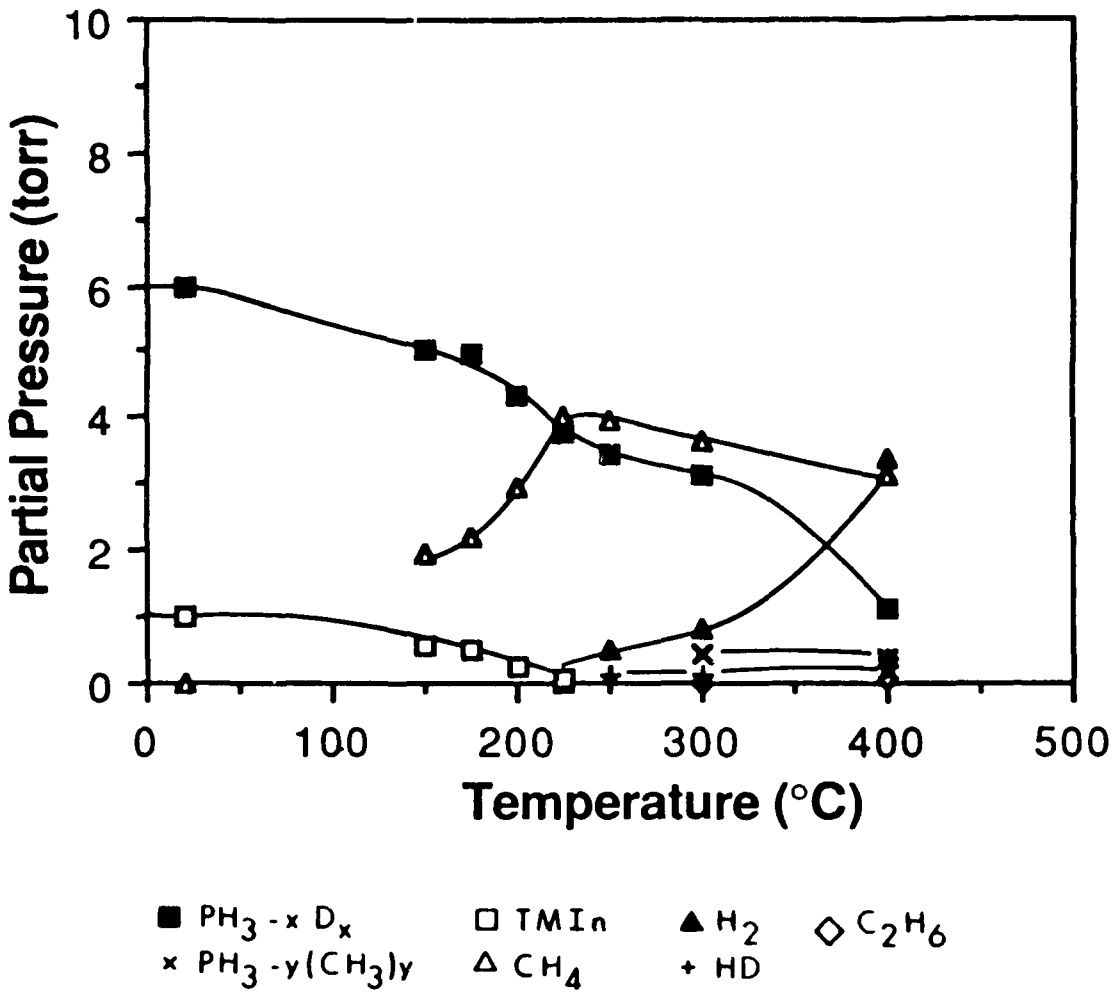

Dunham et al
Fig 3

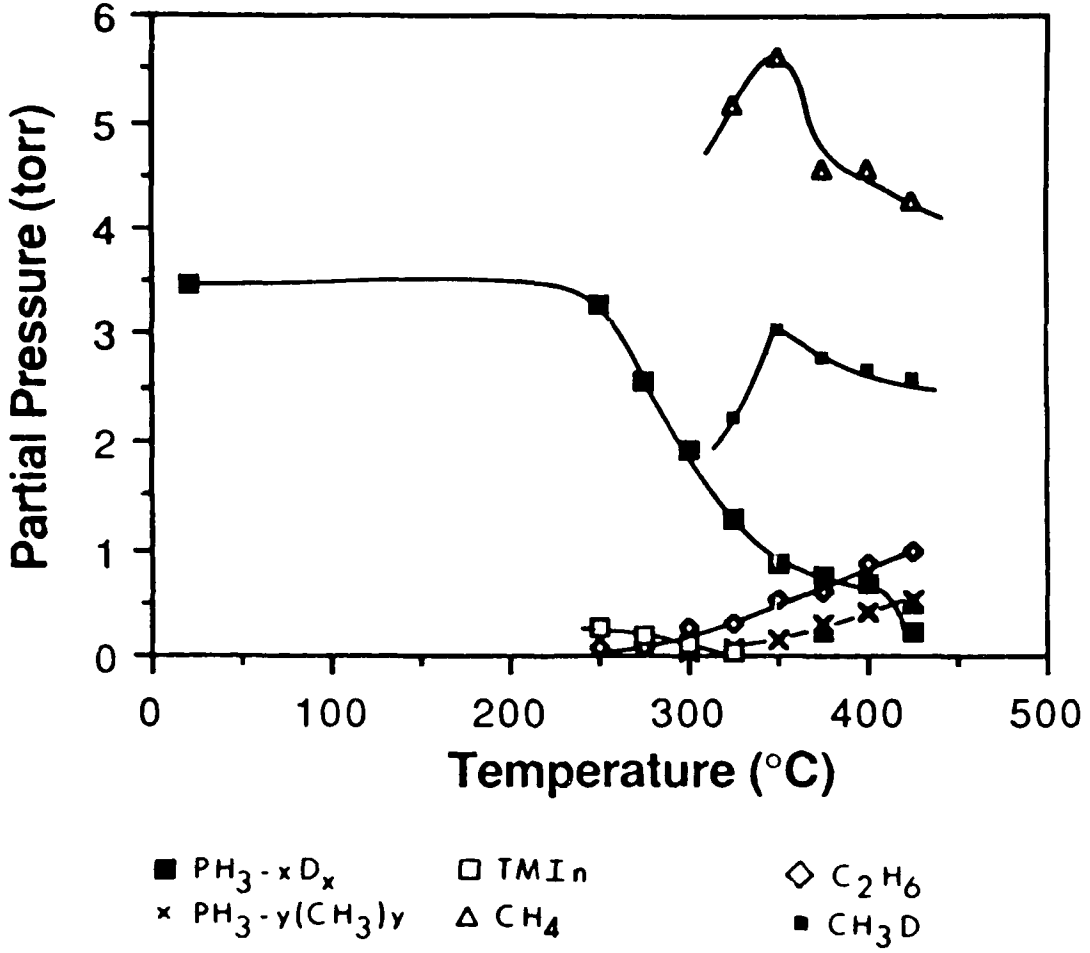

Buchan et al
Fig. 9

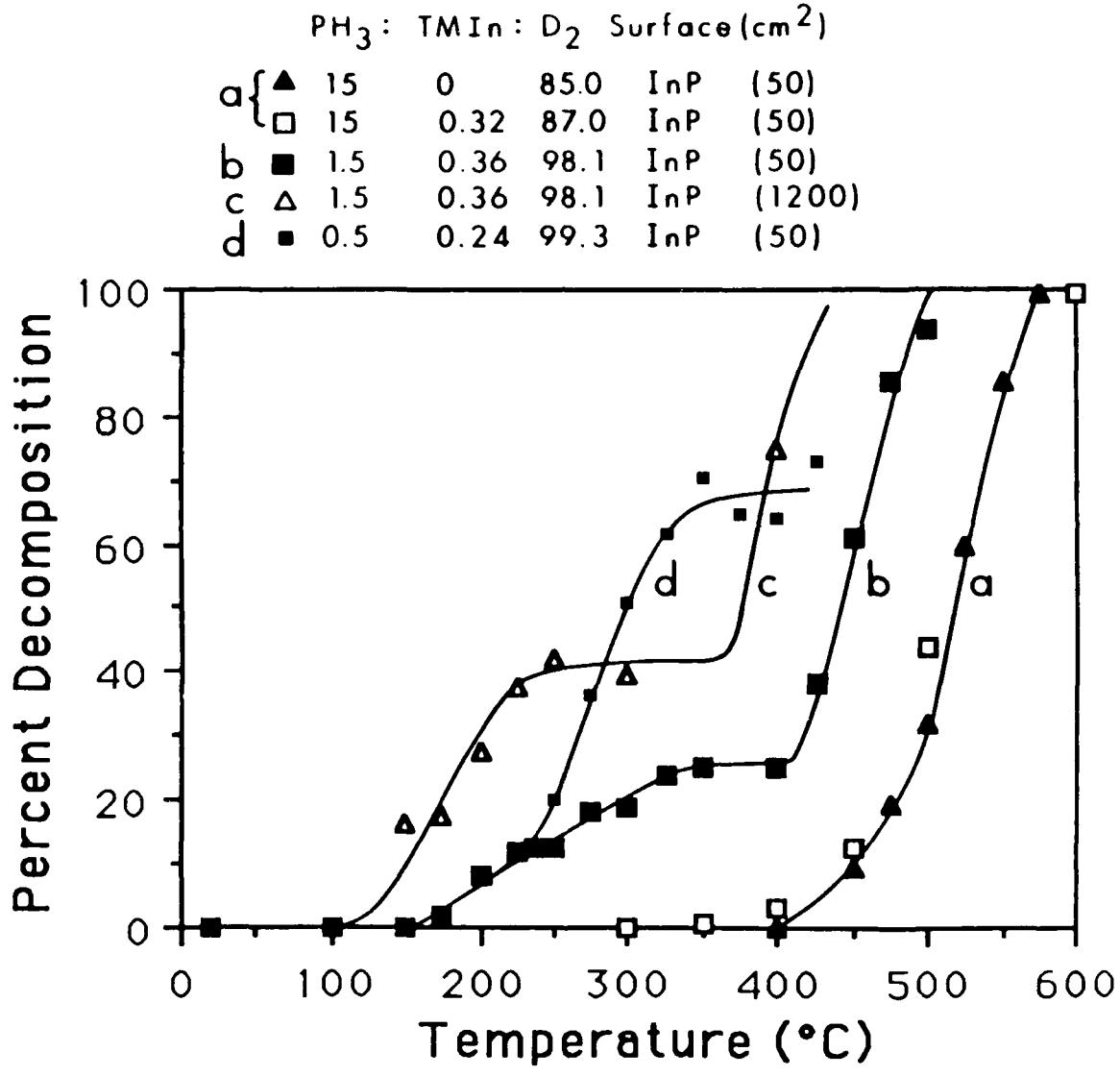
PH3 : TMIn : D2 Surface(cm2)
a ▲ 15 0 85.0 InP (50)
□ 15 0.32 87.0 InP (50)
b ■ 1.5 0.36 98.1 InP (50)
c △ 1.5 0.36 98.1 InP (1200)
d ▪ 0.5 0.24 99.3 InP (50)
Percent Decomposition
100
80
60
40
20
0
0
100
200
300
400
500
600
Temperature (°C)
d
c
b
a

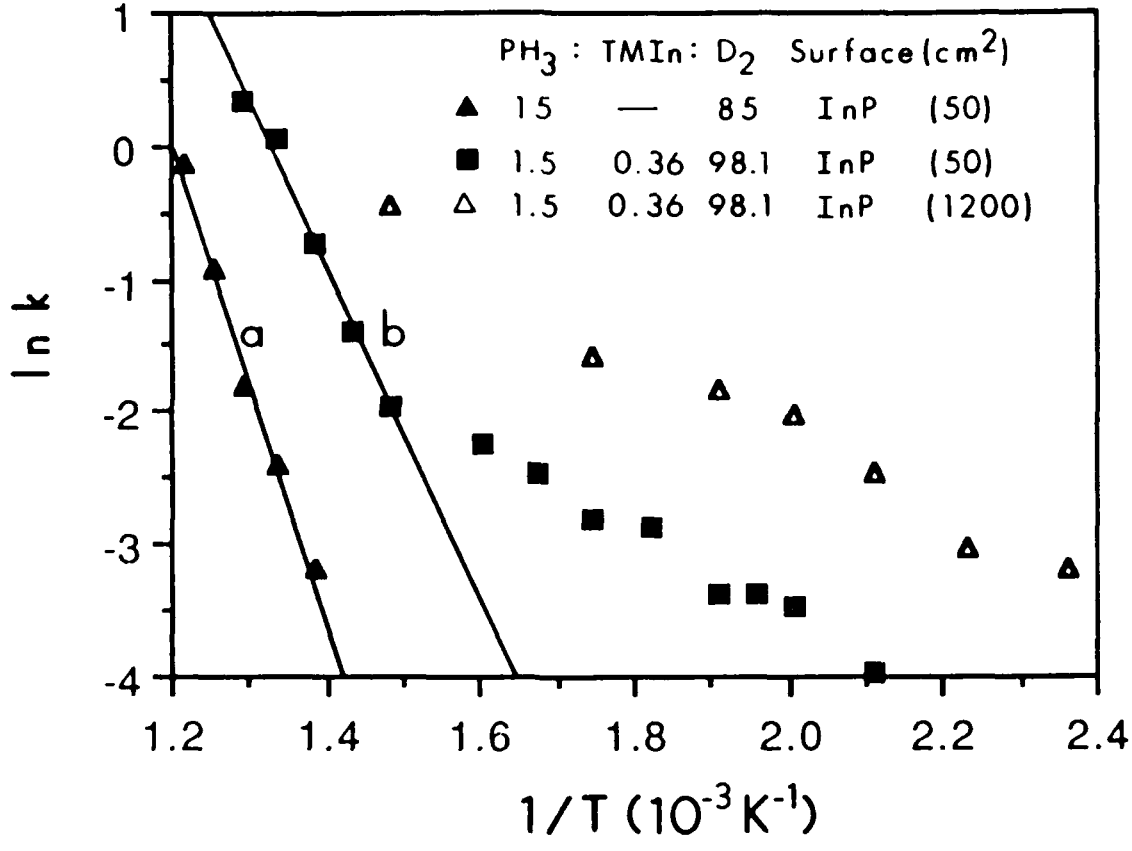
PH3 : TMIn : D2 Surface(cm2)
▲ 15 — 85 InP (50)
■ 1.5 0.36 98.1 InP (50)
△ 1.5 0.36 98.1 InP (1200)
a
b
ln k
1
0
-1
-2
-3
-4
1.2
1.4
1.6
1.8
2.0
2.2
2.4
1/T (10-3 K-1)

Fig 6

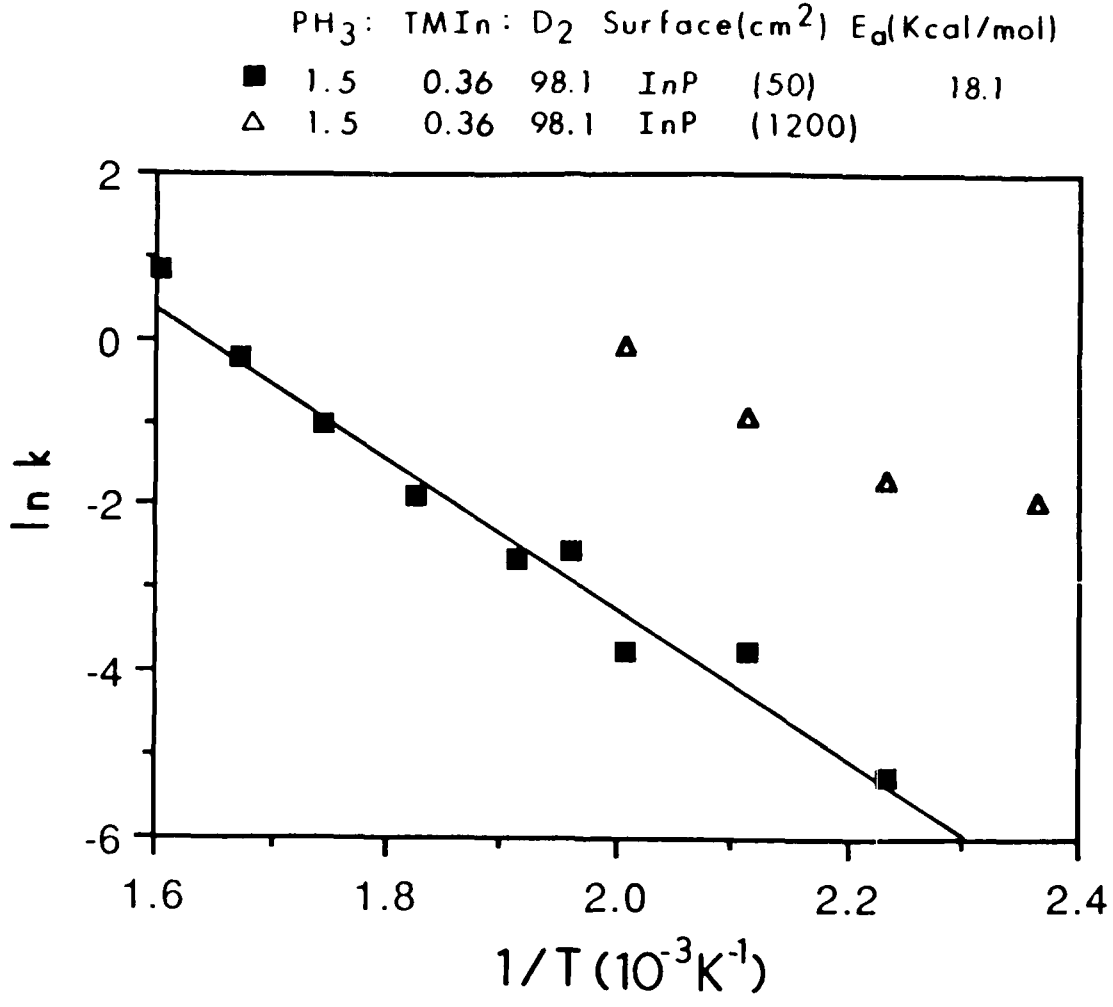
PH3: TMIn: D2 Surface(cm2) Ea(Kcal/mol)
■ 1.5 0.36 98.1 InP (50) 18.1
△ 1.5 0.36 98.1 InP (1200)
2
0
-2
-4
-6
ln k
1.6
1.8
2.0
2.2
2.4
1/T (10-3K-1)

Decomposition Mechanisms of Tertiarybutylarsine

C. A. Larsen, N. I. Buchan, S. H. Li, and G. B. Stringfellow

Departments of Materials Science and Engineering

and Electrical Engineering

University of Utah

Salt Lake City, Utah 84112

Abstract

As a new source compound to replace AsH_3 for organometallic vapor phase epitaxy (OMVPE) of III/V semiconductors, tertiarybutylarsine (TBAs) has the advantages of low decomposition temperatures, low toxicity, and low carbon contamination in OMVPE grown GaAs layers. The vapor pressure of TBAs was measured, and is given by

$$\log_{10}P \text{ (mm Hg)} = 7.500\text{-}1562.3/T \text{ (K)}.$$

The decomposition mechanisms of TBAs were studied in a D_2 ambient using a time-of-flight mass spectrometer to analyze the gaseous products. The dominant route is intramolecular coupling yielding AsH and isobutane. At higher temperatures β-elimination becomes important, producing AsH_3 and isobutene. The reactions are catalyzed by GaAs surfaces, but not by silica. The homogeneous coupling mechanism dominates in all cases. The temperature dependence of the reaction rates was studied, and Arrhenius parameters for the rate constants are given.

1. Introduction

Organometallic vapor phase epitaxy (OMVPE) has progressed from a laboratory phenomenon to a process which promises to become a commercially viable method for making III/V semiconductor devices such as high speed logic circuits and fiber optic system components (1). Great strides have been made by studying macroscopic aspects of the OMVPE process such as growth rate and solid composition vs. gas phase composition and temperature (2) and intentional and unintentional doping as a function of temperature and V/III ratio (3). These studies are useful for developing an empirical set of parameters, and have led to a thorough understanding of OMVPE thermodynamics. They do not, however, represent an efficient approach to elucidate the microscopic mechanisms of crystal growth. Attention has been given to the basic phenomena of OMVPE, including transport phenomena in the various reactor types (4) interactions at the gas-solid interface (5), and, perhaps most important, the chemical reactions of the precursors leading to growth (6-10). Careful analysis of the reaction mechanisms is of course essential for better understanding and modeling of the overall process, and may be useful for further developments such as scale-up of the process, selective epitaxy

(11), photon-asisted growth (12) , and atomic layer epitaxy (13).

Another application of chemical studies is in the design of new source materials. There has been some success in the use of pre-formed adducts, such as $Et_3In:PEt_3$ (14), $Me_3In:PMe_3$ (15) and $ClEt_2Ga:AsEt_3$ (16). However, PH_3 and AsH_3 are still used almost universally as the group V sources for the OMVPE growth of III/V semiconductor materials. They are readily available in high purity form. But their use presents some serious drawbacks. They are highly toxic and inflammable. Storage of large quantities in high pressure cylinders exacerbates the problem. As a result costly safety measures and equipment are involved in their use. Other possible Group V materials such as trialkylarsines are not good alternatives to the hydrides because of higher decomposition temperatures and high background carbon levels in the epilayers (17).

Thus, the need for research into new source compounds is imperative. One group of compounds which has been shown to give very good results is the tertiarybutyl derivatives of PH_3 and AsH_3 (17-21). The structural formula of tertiarybutylarsine (TBAs) is shown below. The large C atom would result in a H-As-C bond angle slightly larger than the H-As-H angle, which is expected to be close to 91.83 degrees as in AsH_3 (22). The *t*-butyl ligand leads to

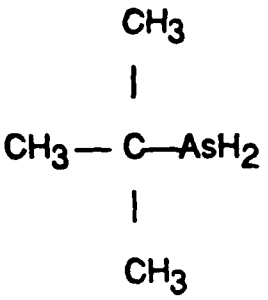

lower decomposition temperatures. This was presumed to be due to a weak As-C bond as compared with the As-H bond. TBAs has been used to grow GaAs layers whose morphology is as good as AsH_3-grown material (20, 21). In addition, the carbon contamination with TBAs appears to be less than with AsH_3 in spite of the large "extra" alkyl group (20). It is relatively stable in air, and is less toxic than AsH_3 (the LC_{50} for TBAs is 70 ppm (23)). It is stored in stainless steel bubblers at atmospheric pressure as are other common sources like trimethylindium (TMIn) and trimethylgallium (TMGa). Thus it appears to be an excellent choice to replace AsH_3 in OMVPE reactors.

The preliminary encouraging results with TBAs have prompted a more detailed investigation into the mechanisms of the decomposition and growth reactions. In this paper we present the results of our studies of TBAs pyrolysis in D_2, and give reaction mechanisms consistent with our observations. In a companion paper (24) we give our results for mixtures of TBAs and TMGa. Our findings should be of use in the search for even better starting materials, as well as in understanding III/V growth

reactions in general.

2. Experimental apparatus

The studies were done in an atmospheric pressure flow tube reactor described in detail elsewhere (25). The key feature of the experiments is the use of D_2 rather than H_2 as the carrier gas. This allows the reaction products to be isotopically labelled and permits us to distinguish between TBAs-D_2 and TBAs-TBAs interactions. The gaseous products are admitted to a CVC Model 2000 time-of-flight mass spectrometer, where the products can be identified and the relative amounts determined. Thus the steps in the reaction mechanism and the Arrhenius parameters can be studied. A total flow rate of 40 sccm through the reactor was used for all experiments.

The TBAs was Electronic Grade, obtained from American Cyanamid Company. The D_2 was C. P. Grade from Union Carbide Corp., Linde Division. Before use it was passed through a catalytic chamber and molecular sieve to remove traces of O_2, H_2O, and D_2O. The unpacked reactor tube had a surface area of approximately 50 cm^2. For some of the experiments the reactor surface was increased to approximately 1200 cm^2 by packing with silica chips. GaAs surfaces were deposited *in situ* by decomposing TMGa-TBAs mixtures.

3. Results

The mass spectrum of a 3 % mixture of TBAs in D_2 is given in Fig. 1. The relative heights of the twenty highest peaks are tabulated in Table I. The parent peak, at m/e = 134, is severely attenuated. The principal peak appears at m/e = 57, corresponding to $C_4H_9^+$. None of the decomposition products has any significant contribution at that mass number, so it was used to monitor the TBAs concentration.

As a first experiment it was necessary to measure the temperature dependence of the TBAs vapor pressure. The TBAs concentration was measured as a function of the source bubbler temperature, with the data normalized to a measurement from an earlier study (20), which showed that the vapor pressure was 96 Torr at 10.0 °C. A least squares fit of the data, shown in Fig.2, provides the vapor pressure equation

$$\log P \text{ (Torr)} = 7.500 - 1562.3/T(K).$$

The boiling point is calculated to be 65.1 °C, which correlates well with the value of 65°C given by Alfa Products (26).

Fig. 3 is a plot of percent decomposition of TBAs in D_2 vs. temperature for: i) 3% TBAs in an unpacked silica tube, ii) 3% TBAs in a packed silica tube, iii) 0.3% TBAs in an unpacked silica tube, iv) 3% TBAs in an unpacked GaAs coated tube, and v) 3 % TBAs in a packed GaAs coated tube. The difference in pyrolysis temperatures for the unpacked and packed silica tube is slight. The GaAs surface in the unpacked tube lowers the

decomposition temperature by only 10°C, but the high GaAs surface decreases the pyrolysis temperature markedly. Thus the decomposition is almost completely homogeneous except at very high GaAs surface areas. This is in marked contrast to other hydride and organometallic compounds of group V elements which are strongly catalyzed by both silica and III/V surfaces (27-30). The reaction order was found by measuring the decomposition of a 3 % TBAs mixture at a series of flow rates in an unpacked tube. The results are plotted in Fig.4 assuming first order kinetics, and the linear curve confirms the assumption.

The temperature dependence of the product partial pressures for the decomposition of a 3 % TBAs mixture are shown in Figs. 5-8. Fig. 5 gives products for the unpacked silica tube. The major products are isobutane (C_4H_{10})and H_2. The C_4H_{10} appears at the same temperature at which the TBAs begins to decompose, i.e. around 300°C. The other products are isobutene (C_4H_8) and AsH_3. The ratios of C_4H_8 to AsH_3 are approximately 1:1 up to 450°C, at which temperature AsH_3 begins to decompose (28). AsH_3 decomposition coincides with H_2 production. The decline in C_4H_{10} is merely due to increased production of C_4H_8. The C_4H_{10} and C_4H_8 concentrations were determined by monitoring the peaks at m/e = 43 and 56, respectively.

Increasing the surface area gives rise to the products shown in Fig. 6. The main features are identical with those of Fig. 5. The only major difference is the lower temperature for the appearance of H_2. This may be

explained in terms of lower decomposition temperatures of AsH_3 due to surface catalysis (31). Again, the C_4H_8 and AsH_3 curves coincide initially. Fig. 7 gives the results for the unpacked GaAs coated tube. The plot is qualitatively the same as for the previous two cases. Finally, a high surface area of GaAs gives the results shown in Fig. 8. The AsH_3 partial pressure is quite small, as expected for the catalytically active surface. The C_4H_8 is also significantly attenuated. There was no evidence in any of the experiments that deuterated species were formed. It is clear that TBAs does not react with the D_2 ambient as part of the decompsition mechanism.

The data from the pyrolysis curves were used to construct the Arrhenius curves shown in Fig. 9. The correponding parameters are given in Table II. It is seen that the highest activation energy is for the unpacked silica tube (curve a). The data for the packed silica tube (b) closely follow curve a except at low temperatures where the curve deviates. This deviation may indicate a different reaction mechanism on silica at low temperatures (e.g., heterogeneous catalysis). However, if this were the case, the activation energy of this new reaction would be much smaller than for the high GaAs surface area (curve d) which plainly exhibits strong surface catalysis. A more likely explanation is simply difficulty in accurately measuring the percent pyrolysis at the low conversions (see Fig. 3). When these data points are ignored the Arrhenius parameters are quite close to those from curve a. The unpacked GaAs coated tube has a

lower E_a and lower A factor (curve c). Finally, a high GaAs surface area (curve d) results in the lowest pre-exponential factor and activation energy of all the cases.

4. Discussion

A. Free Radical Reaction Hypothesis

A key experimental observation is that *no deuterated* species are formed. If the ligands were cleaved homolytically they would encounter D_2 molecules and form HD or C_4H_9D. This was verified by computer simulation of a free radical reaction scheme, using the following steps:

$$TBAs \rightarrow C_4H_9 + H + AsH \quad (1)$$

$$C_4H_9 + D_2 \rightarrow C_4H_9D + D \quad (2)$$

$$2\ C_4H_9 \rightarrow C_8H_{18} \quad (3)$$

$$C_4H_9 + D \rightarrow C_4H_9D \quad (4)$$

$$C_4H_9 + H \rightarrow C_4H_{10} \quad (5)$$

$$H + D_2 \rightarrow HD + D \quad (6)$$

$$2\ D \rightarrow D_2 \quad (7)$$

$$2\ H \rightarrow H_2 \quad (8)$$

$$H + D \rightarrow HD \quad (9)$$

The rate constant for step 1 was taken as the k_a for the silica tube above.

If TBAs were to decompse homolytically the expected products are C_4H_9 and AsH_2, but release of one H atom was assumed in step 1 as the only source of any C_4H_{10} at all in the subsequent steps. The rate constant for step 2 has not been reported, but was estimated from ΔH°_f and ΔS°_f values for the reactants and products (32), together with the known rate constant for the reverse reaction (33). The k's for steps 4 and 5 were based on the reaction

$$A + B \rightarrow AB$$

with zero activation energy. For such a collision limited reaction the rate constant is given by (32)

$$k = P_a P_b (\pi d_{ab}^2/\sigma_{ab})(8RT/\pi\mu_{ab})^{1/2}$$

where P_a and P_b are the probabilities that a collision between A and B will proceed to reactants (chiefly dependent on orientation factors), d_{ab} is the reaction cross section, σ_{ab} is a symmetry factor (1 for $A \neq B$ and 2 for $A = B$), and μ_{ab} is the reduced mass of the reactants. Collision radii of 3.0 Å for *t*-butyl and 0.5 Å for H and D were used. A value for P_a of 0.05 was calculated from the known rate constant of step 3. This small reaction probability is expected because of the large degree of steric hindrance in the *t*-butyl radical. Recombinations of this radical involve attack on the central C atom. A collision in the plane of the radical, for example, would not result in a reaction. For H and D atoms $P_b = 1.0$, which then permits an

accurate calculation of the rate constants. All other k's have been reported. Table III lists the values of the rate constants for all reactions and the sources of the data. A temperature of 427 °C and flow rate of 40 sccm were used. The temperature was chosen to give the maximum TBAs decomposition and hence the highest possible radical concentrations. Under these conditions the predicted C_4H_{10}, HD, and C_4H_9D partial pressures are 3.70×10^{-2}, 28.9 and 28.8 Torr, respectively. Reference to Fig.5 shows that this model gives results which are in marked disagreement with our observations. Neither C_4H_9D nor HD was detected at all.

B. Coupling and β-elimination Model

The data are more consistent with another reaction pathway which does not involve free radicals. Production of both C_4H_{10} and C_4H_8 are unimolecular proceses, as demonstrated by the linear dependence of their individual partial pressures on initial TBAs concentration (shown in Fig. 10 for TBAs concentrations of 3.0, 0.6 and 0.3 %). Also, the reaction is largely homogeneous. The following mechanism accounts for our observations for the unpacked silica tube experiments:

$$C_4H_9AsH_2 \rightarrow C_4H_{10} + AsH \qquad (10)$$

$$AsH \rightarrow AsH(ads) \qquad (11)$$

$$AsH(ads) \rightarrow As + 1/2\ H_2 \qquad (12)$$

$$C_4H_9AsH_2 \rightarrow C_4H_8 + AsH_3 \qquad (13)$$

The first step is a classic example of reductive coupling, known for several transition metal compounds (34,35) and for some trivalent P compunds (36). To our knowledge this is the first reported example of the process for As compounds. The transition state is a three centered complex between the central As atom, the central carbon atom on the *tert*-butyl ligand, and one of the H atoms bonded to the As. The leaving group is a complete isobutane molecule. Reactions between the AsH and the D_2 ambient appear to be unimportant, based on the absence of HD and $AsHD_2$. The stability of the AsH group is further demonstrated by the fact that it does not yield H_2 until temperatures are reached at which the AsH_3 from step 13 also decomposes.

The last step, yielding the isobutene and AsH_3, is a ß-elimination process, also well known for other main-group organometallic systems (37). In β–elimination, the *tert*-butyl ligand donates one of its hydrogen atoms to the central As atom and subsequently leaves as isobutene. Thus the C_4H_8 and AsH_3 partial pressures track each other in all cases until temperatures are reached at which AsH_3 decomposes. The possibility of some C_4H_8 being produced by the dehydrogenation of C_4H_{10} was investigated, by passing a 3 % mixture of C_4H_{10} in D_2 over a GaAs-coated packed tube (to maximize the possibility of catalytic reactions) at the same flow rate as for the other experiments. There was no decline in

C_4H_{10} concentration, and no C_4H_8 was detected, even at temperatures as high as 600 °C.

It should be noted that, since As is a non-metal, it is given an oxidation number of -3 for arsines and their organic derivatives. Hence the coupling reaction should correctly be termed an oxidative process. Similarly, the β-elimination is strictly a β-proton elimination, rather than a hydride pathway. These distinctions, however, are formalisms where As, which forms mostly covalent bonds with hydrogen, is involved. The mechanisms are of the same class as the corresponding reactions with, say, transition metals as the central atom. This problem of nomenclature at the expense of a general mechanistic theory is present for several organometallic systems. One attempt to reslove the dilemma is given in Ref. 38 At this stage of main-group reaction classification we prefer merely to refer to step 10 as coupling and step 13 as β-elimination.

Homogeneous Reactions

It has been shown that the decomposition in the presence of silica yields two hydrocarbon products by parallel, unimolecular, completely homgeneous steps. Thus the rate constant for curve a in Fig. 9, k_a, is the sum of the two individual rate constants:

$$k_a = k_{10} + k_{13}.$$

These rate constants can be separated by virtue of the fact that the

branching ratio is given by the product ratio, since both processes are unimolecular:

$$k_{10}/k_{13} = [C_4H_{10}]/[C_4H_8].$$

Fig. 11 is an Arrhenius plot of the values of k_{10} and k_{13} determined using this analysis. The two rate constants are given by

$$\log_{10}k_{10}\ (sec^{-1}) = 13.08 - 41.48\ (kcal/mol)\ /2.303RT$$

$$\log_{10}k_{13}\ (sec^{-1}) = 14.24 - 48.49\ (kcal/mol)\ /2.303RT.$$

The pre-exponential factors for these rate constants are comparable to those of other unimolecular processes having three- and four-center transition states, which typically are near $10^{13.5}$ sec^{-1} (31). A lower A-factor would be expected for the four-center β-elimination compared to the coupling reaction. The higher measured value indicates a "loose" transition state. The activation energies are more difficult to predict, because the bond dissociation energies and geometry of the TBAs molecule are unknown. However, they provide a lower limit for the $H_2As\text{-}C(CH_3)_3$ bond strength of approximately 50 kcal/mol. This may be compared with trimethylarsine, for which the bond dissociation energy of the $(CH_3)_2As\text{-}CH_3$ bond is approximately 63 kcal/mol (38). Because of the greater stability of the *tert*-butyl radical (39) the As-C bond strength in TBAs is most likely several kcal/mol less than in trimethylarsine.

Heterogeneous Reactions

In contrast to silica surfaces, when GaAs is present heteogeneous reactions also become important. Since the same products are observed for GaAs coated tubes (with different ratios, however), it can be concluded that the GaAs surface serves mainly to enhance the rates of the same reactions listed above. Then the decomposition proceeds according to the following mechansm:

$$TBAs + s \leftrightarrow TBAs\ (ads) \qquad (14)$$

$$TBAs(ads) \rightarrow C_4H_{10} + AsH\ (ads) \qquad (15)$$

$$TBAs(ads) \rightarrow C_4H_8 + AsH_3 \qquad (16)$$

where s represents a vacant surface site. The rate law for this scheme is

$$d[TBAs]/dt = k_{het}KS[TBAs]/(1 + K[TBAs])$$

where k_{het} is the overall heterogeneous rate constant, K is the adsorption equilibrium constant for TBAs, and S is the total concentration of surface sites. k_{het} can be derived by subtracting the overall homogeneous rate constant (k_a in Table II) from the data of curves c and d in Fig. 9, taking into account the increased surface area for curve d. The following equations then result from k_c and k_d, respectively:

$$\log_{10} k_{het,c}\ (sec^{-1}) = 9.31 - 30.15\ (kcal/mol)/2.303RT$$

$$\log_{10} k_{het,d}\ (sec^{-1}) = 9.01 - 29.66(\ kcal/mol)/2.303RT.$$

The remarkable similarity of these values lends support to the procedure. The high surface area case gives the more reliable values and so was used for the calculations described below and in Ref 23.

As with the gas phase reactions, the branching ratio for the surface reactions equals the product ratio at low partial pressures of TBAs. The rate constants for steps 15 and 16 were determined by subtracting k_{10} and k_{13}, respectively, from the total Arrhenius plots for C_4H_{10} and C_4H_8 production (shown in Fig. 12). The resulting equations are

$$\log_{10} k_{15}\ (sec^{-1}) = 8.82 - 29.18\ (kcal/mol)/2.303RT$$

$$\log_{10} k_{16}\ (sec^{-1}) = 9.99 - 36.37(\ kcal/mol)/2.303RT.$$

The surface catalysis is reflected in the lower A-factors compared with the homogeneous reactions (due to the lower entropy of adsorbed species), and in the lower activation energies (due to weakening of the bonds in TBAs upon formation of As-surface bonds). As with the gas-phase steps, both Arrhenius parameters for the β-elimination are higher than for the coupling route.

It is worthwhile to interject some comments regarding these rate constants. First, the preexponential factors include the surface site concentration. On a given surface this term is specific for each reacting species and is actually the concentration of active sites. Adsorption studies can provide reliable values for S in the above equations. The activation energy, also, requires care in interpretation. The adsorption

equilibrium constant has a temperature dependence, so the measured activation energy is given by

$$E_{meas} = E_a + \Delta H_{ads} \; (\Delta H_{ads} < 0).$$

For simplicity Langmuir behavior is usually assumed for surface reactions, i.e., that the enthalpy of adsorption is not a function of surface coverage. Schlyer and Ring, however, showed (5) that for adsorption of AsH_3 on GaAs the Langmuir isotherm is *not* applicable. From their data it appears that the Freundlich isotherm more nearly describes adsorption on III/V semiconductor surfaces.

The mechanism for TBAs decomposition is significantly different from that of AsH_3. The latter is highly surface catalyzed, even by silica, and probably does not involve reductive coupling. Evidence for this is found in the work of Tamaru (40), who studied the decomposition of mixtures of AsH_3 and AsD_3. He reported finding "large amounts" of HD. No quantitative data were given. If the reaction were by the coupling route the ratio of H_2:HD:D_2 would be 1:0.4:1,whereas the ratio would be 1:2:1 if there were no coupling. If it is assumed that the "large amount" of HD was in comparison with the H_2 and D_2, then the coupling route is not dominant. Rather, the decomposition of AsH_3 proceeds by stepwise removal of the H atoms.

4. Summary

It has been shown that TBAs decomposition occurs by two well-defined

parallel routes. In all cases coupling is the dominant route. β-elimination becomes important at higher temperatures. The reactions are not catalyzed by silica surfaces, but GaAs surfaces increase the reaction rates of both mechanisms. Coupling produces isobutane and AsH, which is stable enough to diffuse to the surface before any reaction with D_2 can take place. The β-elimination yields isobutene and AsH_3 in nearly one-to one ratios at low temperatures before AsH_3 pyrolysis is initiated. These mechanisms are substantially different from AsH_3 which decomposes primarily by heterogeneous stepwise removal of individual H atoms.

5. Acknowledgements

This work was supported by a grant from the U. S. Air Force, Contract # AFSOR-87-0233. The authors also wish to thank American Cyanamid company for supplying the tertiarybutylarsine.

References

1. G. B. Stringfellow, Semiconductors and Semimetals, 22A (1985) 209; M. J. Ludowise, J. Appl. Phys. 58 (1985) R31; P. M. Frijlink, in: Heterojunctions and Semiconductor Superlattices, Eds.G. Allan, N. Boccara, M. Larnoo and M. Voss (Springer-Verlag, Berlin, 1986) p. 226
2. J. Yoshino, T. Iwamoto, and H. Kukimoto, J. Crystal Growth 55 (1981) 74; D. W. Shaw, J. Electrochem. Soc. 115 (1986) 405
3. G. B. Stringfellow, J. Crystal Growth 75 (1986) 91
4. H. Moffat and K. F. Jensen, J. Crystal Growth 77 (1986) 108; N. Shibata and S. Zembutsu, Japan. J. Appl. Phys. 26 (1987) 1416
5. D. J. Schlyer and M. A. Ring, J. Organometallic chem. 114 (1976) 9
6. C. A. Larsen, N. I. Buchan and G. B. Stringfellow, J. Crystal Growth 85 (1987)148
7. M. Yoshida, H. Watanabe, and F. Uesugi, J. Electrochem. Soc. 132 (1985) 677
8. J. Nishizawa and T. Kurabayashi, J. Electrochem. Soc. 130 (1983) 413
9. S. P. DenBaars, B. Y. Maa, P. D. Dapkus, A. D. Danner, and H. C. Lee, J. Crystal Growth 77 (1986) 188
10. J. E. Butler, N. Bottka, R. S. Sillman, and D. K. Gaskill, J. Crystal Growth 77(1986) 163
11. K. Kamon, S. Takagishi, and H. Mori, Japan. J. Appl. Phys. 25 (1986) L10
12. M. Hanabusa, Materials Science Reports 2 (1987) 51
13. B. J. McDermott, N. A. El-Masry, M. A. Tischler, and S. M. Bedair, Appl.

Phys. Lett. 51 (1987) 1830

14. R. H. Moss and J. S. Evans, J. Crystal Growth 55 (1981) 129
15. R. Karlicek, J. A. Long, and V. M. Donnelly, J. Crystal Growth 68 (1984) 123
16. F. Maury and G. Constant, J. Crystal Growth 62 (1983) 568
17. G. B. Stringfellow, J. Electron. Mater. (submitted)
18. C. H. Chen, C. A. Larsen, G. B. Stringfellow, D. W. Brown, and A. J. Robertson, J. Crystal Growth 77 (1986) 11
19. C. H. Chen, D. S. Cao and G. B. Stringfellow, J. Electron. Mater. 17 (1988) 67
20. C. H. Chen, C. A. Larsen, and G. B. Stringfellow, Appl. Phys. Lett. 50 (1987) 218
21. R. M. Lum, J. Klingert, and M. G. Lamont, Appl. Phys. Lett. 50 (1987) 284
22. *CRC Handbook of Chemistry and Physics*, 61st edition, Ed. R. C. Weast (CRC Press, Boca Raton, Florida, 1980)
23. Private communication, American Cyanamid Company
24. C. A. Larsen, N. I. Buchan, S. H. Li, and G. B. Stringfelow, J. Crystal Growth (submitted, companion paper)
25. N. I. Buchan, C. A. Larsen, G. B. Stringfellow, J. Crystal Growth (submitted)
26. "Organometallics for Vapor Phase Epitaxy-Literature and Product Review" (Morton Thiokol, Inc., Alfa Products, 1986) p. 73
27. M. J. Cherng, H. R. Jen, C. A. Larsen, G. B. Stringfellow, H. Lundt, and P. C. Taylor, J. Crystal Growth 77 (1986) 408
28. I. A. Frolov, E. M. Kitaev, B. L. Druz', and E. B. Sokolov, Zh. Fiz. Khim. 51

(1977) 1106

29. C. A. Larsen, N. I. Buchan, and G. B. Stringfellow, Appl. Phys. Lett. (submitted)

30. C. A. Larsen and G. B. Stringfellow, J. Crystal Growth 75 (1986) 247

31. G. G. Devyatykh, V. M. Kedyarkin, and A. D. Zorin, Russ. J. Inorg. Chem 10 (1965) 833

32. Sidney W. Benson, *Thermochemical Kinetics* (Wiley-Interscience, 1976)

33. *CRC Handbook of Bimolecular and Termolecular Gas Reactions*, vol.2, Eds. J. A. Kerr and S. J. Moss (CRC Press, Boca Raton, Florida, 1981)

34. Jay K. Kochi, *Organometallic Mechanisms and Catalysis* (Academic Press, New York, 1978)

35. J. J. Low and W. A. Goddard III, Organometalics 5 (1986) 609

36. F. Mathey, Angew. Chem. Int. Ed. Engl. 26 (1987) 275

37. M. E. O'Neill and K. Wade, in: *Comprehensive Organometallic Chemistry: The Synthesis, Reactions and Structures of Organometallic Compounds*, Eds. G. Wilkinson, F. G. A. Stone, and E. W. Abel (Pergamon Press, Oxford, 1982) vol. I, p. 7

38. R. H. Crabtree and G. G. Hlakty, Inorg. Chem.19 (1980) 571

39. S. J. W. Price and J. P. Richard, Can. J. Chem. 48 (1970) 3209

40. R. T. Morrison and R. N. Boyd, *Organic Chemistry*, 3rd edition (Allyn and Bacon, Inc., Boston, 1975) p. 103

41. K. Tamaru, J. Phys. Chem. 59 (1955) 777

Table I. Mass Spectrum of TBAs

3 % TBAs in D_2, Ionization Potential = 70 eV

m/e	Species	Rel. Height (%)
27	$C_2H_3^+$	18.1
29	$C_2H_5^+$	49.9
39	$C_3H_3^+$	18.7
41	$C_3H_5^+$	59.1
43	$C_3H_7^+$	9.3
55	$C_4H_7^+$	8.9
57	$C_4H_9^+$	100 (principal peak)
58	$C_4H_{10}^+$	7.1
75	As^+	2.5
76	AsH^+	3.8
77	AsH_2^+	1.8
78	AsH_3^+	1.9
89	CH_2As^+	3.2
91	$CH_2AsH_2^+$	4.5
101	$C_2H_2As^+$	1.3
103	$C_2H_4As^+$	1.5
105	$C_2H_6As^+$	1.9
117	$C_3H_6As^+$	2.2
119	$C_3H_6AsH_2^+$	2.3
132	$C_4H_9As^+$	2.3
134	$C_4H_9AsH_2^+$	4.8 (parent peak)

Table II. Rate Constants from Decomposition Curves of Fig. 3

Rate Constant	Surface	$\log_{10} A$ (sec^{-1})	E_a (kcal/mol)
k_a	50 cm^2 SiO_2	13.18	41.64
k_b	1200 cm^2 SiO_2	12.16	38.14
k_c	50 cm^2GaAs	11.40	35.43
k_d	1200 cm^2 GaAs	10.60	30.23

Table III. Rate Constants for Free Radical Model of TBAs Decomposition

Reaction	Rate Constant[a]	Units	Reference
1	$10^{13.2}$ $e^{-41.6/RT}$	sec^{-1}	Present Work
2	$10^{11.2}$ $e^{-15.2/RT}$	$cm^3/mol\text{-}sec$	32,33
3	$10^{11.8}$	"	32
4	$10^{13.6}$	"	32
5	$10^{13.5}$	"	32
6	$10^{13.7}$ $e^{-9.39/RT}$	"	33
7	$10^{15.6}$	$cm^6/mol^2\text{-}sec$	33
8	$10^{15.6}$	"	33
9	$10^{15.6}$	"	33

a. Activation energies are in kcal/mol.

Figure Captions

Fig. 1. Mass spectrum of 3 % TBAs in D_2. Ionization potential = 70 eV.

Fig. 2. Vapor presure of TBAs vs. temperature.

Fig. 3. Decomposition of TBAs in D_2 vs. temperature.■, 3 % TBAs, 50 cm^2 SiO_2;○,3 % TBAs , 1200 cm^2 SiO_2; △, 0.3 % TBAs, 50 cm^2 SiO_2; □ , 3 % TBAs, 50 cm^2 GaAs;●,3 % TBAs, 1200 cm^2 GaAs.

Fig. 4. ln P/P_o vs. residence time for 3 % TBAs in D_2 at 362 °C.

Fig. 5. Decomposition products of 3 % TBAs in D_2 ; surface is 50 cm^2 SiO_2.

Fig. 6. Decomposition products of 3 % TBAs in D_2; surface is 1200 cm^2 SiO_2.

Fig. 7. Decomposition products of 3 % TBAs in D_2; surface is 50 cm^2 GaAs.

Fig 8. Decomposition products of 3 % TBAs in D_2; surface is 1200 cm^2 GaAs.

Fig. 9. First-order Arrhenius plot for TBAs. a, 50 cm^2 SiO_2; b, 1200 cm^2SiO_2; c, 50 cm^2 GaAs; d, 1200 cm^2 GaAs.

Fig. 10. Partial pressures of C_4H_{10} (a) and C_4H_8 (b) as functions of input TBAs partial pressure.■, 3 %,TBAs;▲, 0.6% TBAs; ●, 0.3 % TBAs.

Fig. 11. Arrhenius plots of rate constants for C_4H_{10} and C_4H_8 production for 3 % TBAs in D_2, 50 cm^2 SiO_2.

Fig. 12. Arrhenius plots of rate constants for C_4H_{10} and C_4H_8 production for 3 % TBAs in D_2, 1200 cm^2 GaAs.

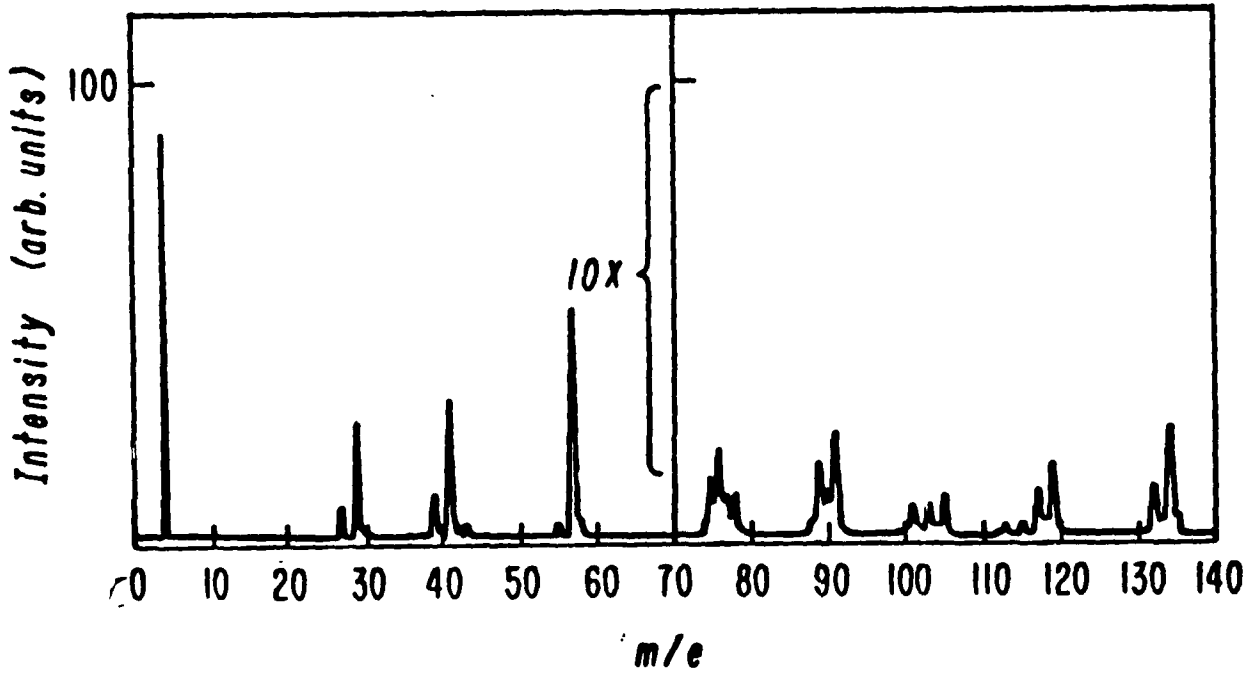
Intensity (arb. units)
100
10x
0
10
20
30
40
50
60
70
80
90
100
110
120
130
140
m/e

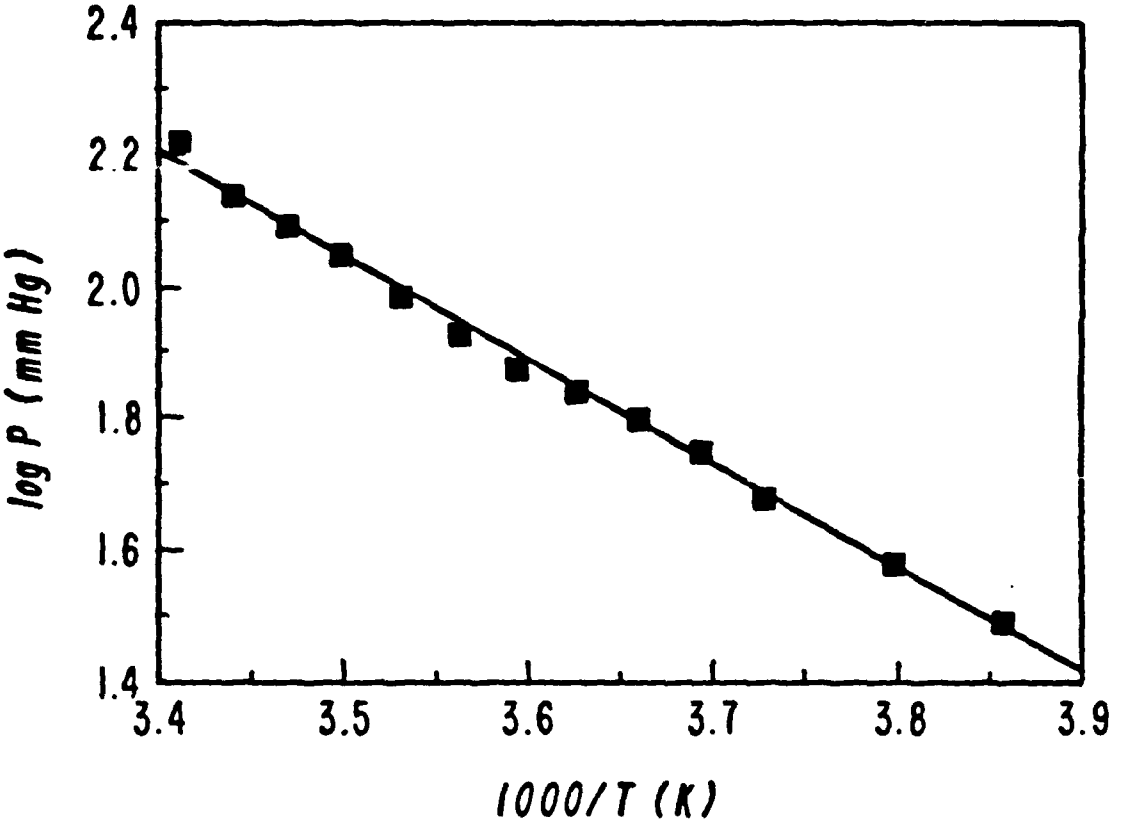
2.4
2.2
2.0
1.8
1.6
1.4
log P (mm Hg)
3.4
3.5
3.6
3.7
3.8
3.9
1000/T (K)

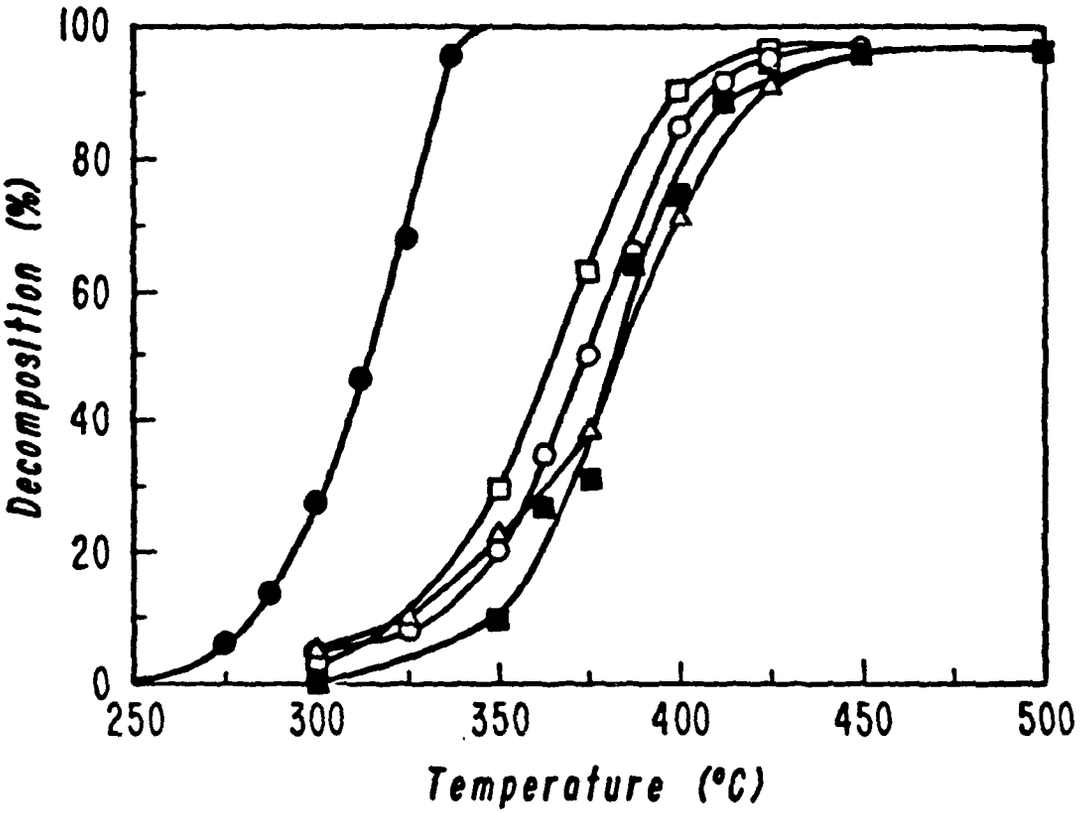
100
80
60
40
20
0
Decomposition (%)
250
300
350
400
450
500
Temperature (°C)

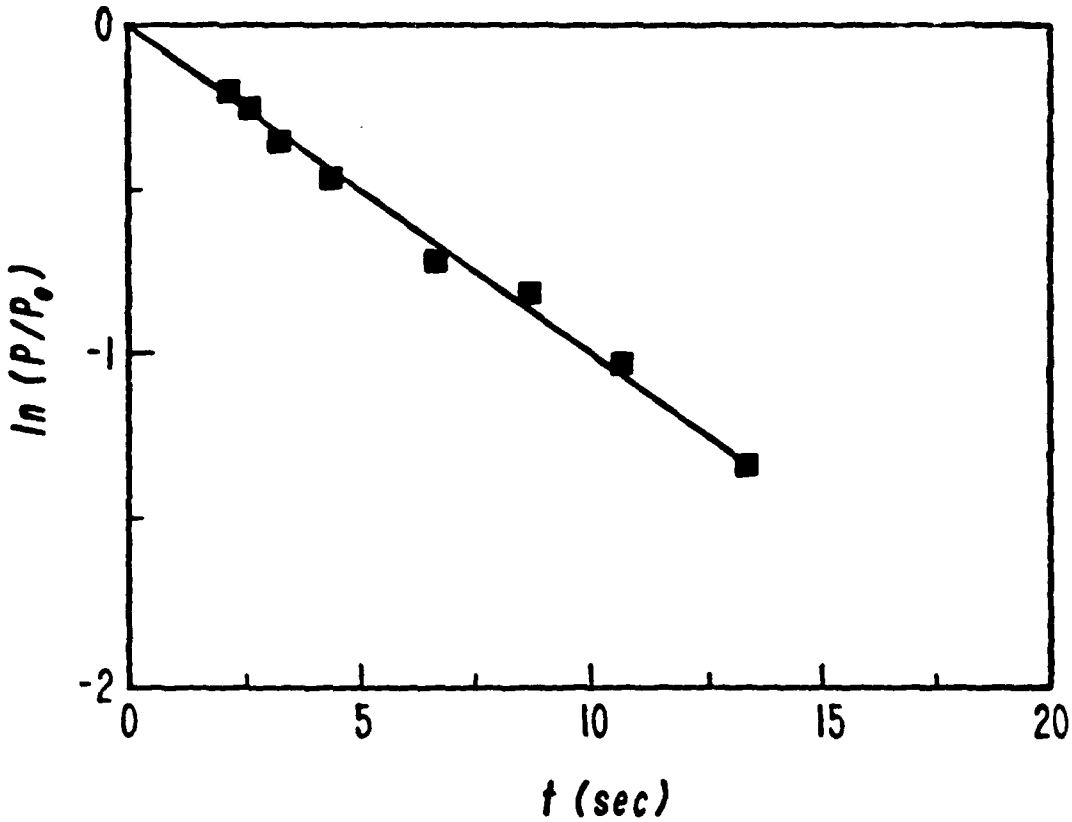
0
-1
-2
ln (P/P₀)
0
5
10
15
20
t (sec)

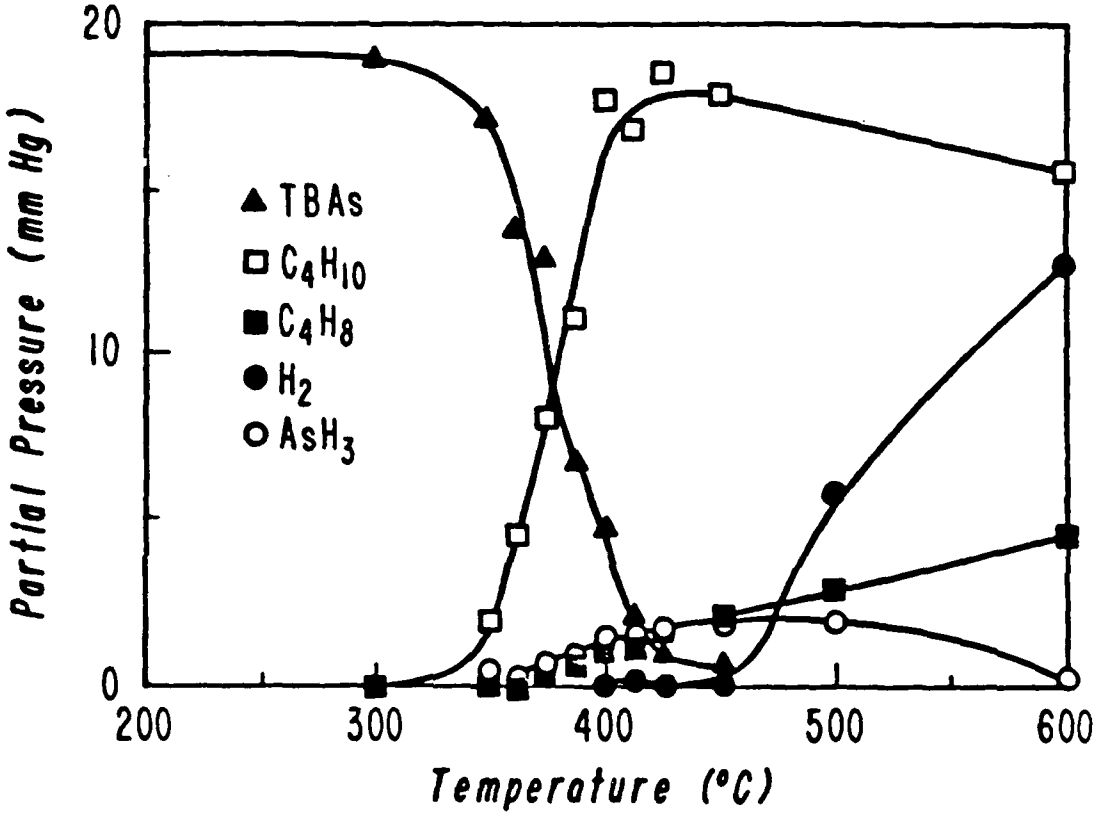
20
10
0
200
300
400
500
600
Partial Pressure (mm Hg)
Temperature (°C)
▲ TBAs
□ C_4H_{10}
■ C_4H_8
● H_2
○ AsH_3

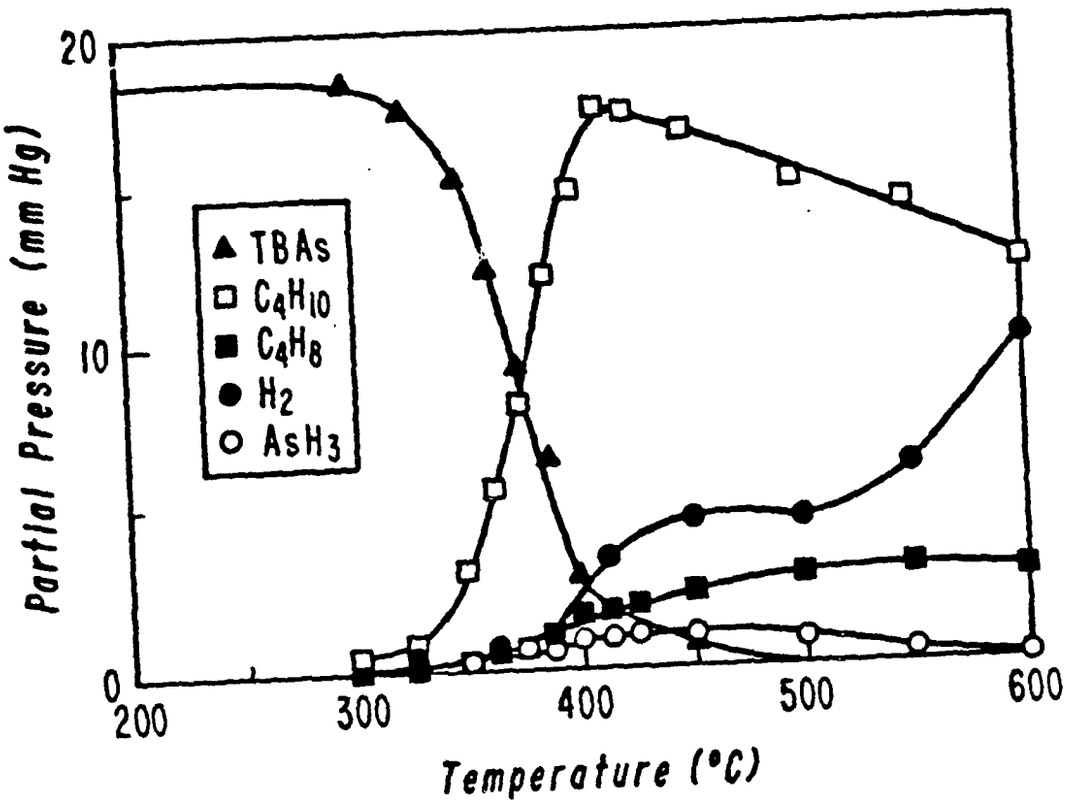
20
10
0
200
300
400
500
600
Partial Pressure (mm Hg)
Temperature (°C)
▲ TBAs
□ C_4H_{10}
■ C_4H_8
● H_2
○ AsH_3

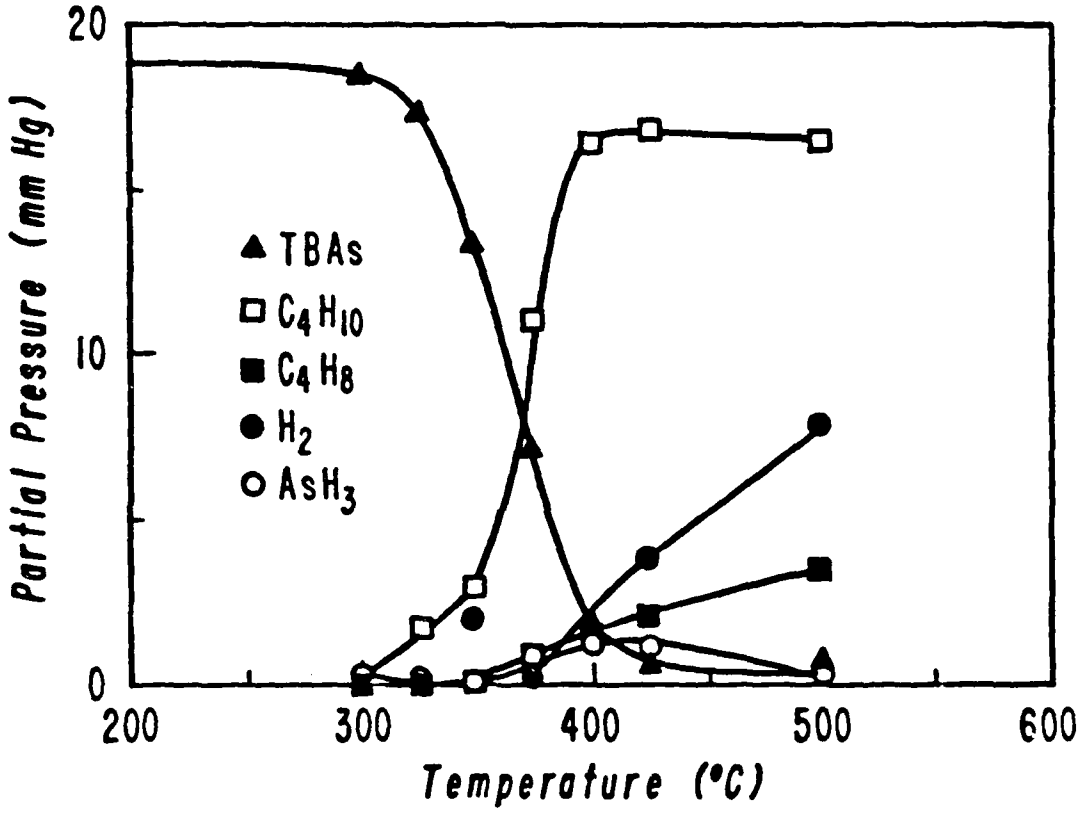
20
10
0
200
300
400
500
600
Partial Pressure (mm Hg)
Temperature (°C)
▲ TBAs
□ C_4H_{10}
■ C_4H_8
● H_2
○ AsH_3

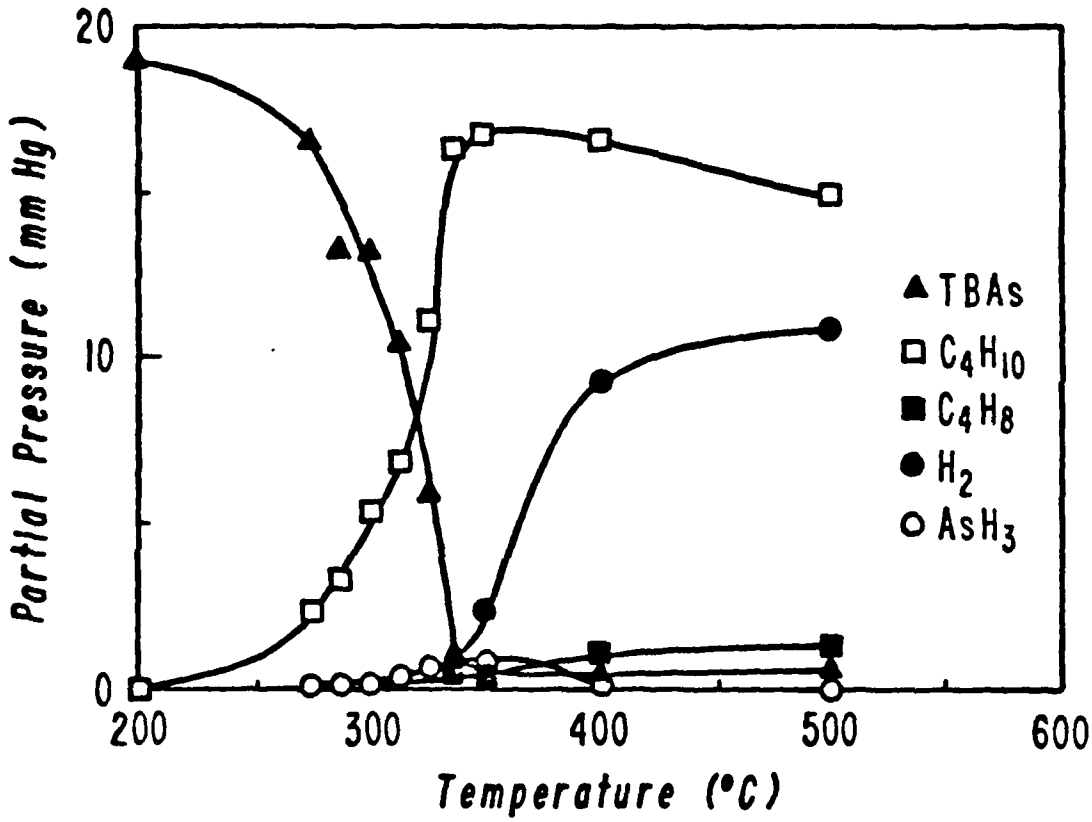
20
10
0
200
300
400
500
600
Partial Pressure (mm Hg)
Temperature (°C)
▲ TBAs
□ C_4H_{10}
■ C_4H_8
● H_2
○ AsH_3

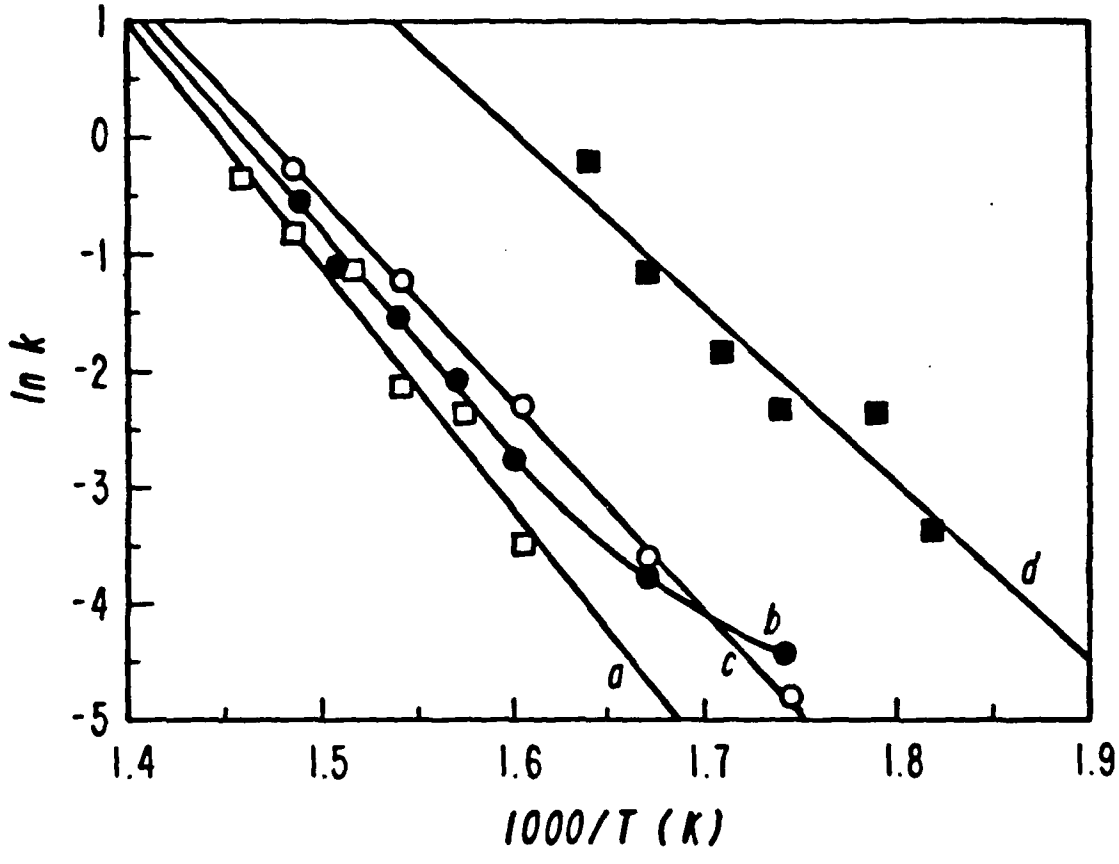
1
0
-1
-2
-3
-4
-5
ln k
1.4
1.5
1.6
1.7
1.8
1.9
1000/T (K)
a
b
c
d

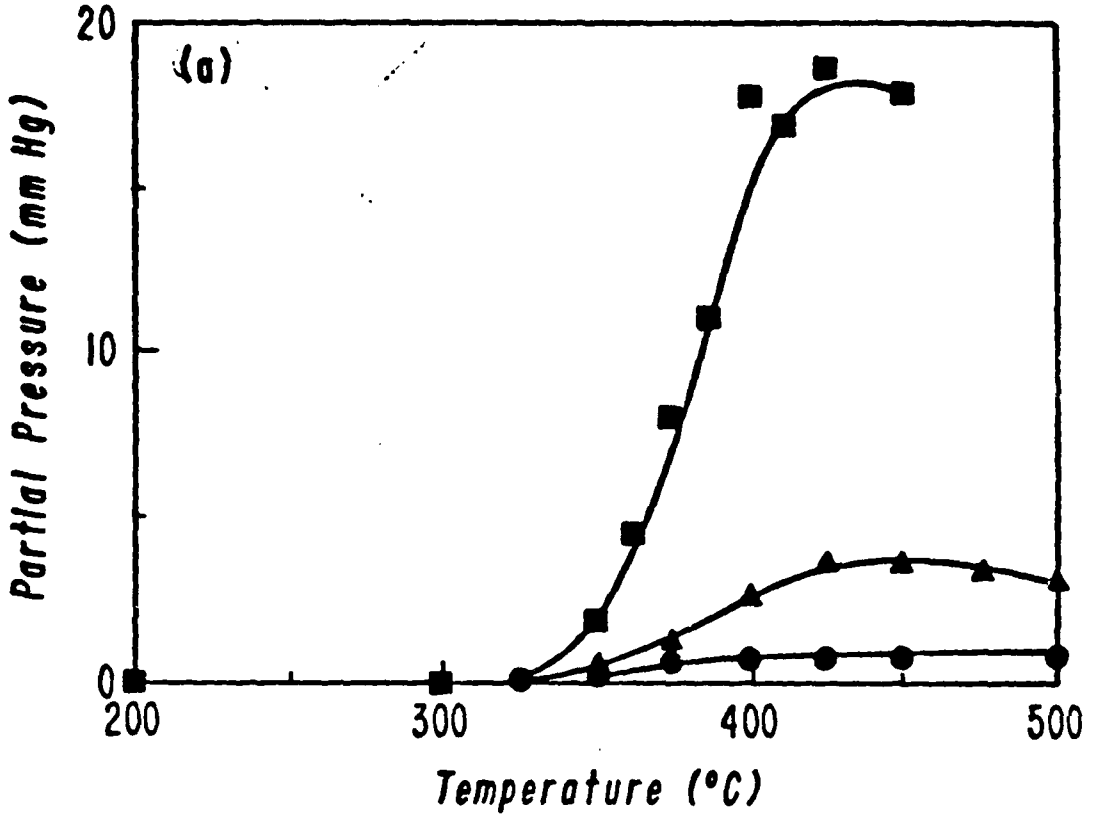
(a)
Partial Pressure (mm Hg)
20
10
0
200
300
400
500
Temperature (°C)

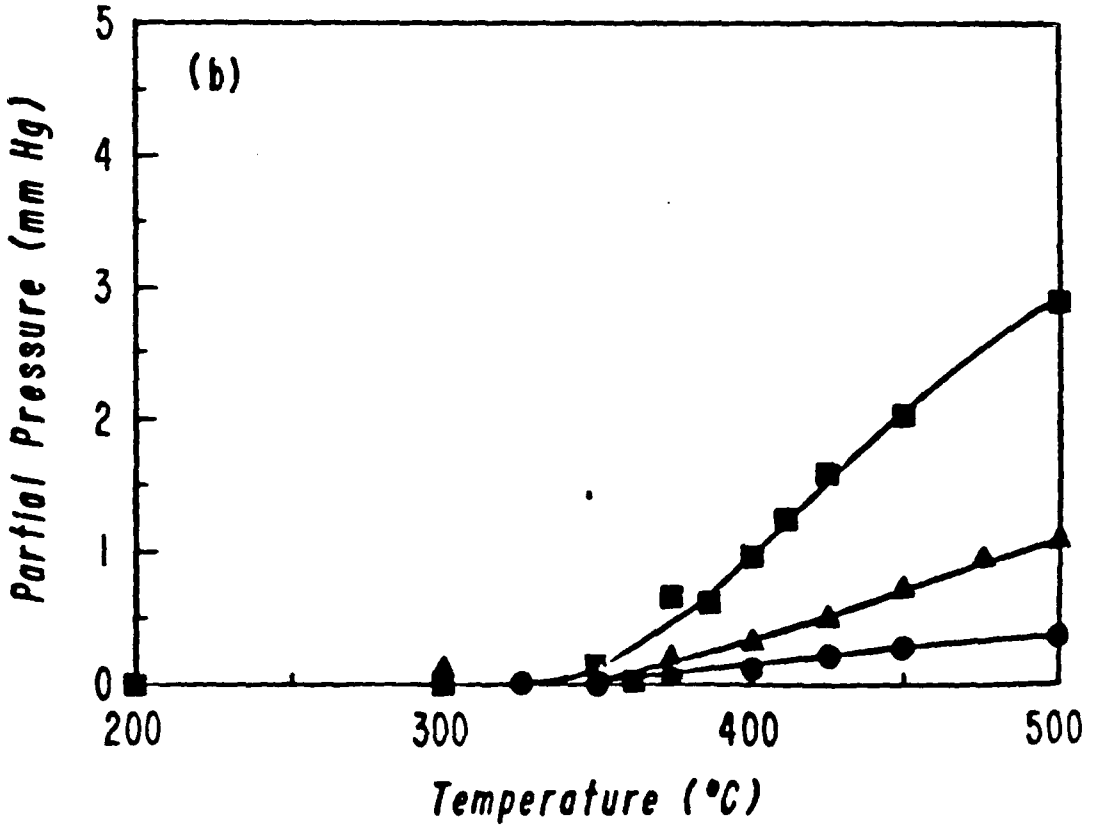
(b)
Partial Pressure (mm Hg)
5
4
3
2
1
0
200
300
400
500
Temperature (°C)

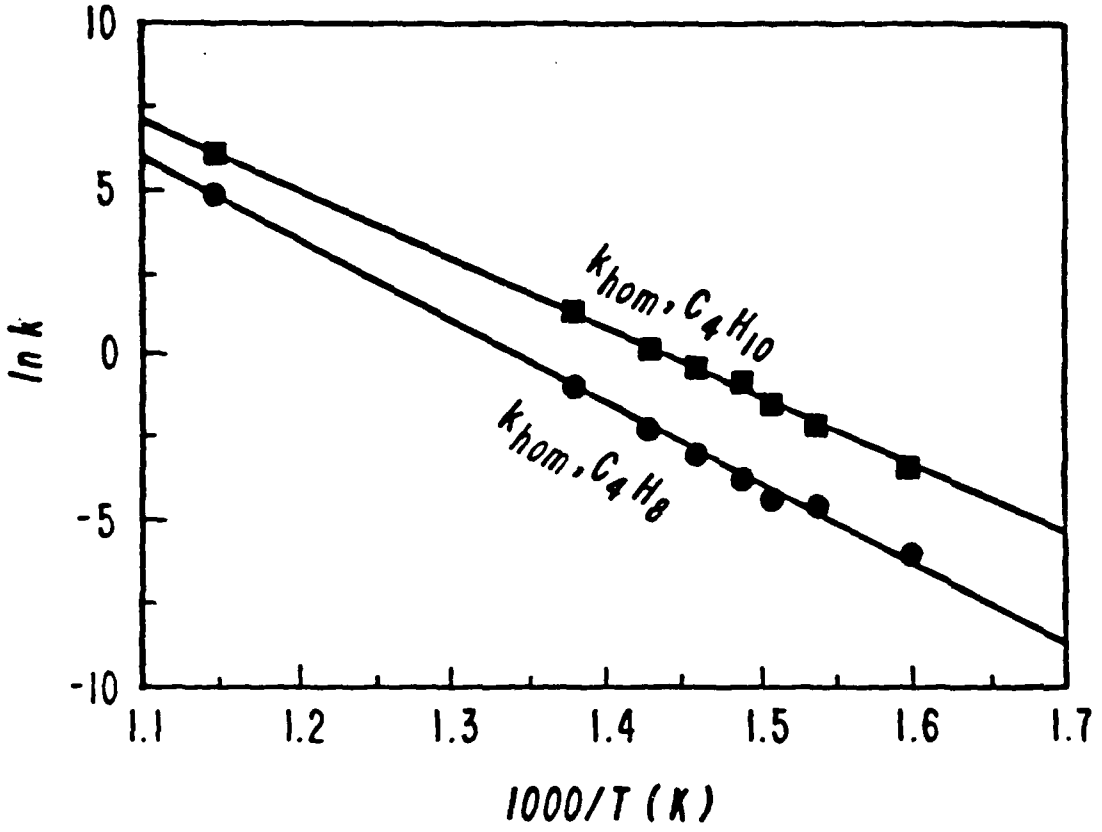
10
5
0
-5
-10
ln k
1.1
1.2
1.3
1.4
1.5
1.6
1.7
1000/T (K)
khom, C4H10
khom, C4H8

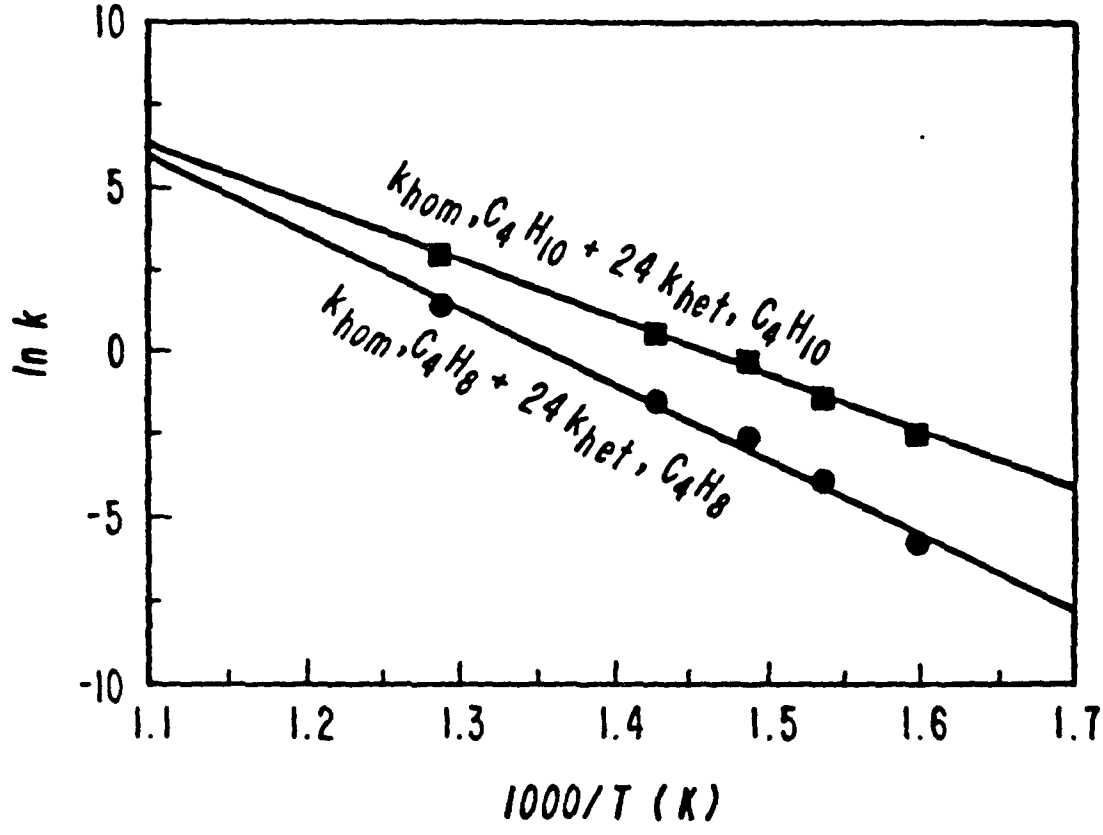
10
5
0
-5
-10
ln k
1.1
1.2
1.3
1.4
1.5
1.6
1.7
1000/T (K)
khom, C4H10 + 24 khet, C4H10
khom, C4H8 + 24 khet, C4H8

Mechanisms of GaAs Growth Using Tertiarybutylarsine and Trimethylgallium

C. A. Larsen, S. H. Li, N. I. Buchan, and G. B. Stringfellow

Departments of Materials Science and Engineering
and Electrical Engineering

University of Utah
Salt Lake City, Utah 84112

Abstract

Tertiarybutylarsine (TBAs) is one of the most promising novel group V sources for organometallic vapor phase epitaxy (OMVPE) of GaAs. The mechanisms of the reactions between TBAs and trimethylgallium (TMGa) were studied in a D_2 flow reactor using a time-of-flight mass spectrometer to analyze the products. TBAs decomposition kinetics are not strongly affected by TMGa, but TBAs alters completely the decomposition pathways of TMGa. The three reactions for TMGa removal are:

$$TMGa(ads) + TBAs(ads) \rightarrow C_4H_8 + products \quad (1)$$

$$TMGa + AsH_3 \rightarrow 3\,CH_4 + GaAs \quad (2)$$

$$TMGa(ads) + 3\,AsH\,(ads) \rightarrow 3\,CH_4 + GaAs + As_2. \quad (3)$$

The AsH_3 and AsH are products of independent TBAs pyrolysis. Reaction (3) is the most important. Another minor reaction proceeds via the formation of gas-phase adducts between TMGa and TBAs. In addition to the experimental data, a numerical model was developed for the system which permits calculation of the rate constants for the reactions. The Arrhenius parameters for the mechanism are given. The results provide insight into the OMVPE process in general.

1. Introduction

In a previous paper (Ref. 1) the decomposition mechanisms of tertiarybutylarsine (TBAs) were described. It was found that there are two main routes. The dominant path is via a unimolecular coupling reaction, wherein the *tert*-butyl ligand forms a bond to one of the H atoms in the transition state. The resulting products are isobutane (C_4H_{10}) and AsH. At higher temperatures, the decomoposition also occurs via β-elimination yielding isobutene (C_4H_8) and AsH_3. Both mechanisms have homogeneous and heterogeneous components on GaAs surfaces, but the reactions are unaffected by silica. In spite of a large excess of D_2, the carrier gas, there was no evidence of any deuterated products.

TBAs has been used to grow layers of GaAs by organometallic vapor phase epitaxy (OMVPE). The materials so produced exhibit morphologies and carrier concentrations similar to layers grown with AsH_3 (2,3). Electron mobilities as high as 55,000 $cm^2/V\text{-}s$ at 77 K have been reported (4), as well as sharp low temperature photoluminesence spectra with resolved exciton recombination peaks. In addition, the GaAs layers have very low concentrations of unintentional carbon contamination.

The use of TBAs has several distinct advantages over the conventional AsH_3. TBAs decomposes at much lower temperatures than AsH_3. It is much safer to use than AsH_3, both because of its inherent lower toxicity (the

LC_{50} is 70 ppm) (5) and because the liquid is stored in stainless steel bubblers at atmospheric pressure, as are other common OMVPE source compounds, instead of high pressure gas cylinders as for AsH_3. Its high vapor pressure (1) makes it perhaps the most appealing non-hydride group V source for the OMVPE process as well as other common III/V manufacturing techniques.

The purpose of this paper is to describe the mechanisms and kinetics of decomposition of mixtures of TBAs and trimethylgallium (TMGa). These studies provide an important link in understanding the growth mechanisms of GaAs and III/V semiconductors in general. They also show why TBAs leads to lower carbon incorporation and hence point the way to further developments in the field of improved design of non-hydride group V source materials.

2. Experimental

The apparatus used to simulate the OMVPE growth process has been described in Ref. 1. The salient features are the use of D_2 to isotopically label the reaction products. The gases leaving the reaction furnace were sampled using a CVC Model 2000 time-of-flight mass spectrometer, where the products are identified and their relative amounts determined. The TBAs was obtained from American Cyanamid Company. The TMGa was specially prepared to contain 50 % ^{13}C by Strem Chemicals, Inc. It was

necessary to use isotopically labeled TMGa because some of the expected products (notably neopentane) have mass spectra which closely resemble those of TBAs and its decomposition products. The peaks we monitored were at m/e = 43, 56, 57, and 58 for C_4H_{10}, C_4H_8, TBAs, and $^{12}C_4{}^{13}CH_{12}$, respectively. The D_2 was purified before use to reduce levels of O_2, H_2O and D_2O to 1 ppm or less.

3. Results

The temperature dependence of the decomposition of TBAs for various conditions is shown in Fig. 1. Included are data from Ref. 1 for the pyrolysis of TBAs with no TMGa in the presence of GaAs surfaces for both low (50 cm^2) and high (1200 cm^2) surface areas. Addition of a small amount of TMGa, to give a V/III ratio of 10:1, has very little effect on the reaction rate. When the TBAs concentration is decreased by one-third the results are still nearly identical to the no-TMGa case. At high surface areas there is a small shift in the slope of the curve due to the TMGa. In all cases the decomposition of TBAs is only slightly affected by TMGa. This contrasts markedly with the TMGa-AsH_3 system in which TMGa significantly lowers the AsH_3 pyrolysis temperature for both high and low GaAs surface areas. Thus TBAs decomposes by the same primary mechanisms with and without TMGa.

The corresponding plot describing the behavior of TMGa is given in Fig.

2. Data from an earlier study (6) for TMGa alone and TMGa with AsH_3 are also shown (note that it impossible to determine the effects of GaAs surfaces on TMGa decomposition, because TMGa forms involatile products which reduce all surfaces to the same type after a few monolayers are deposited). The data show that the decomposition is enhanced somewhat by adding TBAs, but the pyrolysis temperature is nearly independent of the TBAs/TMGa ratio. Increasing the surface area results in a marked lowering of the temperature for the pyrolysis, producing a curve which exhibits two distinct decomposition regimes. Kinetic modeling studies, to be described below, show the anomalous appearance to be due to a kinetic effect.

The temperature dependence of the product partial pressures are given in figs. 3-5. In fig. 3a the major products are plotted for a 10/1 TBAs/TMGa ratio (the TBAs concentration was 3 %) in an unpacked tube. Not surprisingly, the plot is much the same as with no TMGa, described in Ref. 1. That is, the major product is isobutane (C_4H_{10}), with isobutene (C_4H_8) produced at higher temperautres. CH_4 is also one of the major products, but no CH_3D was found. The minor products, as shown in in Fig. 3b, include CH_3AsH_2 (methylarsine), C_5H_{12} (neopentane), and AsH_3 In the case of TBAs alone the AsH_3 and C_4H_8 were produced in nearly one-to one ratios at low temperatures. With added TMGa the AsH_3 is attenuated by GaAs-catalyzed decomposition as well as reaction with TMGa directly. H_2 is created by the decomposition of AsH_3 and also AsH, produced by the same reactions which yield C_4H_{10} (1). No deuterated species were

detected in the product gases.

When the V/III ratio is reduced to 3/1 the results of Fig. 4a and b are obtained. AsH_3 is severly attenuated. The CH_3AsH_2 is reduced by aproximately one-half, while the C_5H_{12} decreased by one-third. No H_2 was detected, from which it may be concluded that the AsH_3 *and* the AsH react with TMGa to yield CH_4 before they decompose independently. Finally, increasing the surface area by a factor of 24 (for the 3:1 ratio) gives the results presented in Fig 5a and b. Again, the main products are C_4H_{10}, C_4H_8, and CH_4. There is more CH_3AsH_2 initially than in fig. 4b, but this decreases above 375 °C due to surface catalysis of its decomposition. There is no detectable AsH_3. The concentration of C_5H_{12} is almost the same as in Fig. 4b. It is important to emphasize that there is no CH_3D or C_2H_6 in any of the cases studied. This indicates that there is no independent decomposition of TMGa. As with the low surface area experiment at this same 3/1 ratio, no H_2 was detected.

The pyrolysis curves may be used to extract kinetic data. Fig. 6 shows the Arrhenius plots for TBAs in the presence of TMGa for the three cases studied. The data for the low surface area experiments lie nearly on the same line. The increased surface area results in a lower A factor and activation energy, as expected for heterogeneous reactions. The rate constants from these curves, together with those of TBAs decomposition alone, are given in Table I, along with other k's of importance for this discussion. The values for the low surface area cases are almost identical

with those of Ref. 1 for low surface areas of GaAs (k_c), as listed in Table I. The kinetic parameters for the high surface area experiment, however, differ significantly from the corresponding data of Ref. 1 (k_d). It was assumed that the reactions were first order in TBAs and independent of (zeroth order in) TMGa. Numerical modeling shows that this assumption is valid for the unpacked tube data, but at high surface areas TBAs-TMGa interactions become important. Results of the simulation provide information about the most important of these combined reactions.

While TMGa has little effect on TBAs decomposition, the converse is not true. TBAs lowers the decomposition temperature of TMGa by 75 °C compared with TMGa alone. Also, as noted above, the products are devoid of any CH_3D and C_2H_6, which are the main products of TMGa decomposition in D_2 (6). Thus there is virtually no independent homogeneous decomposition of TMGa. It is also seen that TMGa-TBAs reactions differ from those between TMGa and AsH_3. In the latter system the main product is CH_4 (6). It was concluded that the TMGa and AsH_3 formed adducts both in the gas phase and on the surface, which subsequently eliminated CH_4 molecules. If the TMGa-TBAs interactions were strictly analogous, C_5H_{12} and CH_4 would be produced in a 1:2 ratio. This is clearly not the case. The fact that some C_5H_{12} is formed, with pressures proportional to the V/III ratio, indicates that adduct reactions do occur. Its insensitivity to surface area shows that those reactions are largely homogeneous. However, adducts are plainly not the major pathway for TMGa decomposition in the presence of

TBAs.

4. Discussion

As a first step in identifying the reaction steps, the Arrhenius plots of Fig. 6 were treated by the methods developed in Ref. 1. The overall rate constants were first separated into contributions from C_4H_{10} and C_4H_8 formation reactions using the product ratio as the branching ratio. Plots of the derived rate constants are shown in Fig. 7 for the 10:1 V/III ratio in the unpacked tube. Each k can be further separated into homogeneous and heterogeneous components, as indicated in the figure. Taking the homogeneous rate constants as k_{10} and k_{13} of Ref. 1 (for homogeneous C_4H_{10} and C_4H_8 production, respectively) allows the calculation of the remaining heterogeneous contributions, yielding

$$\log_{10} k_{het,}C_4H_{10}\ (sec^{-1}) = 8.32 - 28.68\ (kcal/mol)/2.303RT$$

$$\log_{10} k_{het,}C_4H_8\ (sec^{-1}) = 16.45 - 56.75\ (kcal/mol)/2.303RT.$$

The first equation is remarkably similar to that obtained for the heterogeneous production of C_4H_{10} when only TBAs is present (k_{15} in Ref. 1, reproduced here):

$$\log_{10} k_{15} = 8.82 - 29.18\ (kcal/mol)/2.303RT.$$

The close agreement indicates that the dominant route for C_4H_{10}

production on the surface is the same with and without added TMGa. Comparing the above k_{het},C_4H_8 with that of heteogeneous C_4H_8 production with TBAs alone (k_{16}, below),

$$\log_{10} k_{16}(sec^{-1}) = 9.99\text{-}36.37 \text{ (kcal/mol)}/2.303RT$$

however, shows a large discrepancy. In part this may be because the heterogeneous rate constant is small, and relatively large errors are associated with accurately determining its value. Nevertheless, the data strongly suggest a surface reaction between TBAs and TMGa which yields C_4H_8, in addition to that produced by the unimolecular β-elimination reactions of TBAs. The following reaction is the simplest possibility which fits our data:

$$TBAs(ads) + TMGa(ads) \rightarrow C_4H_8 + 2\,CH_4 + GaAs \quad (17).$$

In order to facilitate the bookkeeping of a large number of rate constants the numbering system of Ref. 1 is continued. The reaction is written as a single process, but is probably a series of steps.

Reaction 17 is first order in both TBAs and TMGa. This means the product ratio is not equal to the branching ratio for TBAs decomposition, but must include the TMGa-TBAs reaction. The rate law for C_4H_8 production is given by

$$d[C_4H_8]/dt = (k_{13} + k_{16})[TBAs] + k_{17}\ [TBAs][TMGa].$$

At high V/III ratios and low surface areas reaction 17 is unimportant, so similar values are obtained for C_4H_{10} production with and without TMGa in those cases.

Fig. 8 shows the separated rate constants for the V/III = 3, 50 cm^2 surface area case. Here it would be expected that reaction 17 would be of greater importance. This is borne out by the somewhat lower $k_{het,C_4H_{10}}$ derived from this set of data:

$$\log_{10}k_{het,C_4H_{10}}\ (sec^{-1}) = 7.56 - 26.49\ (kcal/mol)/2.303RT.$$

These are not true values for the kinetic parameters, but rather stem from the increased C_4H_8 production by reaction 17. As shown in Fig. 9, increasing the surface area allows reaction 17 to become more important, and the corresponding (fictitious) rate constant for C_4H_{10} production is

$$\log_{10}k_{het,C_4H_{10}}\ (sec^{-1}) = 5.62 - 20.82\ (kcal/mol)/2.303RT.$$

5. Kinetic Models

It was shown in Ref. 1 that TBAs decomposition proceeded by four elementary steps, and the rate constants for these processes were determined. Our present results indicate that adding TMGa to the system further complicates the reaction mechanisms. The product data has led to

a qualitative understanding of the main steps leading to GaAs growth. However, the complexity of the system does not permit reliable quantitative information to be obtained from simple analytic techniques. Instead, a numerical approach was used to obtain a model of the mechanism, including TMGa-TBAs interactions. This method serves two purposes. First, it allows us to determine rate constants for the new reactions. Second, it provides a check on the hypotheses. If the calculated kinetic parameters are unreasonable, then the proposed reactions probably do not occur and other hypotheses must be formulated. Thus the modeling is necessary for an accurate understanding of the important phenomena involved in GaAs growth using TBAs and TMGa. For the modeling Euler's Theorem for numerical solutions to differential equations was used, as in an earlier study on the decomposition of trimethylindium (7). The final rate contants used in the model are given in Tables I and II.

It has been shown that addition of TMGa results in a heterogeneous TBAs decomposition reaction which produces C_4H_8. Thus, as a first step in developing the model, reaction 17 was added to the set of reactions describing the TBAs decomposition process:

$$TBAs \rightarrow C_4H_{10} + AsH \qquad (10)$$

$$TBAs \rightarrow C_4H_8 + AsH_3 \qquad (13)$$

$$TBAs(ads) \rightarrow C_4H_{10} + AsH(ads) \qquad (15)$$

$$TBAs(ads) \rightarrow C_4H_8 + AsH_3(ads) \qquad (16)$$

$$TBAs(ads) + TMGa(ads) \rightarrow C_4H_8 + products \qquad (17).$$

In the above mechanism the numbering from Ref. 1 is used. The products in reaction 17 are as yet unidentified, but may include CH_4, $(CH_3)_2Ga{:}AsH_2$, and GaAs,among others. Rate constants from Ref. 1 were used for steps 10,13,15,and 16. The Arrhenius parameters for step 17 were adjusted to give the best fit to the TBAs pyrolysis curves (see Fig. 1). This resulted in good agreement for TBAs decomposition, but a poor simulation of TMGa behavior, as shown by curve a in Fig. 10 which compares the experimental and calculated data for TMGa decomposition at a 3:1 V/III ratio with high surface area. As a next level of sophistication it was decided to include reactions between TMGa and the AsH_3 produced in steps 13 and 16:

$$TMGa(g) + AsH_3(g) \rightarrow 3\ CH_4 + GaAs \qquad (18)$$

$$TMGa(ads) + AsH_3(ads) \rightarrow 3\ CH_4 + GaAs \qquad (19).$$

These reactions were investigated in an earlier publication (6), and the data from that study were used to obtain the rate constants. Inclusion of these reaction in the model gave a better fit to the TMGa pyrolysis data (Fig. 10, curve b), but still did not adequately account for the pyrolysis behavior over the entire temperature range. An additional reaction was then included:

$$TMGa(ads) + AsH(ads) \rightarrow CH_4 + products. \qquad (20)$$

The AsH is produced in steps 10 and 15. The reaction apparently occurs entirely on the surface, because a gas-phase interaction would create free methyl radicals which in turn would collide with the D_2 ambient to give CH_3D, none of which was observed. The reacting species is the adsorbed

AsH, as shown. This comes from both the AsH created on the surface (step 15) and that liberated in the gas phase (step 10) which subsequently adsorbs. Again, "P" represents unknown products. At each temperature, the rate constant for step 17 was fixed at the previous figure, and that of step 20 was varied to give the best fit to the experimental TMGa data. This set of reactions was able to account for TMGa decomposition over nearly the entire temperature range, as demonstrated by curve c in Fig. 10. The results obtained from the model are compared with the experimental data in Figs. 11-14. The correlation between the results of the model calculations and the experimental data for TBAs, TMGa, C_4H_{10}, and C_4H_8 are shown for each set of experimental conditions. The only deviation is for the C_4H_8 concentration at high temperatures. It was found that this last discrepancy can be removed by lowering the activation energy for step 16 by 2 kcal/mol. Adjusting the Arrhenius parameters for all of the reactions would in fact result in complete agreement with experiment. Such fine manipulations, however, do not add to the major objective of this work, which is to identify the important steps in the reaction mechanism based on the product distributions and relative reaction rates.

The model shows that reaction 17 does occur to some extent, providing the "extra" source of C_4H_8. But it is not the dominant pathway for TMGa removal. Reaction with AsH_3 is also important, especially the surface reaction at low temperatures. But at higher temperatures, such as those used in typical OMVPE growth, the TMGa mainly reacts with the AsH

produced by independent decomposition of TBAs. It is now possible to resolve the question of the apparent low carbon contamination of GaAs grown with TBAs as compared to AsH_3-grown material (2). There is evidence that the last methyl group on the TMGa molecules is not liberated from the surface until an AsH group donates its H atom to form CH_4 (8). Also, it is known that carbon is preferentially incorporated as an acceptor on the group V sublattice (9). TBAs provides a ready supply of AsH groups which have a dual function. First, they aid in removal of the remaining methyl groups from the TMGa. The adsorbing TMGa readily reacts to give free CH_4 and GaAs. Any excess AsH groups further decompose to yield As_2 and H_2. Second, they effectively compete with carbon species for the As sites in the growing crystal. When AsH_3 is used as the As source it is the TMGa which has the lower decomposition temperature, and the AsH_3 in fact decomposes only by interaction with the TMGa (6). At OMVPE growth temperatures, typically around 600°C, there is probably some independent decomposition of TMGa. The methyl groups dissociating from the TMGa molecules become incorporated into the semiconductor layers unless the V/III ratio is high.

The results of our numerical modeling have shown the importance of several reactions between TMGa and TBAs and/or its decomposition products. By extension these findings provide information about OMVPE reaction mechanisms in general. Also, they should be of use in designing other source compounds to take fuller advantage of the best properties of

TBAs, such as the high concentration of AsH at temperatures below the decomposition temperature of TMGa.

6. Summary

The results presented herein show that TBAs pyrolysis is nearly the same with and without TMGa. This is true both of the nature of the products and their rates of formation. TMGa, on the other hand, is greatly affected by TBAs. No CH_3D or C_2H_6 were found when mixtures of the two were decomposed, and the TMGa decomposition temperatures were significantly lowered. The numerical modeling shows that there is a direct heterogeneous reaction between TBAs and TMGa to produce C_4H_8, but this reaction is of minor importance except at low temperatures. Another minor reaction is the formation of gas-phase adducts which liberate C_5H_{12}. At the temperatures typically used for OMVPE growth, however, most of the TMGa decomposes by reactions with the AsH_3 and especially AsH produced by independent decomposition of TBAs. The high concentration of AsH on the surface leads to low levels of carbon incorporation in the epitaxial GaAs as compared to AsH_3-grown material.

Acknowledgements

This work was supported by a grant from the U. S. Air force, Contract # AFSOR-87-0233. The authors wish to thank American Cyanamid Company

for supplying the tertiarybutylarsine.

References

1. C. A. Larsen, N. I. Buchan, S. H. Li, and G. B. Stringfellow, J. Crystal Growth (submitted, companion paper)
2. C. H. Chen, C. A. Larsen, and G. B. Stringfellow, Appl. Phys. Lett 50 (1987) 218
3. R. M. Lum, J. Klingert, and M. G. Lamont, Appl. Phys. Lett. 50 (1987) 284
4. G. Haake et al. (private communication, reported in G. B. Stringfellow, J. Electron. Mater. (to be published))
5. American Cyanamid Company (private communication)
6. C. A. Larsen, N. I. Buchan, and G. B. Stringfellow, Appl. Phys. Lett. 52 (1988) 480
7. N. I. Buchan, C. A. Larsen, and G. B. Stringfellow, J. Crystal Growth (to be published)
8. T. F. Kuech, E. Veuhoff, T. S. Yuan, V. Deline, and R. Potemski, J. Crystal Growth 77 (1986) 257
9. B. J. Skromme, T. S. Low, T. J. Roth, G. E. Stillman, J. K. Kennedy, and J. K. Abrokwah, J. Electron. Mater. 12 (1983) 433

Table I.

Measured Rate Constants for TBAs Decomposition

Rate Constant	Reaction	$\log_{10} A$	E_a (kcal/mol)
k_a	overall homogeneous decomposition of TBAs (no TMGa)	13.18	41.64
k_c	overall decomposition of TBAs on 50 cm^2 GaAs (no TMGa)	11.40	35.43
k_d	overall decomposition of TBAs on 1200 cm^2 GaAs (no TMGa)	10.60	30.23
k_e	overall decomposition of TBAs on 50 cm^2 GaAs, with 10:1 V/III ratio	11.95	37.68
k_f	overall decomposition of TBAs on 50 cm^2 GaAs, with 3:1 V/III ratio	11.66	36.83
k_g	overall decomposition of TBAs on 1200 cm^2 GaAs, with 3:1 V/III ratio	8.38	24.44
k_{10}	homogeneous production of C_4H_{10} (no TMGa)	13.08	41.48

k_{13}	homogeneous production of C_4H_8 (no TMGa)	14.24	48.49
k_{15}	heterogeneous production of C_4H_{10} (no TMGa)	8.82	29.18
k_{16}	heterogeneous production of C_4H_8 (no TMGa)	9.99	36.37
k_{TMGa}	overall decomposition of TMGa in D_2	14.67[a]	52.88
k_{As}	AsH_3 decomposition in D_2, 50 cm^2 GaAs	11.02[a]	39.82

a. From unpublished data of Ref. 6.

Table II.

Rate Constants for Numerical Modeling of TBAs-TMGa Reactions

Reaction	$\log_{10} A$	E_a (kcal/mol)
17[a]	13.0	22.5
18[b]	26.45	63.15
19[b]	0.435	11.27
20[a]	14.90	28.5

a. Adjusted values, as explained in text.

b. From data of Ref. 6

Figure Captions

Fig.1. Percent Decomposition of TBA in D_2 vs. temperature. ○ , 3.0 % TBAs, 50 cm^2 GaAs (no TMGa; data fromRef. 1); ■ , 3.0 % TBAs, 0.3 % TMGa, 50 cm^2 GaAs; ● , 0.9 % TBAs, 0.3 % TMGa, 50 cm^2 GaAs; ▲ , 3.0 % TBAs, 1200 cm^2 GaAs (no TMGa; data from Ref. 1); △ 0.9 % /TBAs, 0.3 % TMGa, 1200 cm^2 GaAs.

Fig. 2. Percent decomposition of TMGa in D_2 vs. temperature. □ , 3.0 % TMGa, 50 cm^2 Ga; ○ , 0.3 % TMGa, 0.3 % AsH_3, 50 cm^2 GaAs (data from Ref. 6); ■ , 3.0 % TBAs, 0.3 % TMGa, 50 cm^2 GaAs; ● , 0.9 % TBAs, 0.3 % TMGa, 50 cm^2 GaAs; △ 0.9 % TBAs, 0.3 % TMGa, 1200 cm^2 GaAs.

Fig. 3. Major (a) and minor (b) decomposition products of 3.0 % TBAs, 0.3 % TMGa mixture in D_2. Surface is 50 cm^2 GaAs.

Fig. 4. Major (a) and minor (b) decomposition products of 0.9 % TBAs, 0.3 % TMGa mixture in D_2. Surface is 50 cm^2 GaAs.

Fig. 5. Major (a) and minor (b) decomposition products of 0.9 % TBAs, 0.3 % TMGa mixture in D_2. Surface is 1200 cm^2 GaAs.

Fig. 6. First order Arrhenius plots of TBAs decomposition with added TMGa in D_2, from data of Fig. 1. ● , 3.0 % TBAs, 0.3 % TMGa, 50 cm^2 GaAs; ○, 0.9 % TBAs, 0.3 % TMGa, 50 cm^2 GaAs; ■, 0.9 % TBAs, 0.3 % TMGa, 1200 cm^2 GaAs.

Fig. 7. Overall first order Arrhenius plots of C_4H_{10} and C_4H_8 formation. Conditions: 3.0 % TBAs, 0.3 % TMGa, 50 cm^2 GaAs.

Fig. 8. Overall first order Arrhenius plots of C_4H_{10} and C_4H_8 formation. Conditions: 0.9 % TBAs, 0.3 % TMGa, 50 cm^2 GaAs.

Fig. 9. Overall first order Arrheunius plots of C_4H_{10} and C_4H_8 formation. Conditions: 0.9 % TBAs, 0.3 % TMGa, 1200 cm^2 GaAs.

Fig.10. Effects of TBAs and decomposition products on TMGa decomposition, as predicted by model. Curve a, TMGa + TBAs (reaction 17). Curve b, TMGa + TBAs and AsH_3 (reactions 17, 18 and 19). Curve c, TMGa + TBAs, AsH_3, and AsH (reactions 17,18,19 and 20). ▲ , experimental data (from Fig. 2). Conditions: 0.9 % TBAs, 0.3 % TMGa, 1200 cm^2 GaAs.

Fig. 11. Correspondence of model with experiment for TBAs decomposition. □, ■ , 3.0 % TBAs, 0.3 % TMGa, 50 cm^2 GaAs.○, ● , 0.9 % TBAs, 0.3 % TMGa, 50 cm^2 GaAs. △, ▲ , 0.9 % TBAs, 0.3 % TMGa, 1200 cm^2 GaAs. Open symbols, calculated results; filled symbols, experimental results.

Fig. 12. Correspondence of model with experiment for TMGa decomposition. Symbols as in Fig. 11.

Fig. 13. Correspoondence of model with experiment for partial pressures of C_4H_{10}. Symbols as in Fig. 11.

Fig. 14. Correspondence of model with experiment for partial pressures of C_4H_8. Symbols as in Fig. 11.

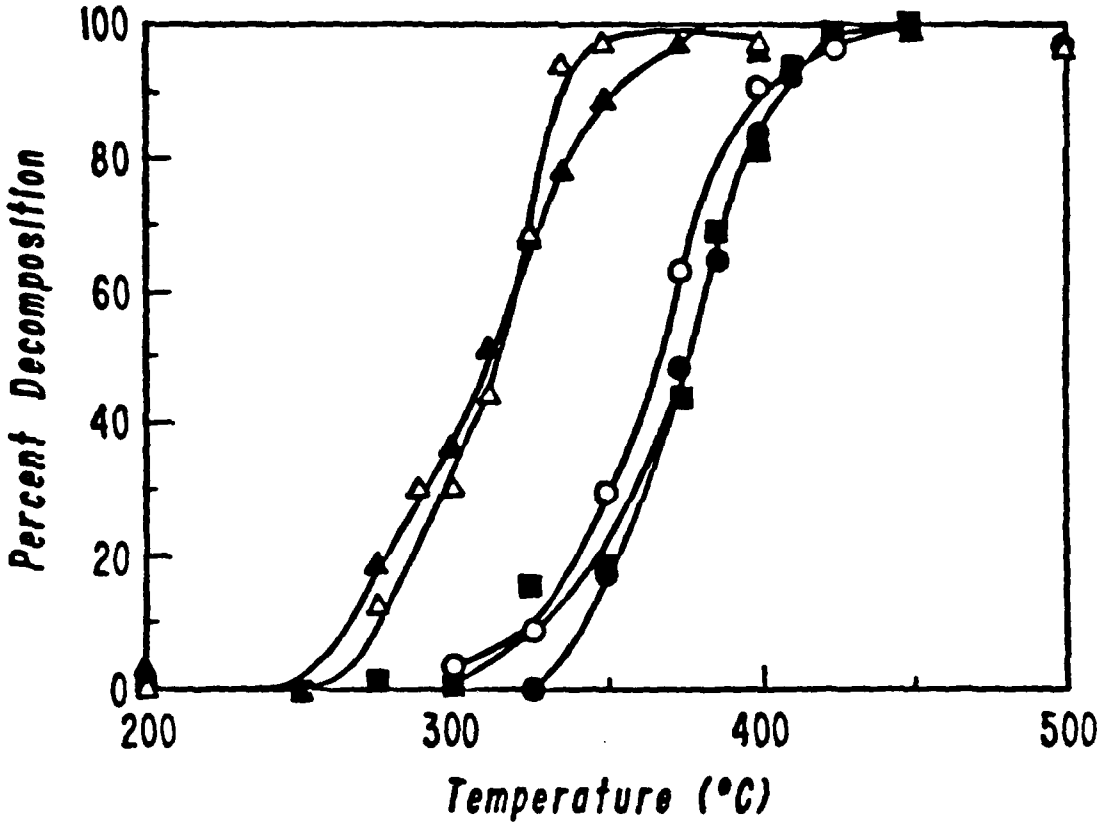
100
80
60
40
20
0
Percent Decomposition
200
300
400
500
Temperature (°C)

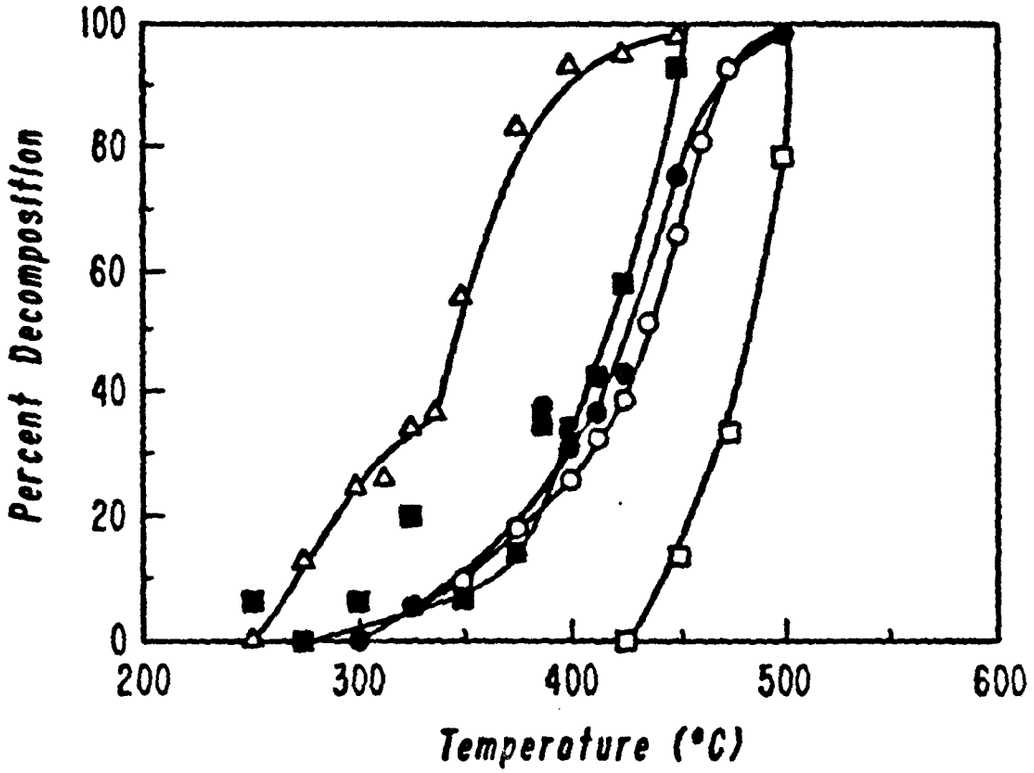
Percent Decomposition
100
80
60
40
20
0
200
300
400
500
600
Temperature (°C)

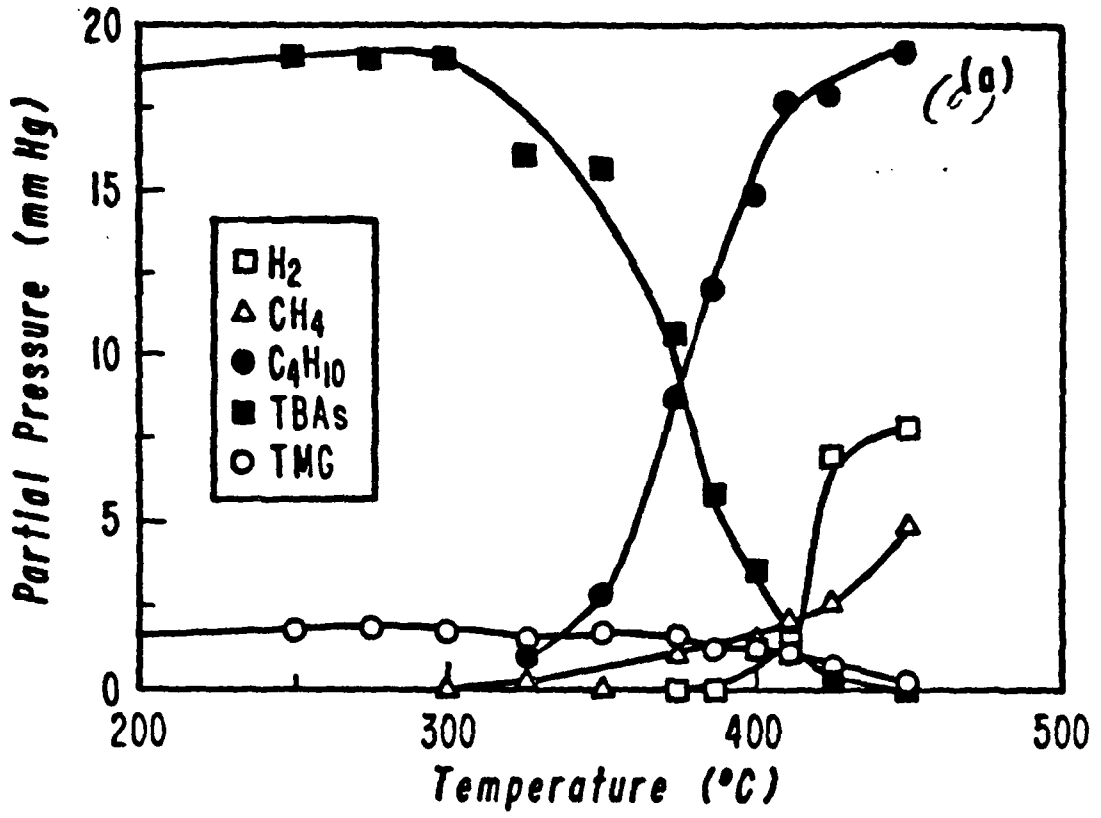
(a)
Partial Pressure (mm Hg)
20
15
10
5
0
200
300
400
500
Temperature (°C)
H2
CH4
C4H10
TBAs
TMG

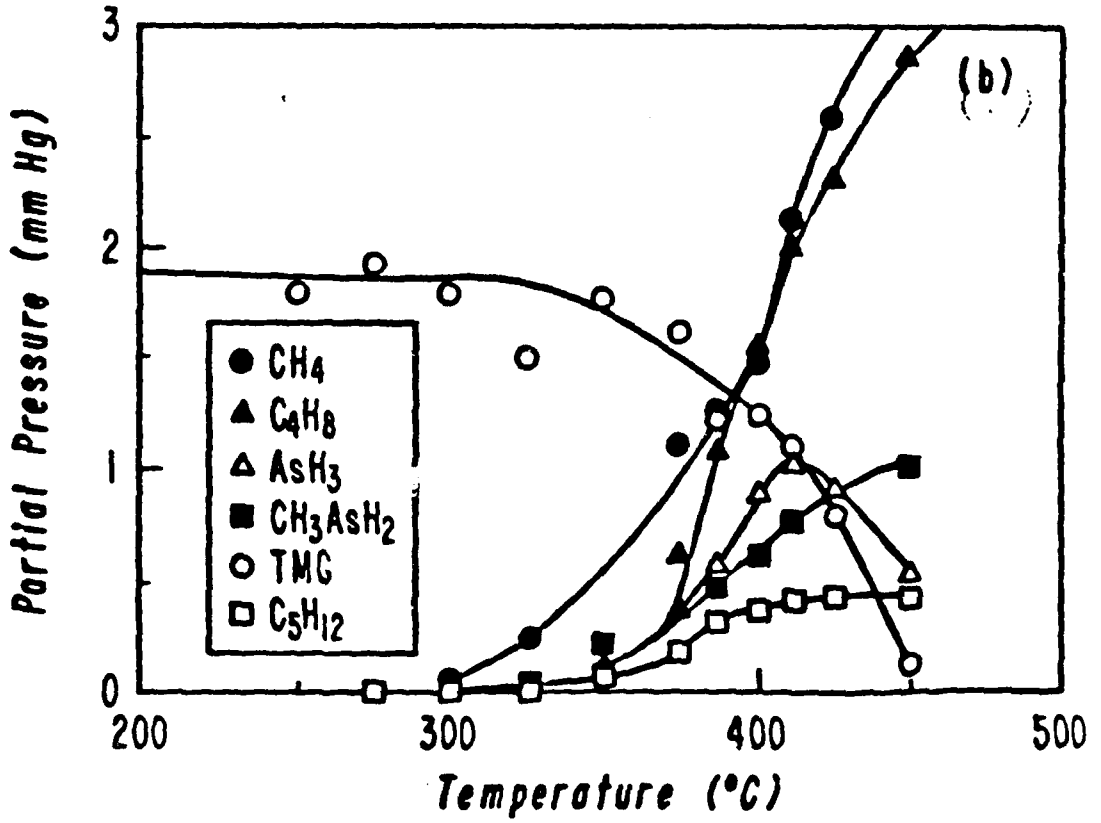
(b)
Partial Pressure (mm Hg)
3
2
1
0
200
300
400
500
Temperature (°C)
CH4
C4H8
AsH3
CH3AsH2
TMG
C5H12

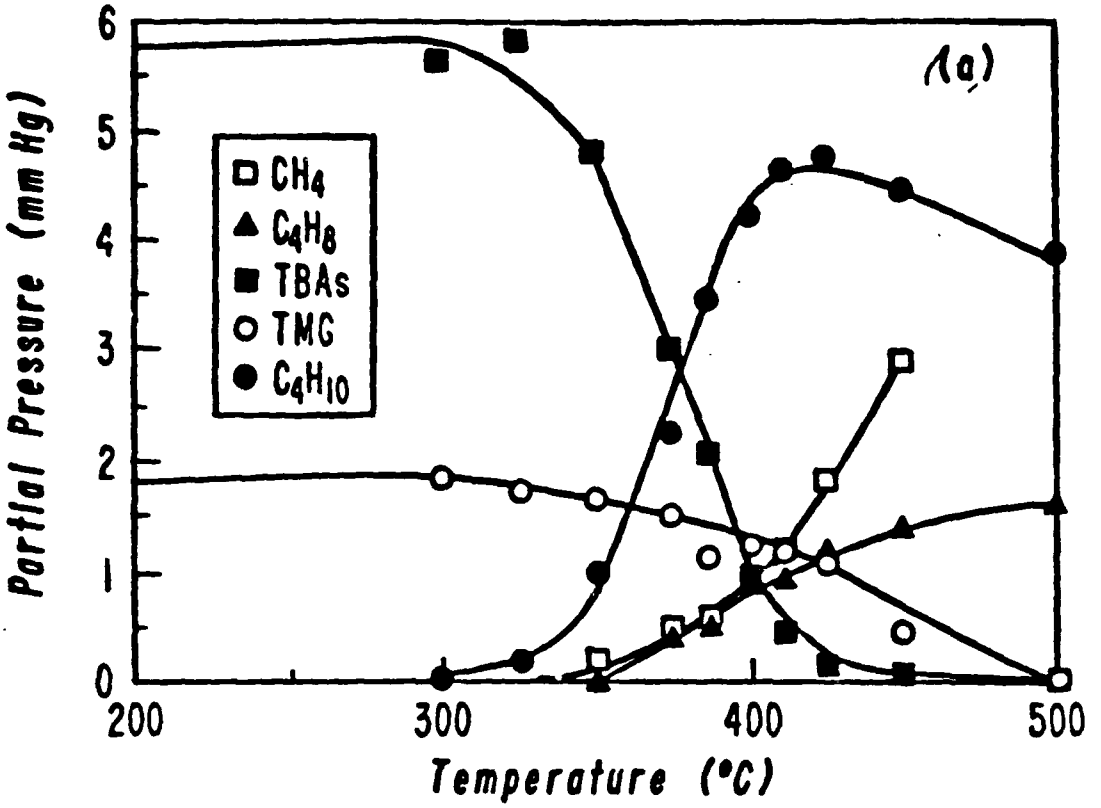
(a)
Partial Pressure (mm Hg)
Temperature (°C)
CH4
C4H8
TBAs
TMG
C4H10
0
1
2
3
4
5
6
200
300
400
500

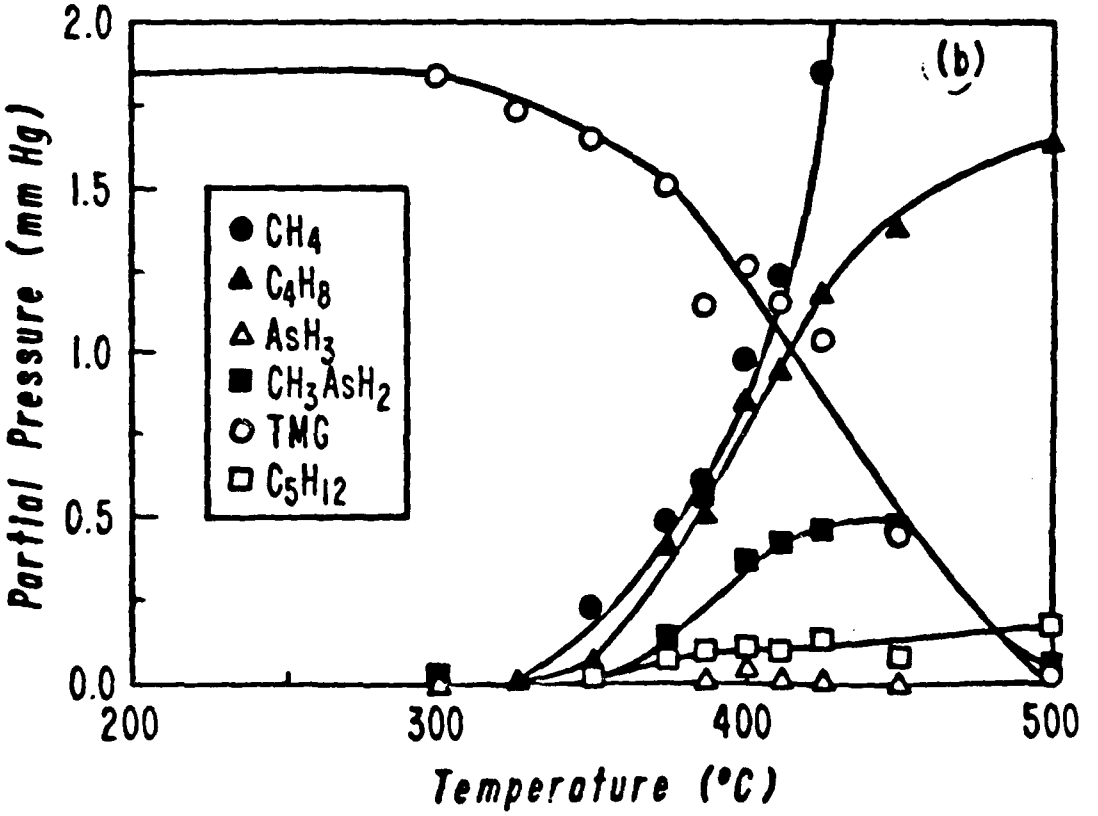
(b)
Partial Pressure (mm Hg)
Temperature (°C)
CH4
C4H8
AsH3
CH3AsH2
TMG
C5H12
0.0
0.5
1.0
1.5
2.0
200
300
400
500

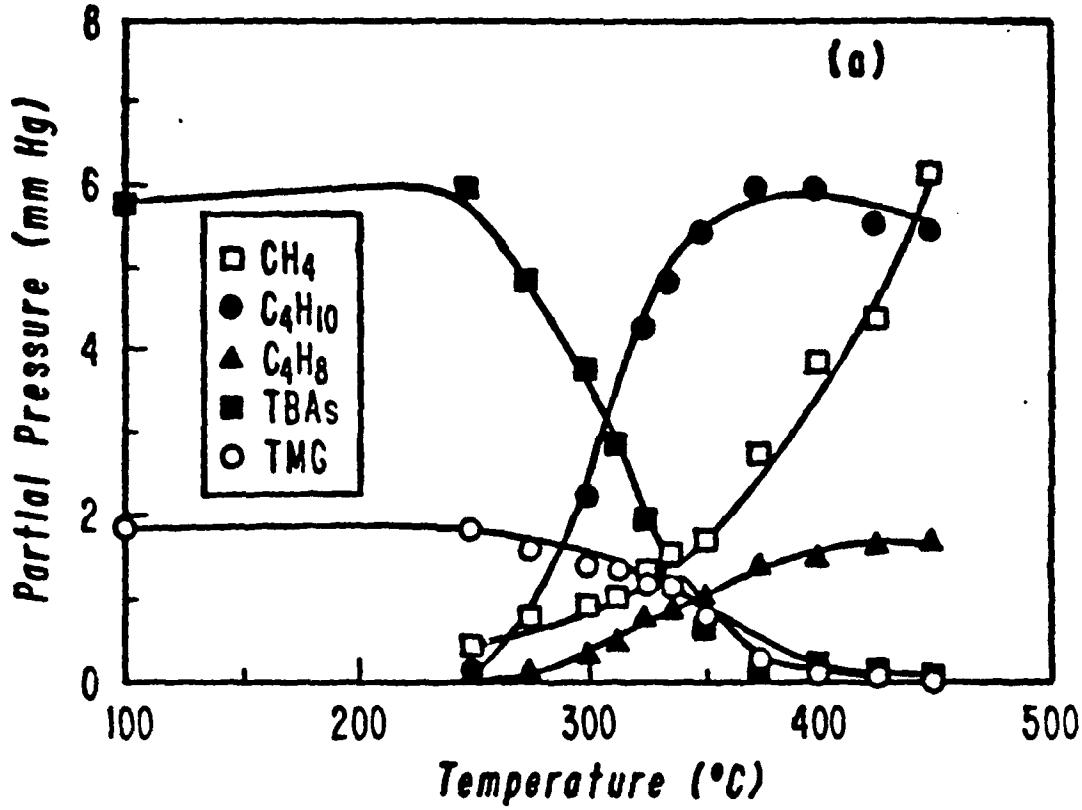
(a)
Partial Pressure (mm Hg)
Temperature (°C)
CH4
C4H10
C4H8
TBAs
TMG
0
2
4
6
8
100
200
300
400
500

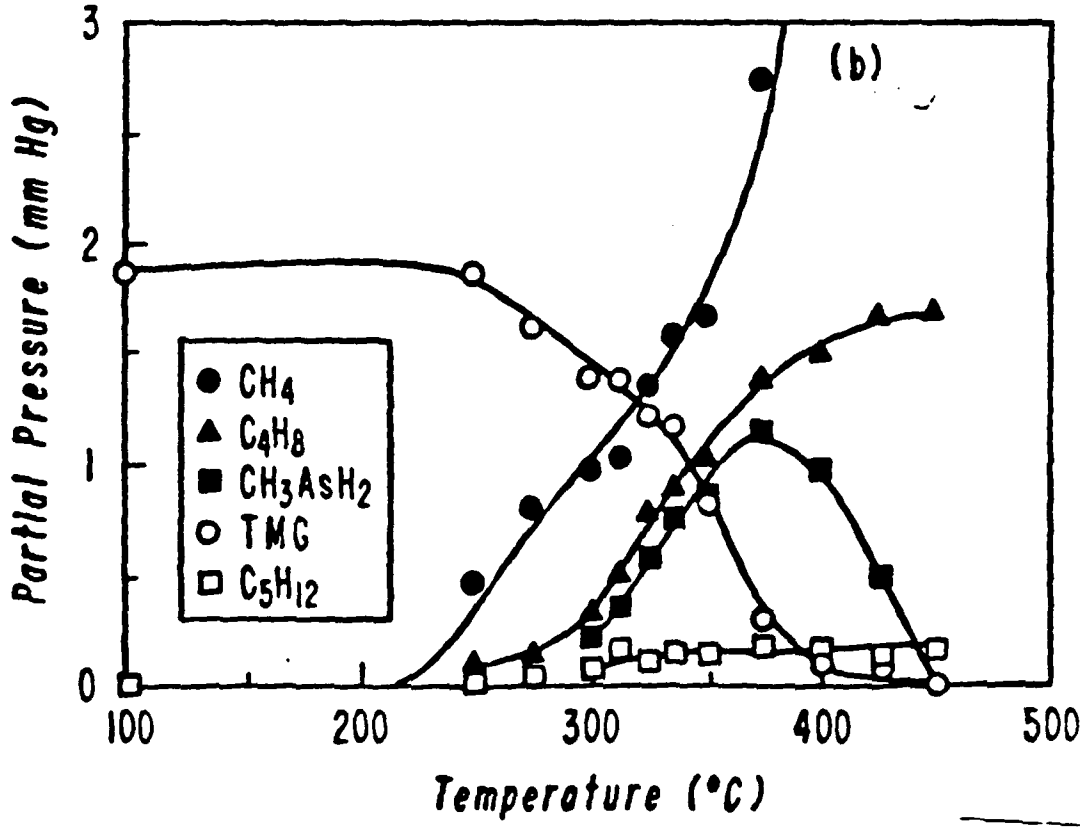
(b)
Partial Pressure (mm Hg)
Temperature (°C)
CH4
C4H8
CH3AsH2
TMG
C5H12
0
1
2
3
100
200
300
400
500

II 5

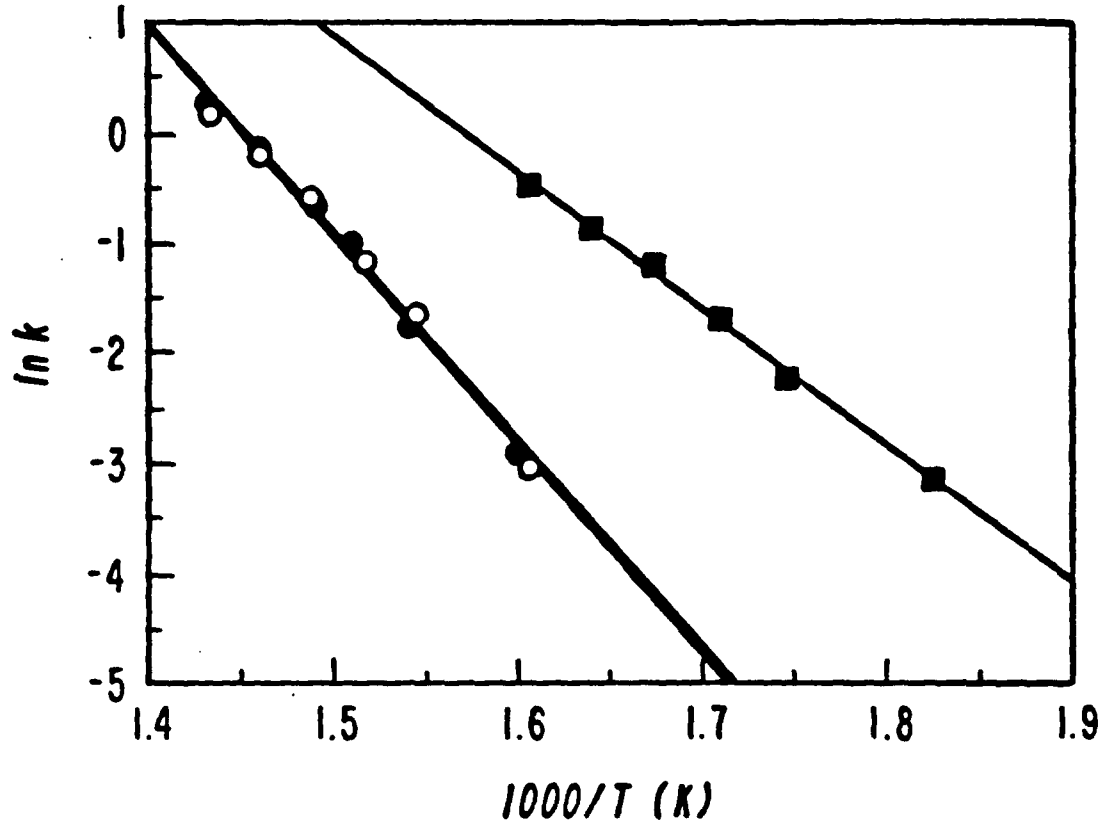
1
0
-1
-2
-3
-4
-5
ln k
1.4
1.5
1.6
1.7
1.8
1.9
1000/T (K)

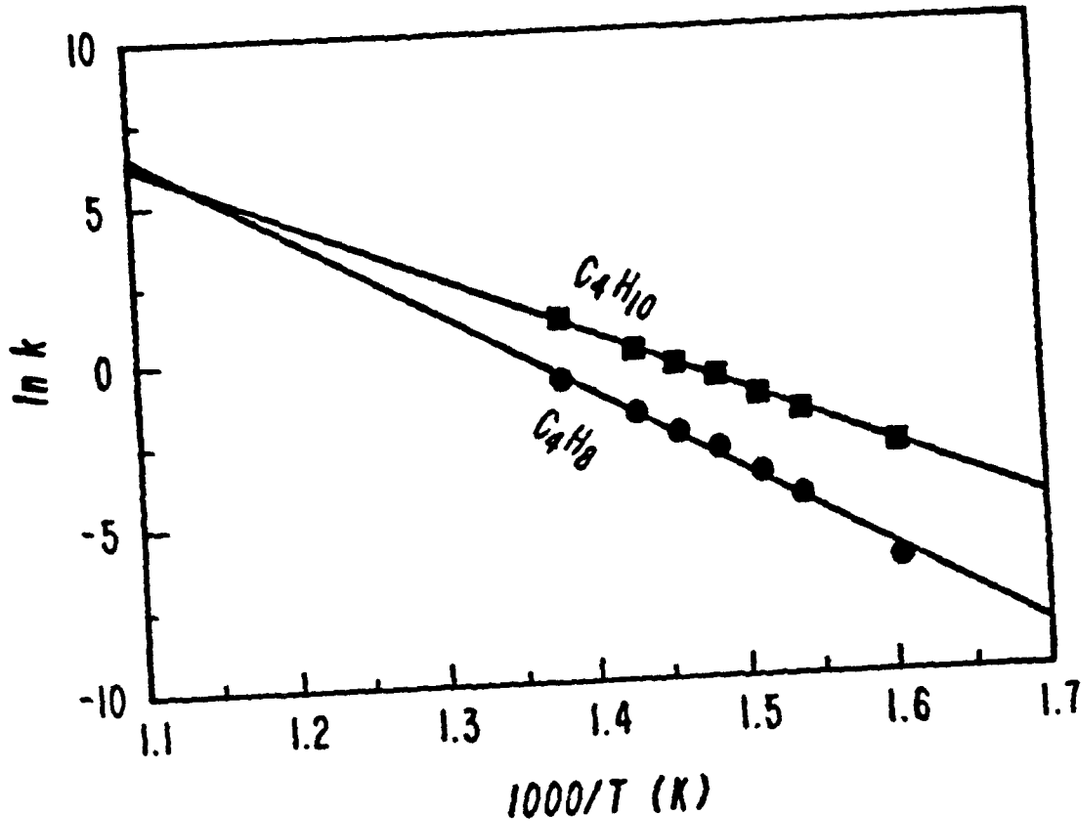
10
5
0
-5
-10
ln k
C_4H_{10}
C_4H_8
1.1
1.2
1.3
1.4
1.5
1.6
1.7
1000/T (K)

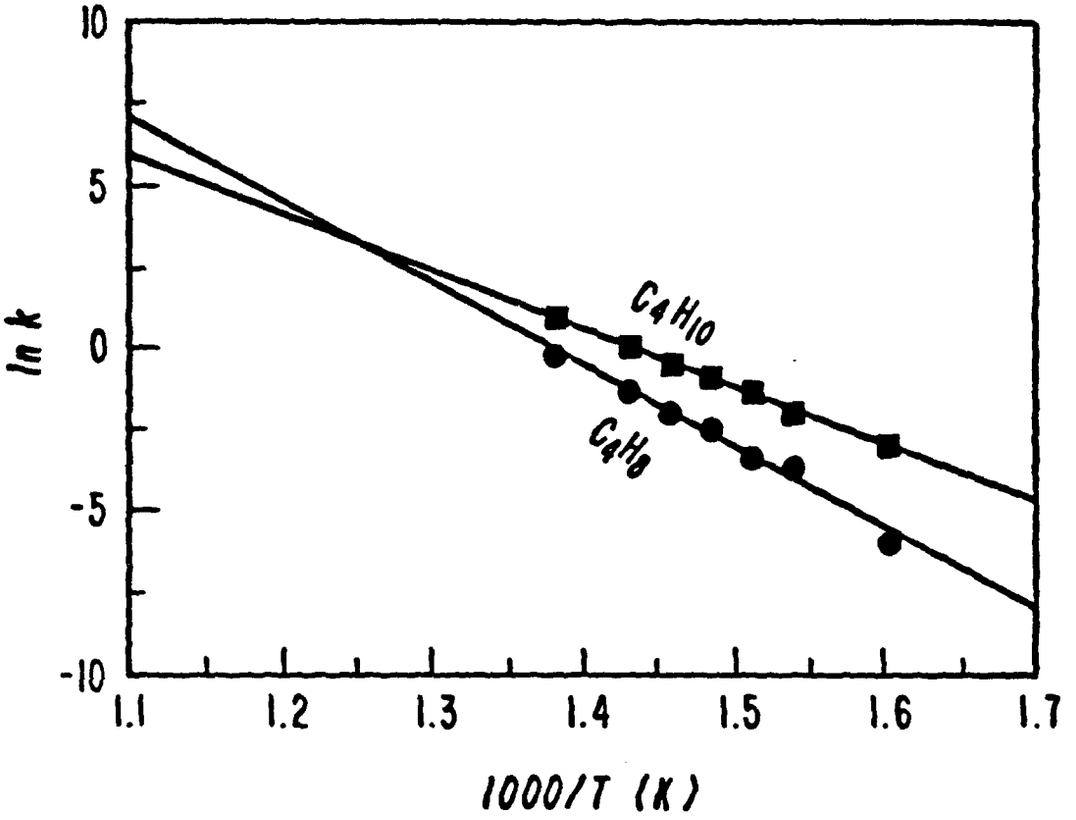
10
5
0
-5
-10
ln k
1.1
1.2
1.3
1.4
1.5
1.6
1.7
1000/T (K)
C4H10
C4H8

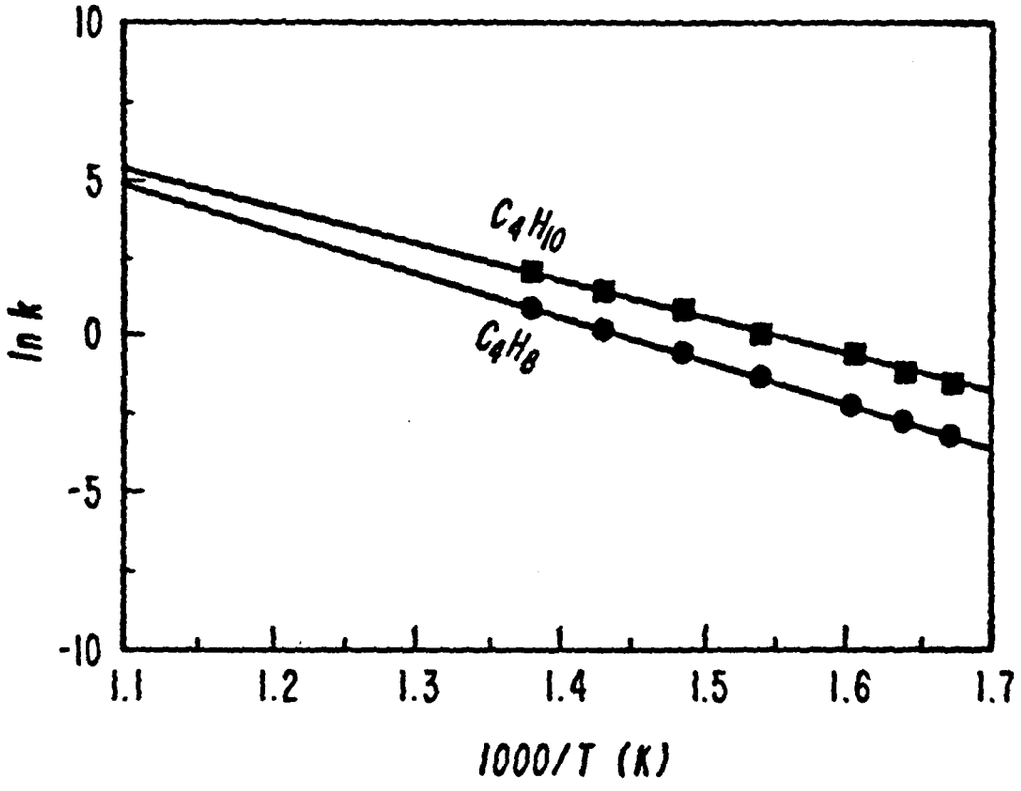
10
5
0
-5
-10
ln k
C_4H_{10}
C_4H_8
1.1
1.2
1.3
1.4
1.5
1.6
1.7
1000/T (K)

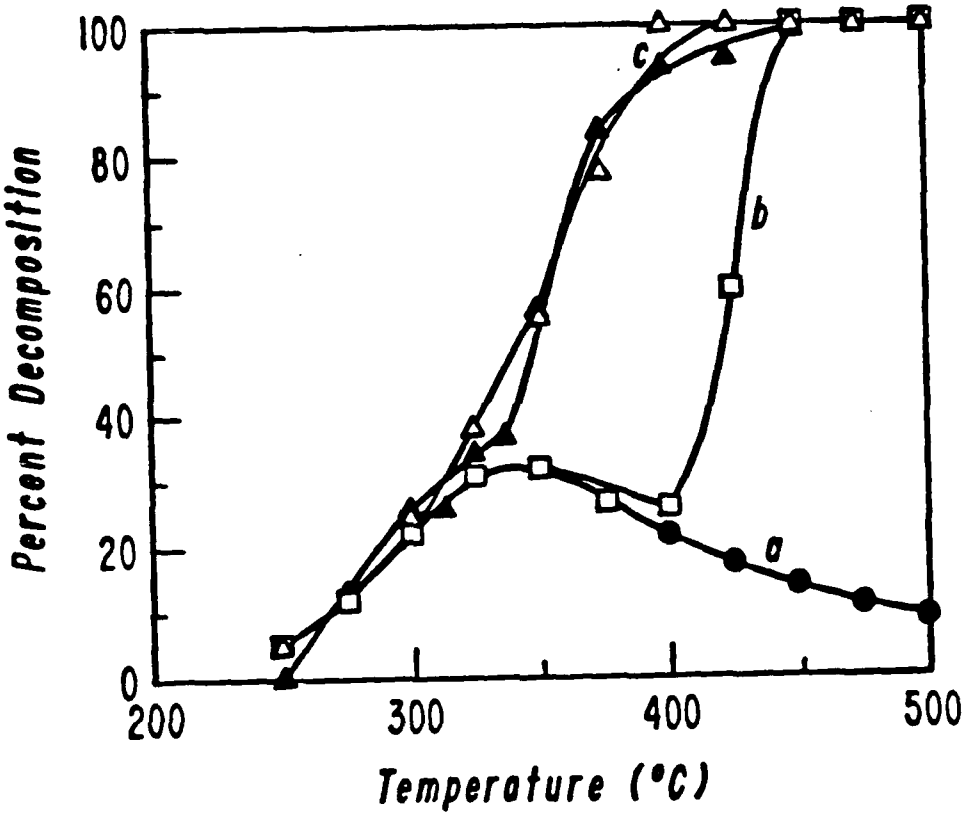
100
80
60
40
20
0
200
300
400
500
Percent Decomposition
Temperature (°C)
c
b
a

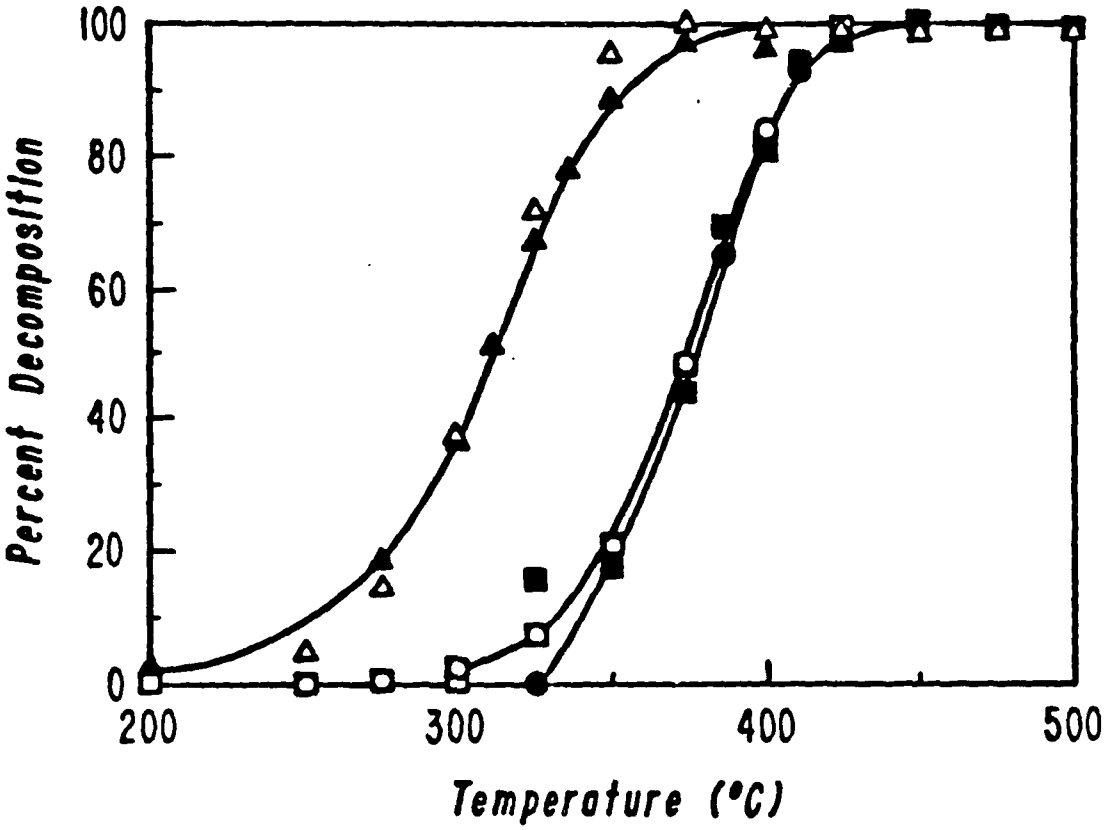
100
80
60
40
20
0
200
300
400
500
Percent Decomposition
Temperature (°C)

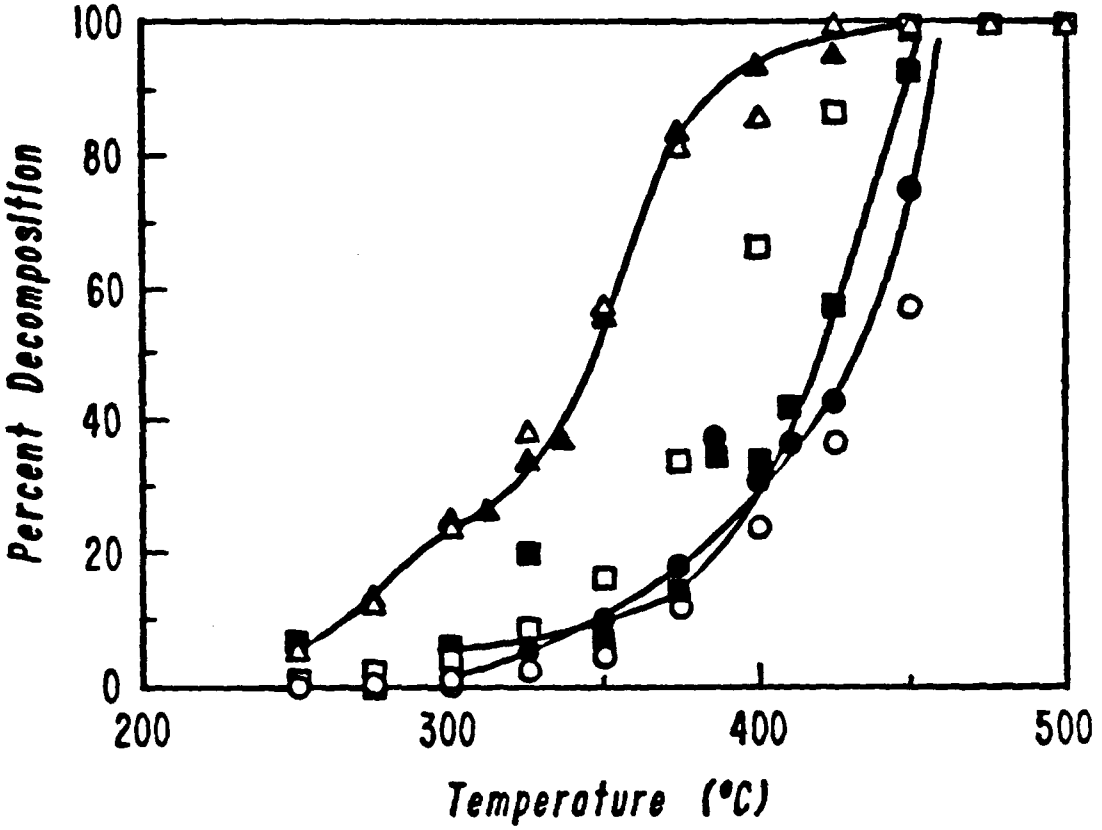
100
80
60
40
20
0
200
300
400
500
Percent Decomposition
Temperature (°C)

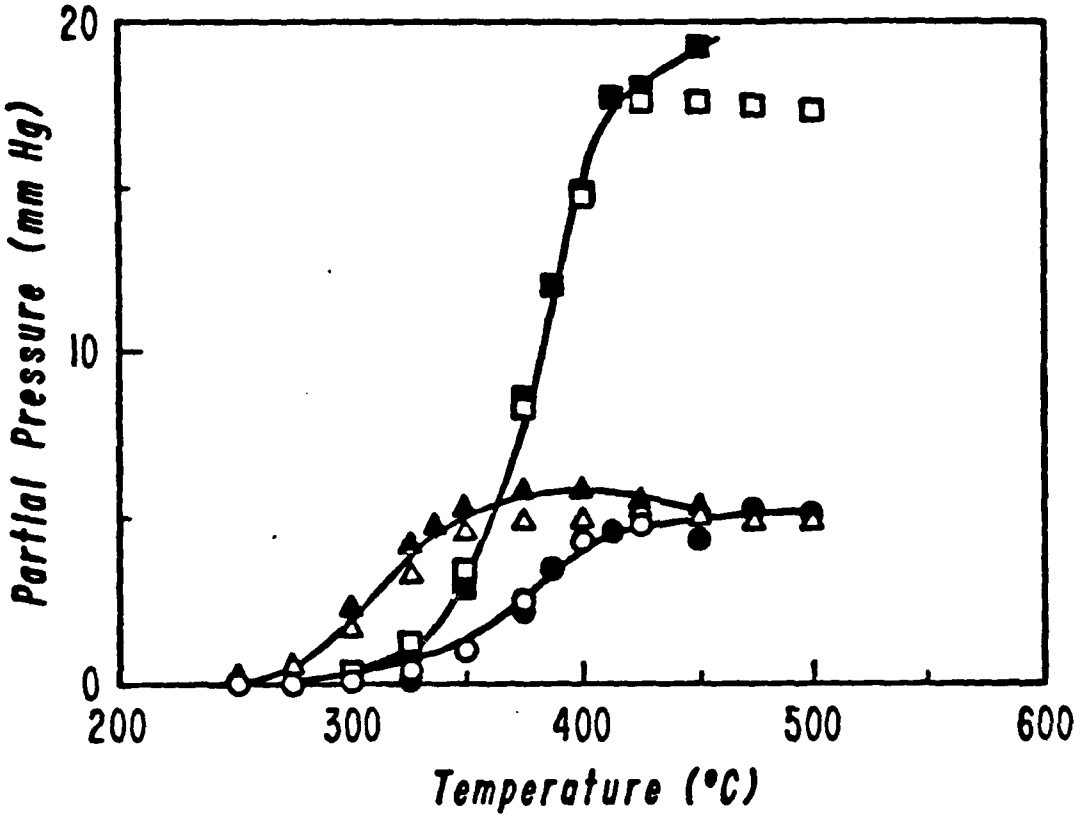
20
10
0
200
300
400
500
600
Partial Pressure (mm Hg)
Temperature (°C)

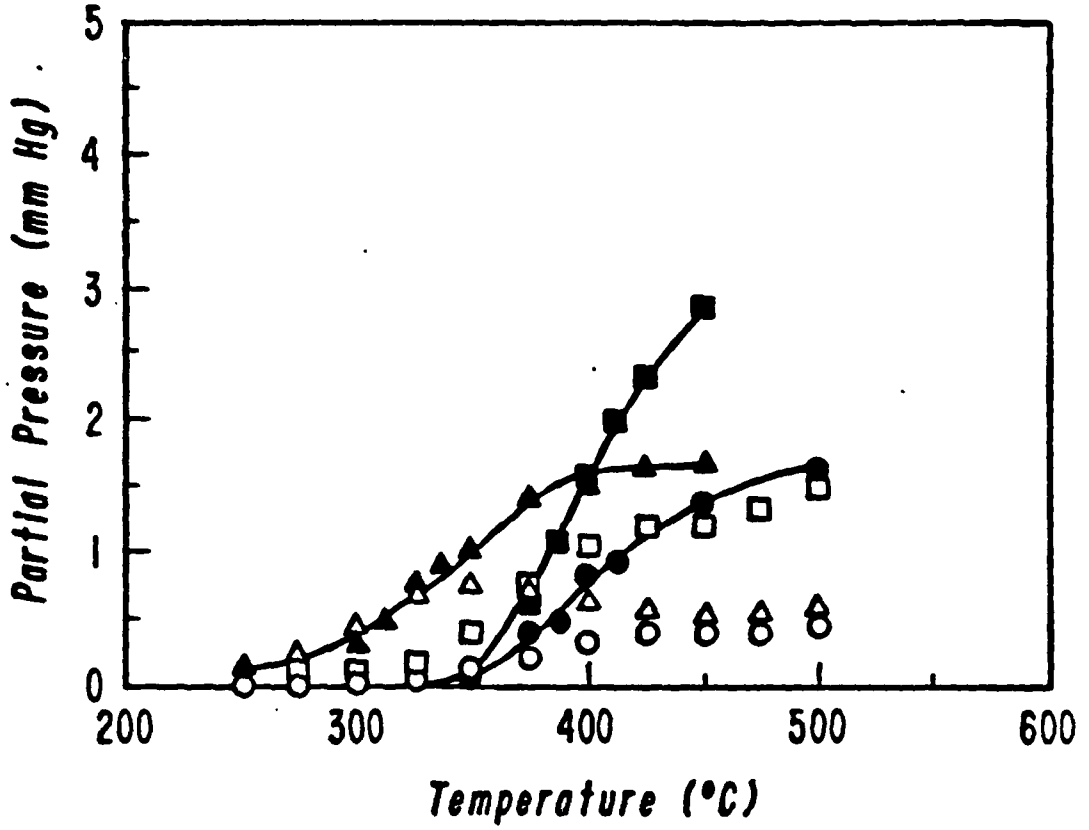
Partial Pressure (mm Hg)
0
1
2
3
4
5
200
300
400
500
600
Temperature (°C)

Elsevier Science Publishers B.V., P.O. Box 1991, Amsterdam

Northprint: JCG0090T

Page: 5

1st proof:

IN ALL CORRESPONDENCE CONCERNING THIS PAPER REFER TO:

CRYS 0090T

Journal of Crystal Growth 00 (1988) JCG0090T
North-Holland, Amsterdam

Copy of Galley Proof with Changes- 7/13/88

GaAs GROWTH USING TERTIARYBUTYLARSINE AND TRIMETHYLGALLIUM

C.A. LARSEN, N.I. BUCHAN, S.H. LI and G.B. STRINGFELLOW

Departments of Materials Science and Engineering and Electrical Engineering, University of Utah, Salt Lake City, Utah 84112, USA

Tertiarybutylarsine (TBAs) is an ideal alternative to highly toxic AsH_3 for organometallic vapor phase epitaxy (OMVPE). Its decomposition was studied in a flow tube reactor using D_2 as the carrier gas. The products were analyzed in a time-of-flight mass spectrometer. The major products are isobutane (C_4H_{10}), isobutene (C_4H_8) and AsH_3. The decomposition proceeds via two routes: intramolecular coupling, to produce C_4H_{10} and AsH, and β-elimination at higher temperatures which yields C_4H_8 and AsH_3. Addition or trimethylgallium (TMGa) has little effect on the rate and product distribution of TBAs decomposition; however, the pyrolysis of TMGa is altered greatly by the presence of TBAs. Numerical modeling shows that the main pathway to remove TMGa is via reaction with the AsH from the coupling step. In OMVPE growth the substrate temperatures are high enough that some TMGa decomposes independently, in which case the AsH serves to prevent adsorption of the CH_3 radicals and thus results in low carbon contamination.

iso-butene (C_4H_8)

1. Introduction

Attention is increasingly being given to the chemical reaction mechanisms occurring in the organometallic vapor phase epitaxial (OMVPE) growth of III/V semiconductors. It is, of course, essential to understand these basic processes in order to intelligently proceed in the further development of the technique. Knowledge of the reaction pathways can aid in modeling transport processes, development of improved techniques such as photon-assisted growth, and, as described in this paper, designing better source compounds. The search for new sources is based on two main factors. Foremost is the extreme safety hazard associated with the use of PH_3 and AsH_3 as the group V precursors. Not only are they highly toxic, but they are stored in large quantities at high pressures. Costly measures are needed to protect personnel in case of serious accidents. The impetus for studying the pyrolysis reactions and kinetics of the new sources is to allow optimization of growth conditions such as growth temperature and V/III ratios to obtain semiconductors with the best electrical and optical properties.

The title compound, tertiarybutylarsine (TBAs), has been investigated as a possible alternative to AsH_3. Its structure is shown below. It is

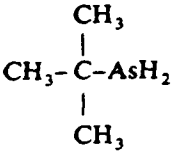

slightly

inherently safer than AsH_3 due to its lower toxicity (the LD_{50} is 70 ppm [1] compared with a TLV of 0.05 ppm for AsH_3 [2]). Also, it is stored in atmospheric pressure bubblers as are other common sources such as trimethylgallium (TMGa) and trimethylindium (TMIn) and has a room temperature vapor pressure of 196 Torr. GaAs layers grown using TBAs have good morphologies [3]. Carbon incorporation is less than in AsH_3 grown samples, and the electrical properties are similar. V/III ratios as low as 3 have been found to give good results. TBAs, then, appears to be an acceptable choice to replace AsH_3 in standard growth reactors. The purpose of this paper is to describe the decomposition mechanisms of TBAs with and without TMGa. As will be shown, these

0022-0248/88/$03.50

REQUEST
Author, please indicate
- printer's errors in BLUE
- author's changes in RED

IMPORTANT
1. Please correct the proofs carefully; the responsibility for detecting errors rests with the author.
2. Restrict corrections to instances in which the proof is at variance with the manuscript
3. Recheck all reference data
4. A charge will be made for extensive alterations
5. Return proofs by airmail within **3 days** of receipt

Thank you

studies demonstrate the reasons for the low carbon contamination and ability to grow high quality GaAs at low V/III ratios. They also help elucidate the mechanisms of OMVPE growth in general.

2. Experimental

The experiments were carried out in a standard flow tube system, as described elsewhere. The reaction consisted of a silica tube of 7.0 mm inside diameter held in a furnace having a hot zone 41.5 cm long. A flow rate of 40 SCCM was used in all experiments, except for the studies with packed tubes. In those cases the flow rate was adjusted according to the void fraction to give residence times equal to the unpacked tube experiments. The main features include the use of D_2 instead of H_2 as the carrier gas, which permits isotopic labeling of the products. The product gases are sampled by a time-of-flight mass spectrometer and analyzed. Information can be obtained as to the identities of the species as well as their relative partial pressures. Thus the steps in the mechanisms can be identified, and kinetic parameters for those steps can be found. The products were monitored using peaks at $m/e = 57$ (^{13}TBAs), 99 (TMGa), 43 (C_4H_{10}), and 58 (C_4H_8). These peaks were chosen based on high intensities for the species noted and lack of significant contributions from other species. The TBAs was Electronic Grade, supplied by American Cyanamid Company. The TMGa was obtained from Strem Chemicals, Inc., and contained 50% ^{13}C. This labeling was necessary because one of the expected products, neopentane, has its principal peak at $m/e = 57$. Thus it would be difficult to separate the contributions from neopentane and TBAs. By using the labeled material the concentrations of neopentane could be determined without interference by reference to the peak at $m/e = 58$.

3. Results and discussion

3.1. TBAs alone

Fig. 1 is a plot of the percent decomposition of TBAs in D_2 versus temperature for various surfaces. Low (50 cm^2) and high (1200 cm^2) surface areas of silica, as well as low GaAs surface areas, give nearly the same decomposition curves. This is in contrast to other group V precursors, notably the hydrides, which are highly catalyzed by both silica and III/V semiconductor surfaces [4–6]. Only when the area of the GaAs surface is increased 24-fold is a significant lowering of the pyrolysis temperature found. Thus is appears that the dominant route for TBAs decomposition is a homogeneous reaction for all cases studied.

Fig. 2 shows the decomposition products for a 3% TBAs mixture in D_2 over 50 cm^2 silica. The products are isobutane (C_4H_{10}), isobutene (C_4H_8), AsH_3, and H_2. No deuterated species were observed. The AsH_3 tracks the C_4H_8 at low temperatures. The H_2 appears at the same temperature at which the AsH_3 and C_4H_8 curves diverge. C_4H_{10} dominates at all temperatures, but eventually it declines as more C_4H_8 is produced at higher temperatures. The process also yielded As_4, whose low vapor pressure resulted in large quantities being deposited on the cold tube walls downstream from the reactor. Increasing the surface area of silica gives a similar product distribution, except that the AsH_3 divergence and simultaneous H_2 appearance occur at a lower temperature. The low and high GaAs surface area cases give similar results. In all cases C_4H_{10} is the major product.

These data are interpreted by proposing two parallel routes for the decomposition, both of

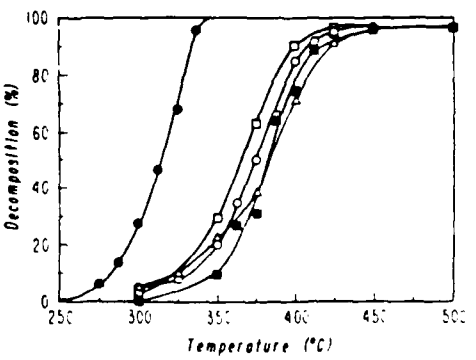

Fig. 1. Decomposition of TBAs in D_2 versus temperature: (■) 3% TBAs, 50 cm^2 SiO_2; (○) 3% TBAs, 1200 cm^2 SiO_2; (△) 0.3% TBAs, 50 cm^2 SiO_2; (□) 3% TBAs, 50 cm^2 GaAs; (●) 3% TBAs, 1200 cm^2 GaAs

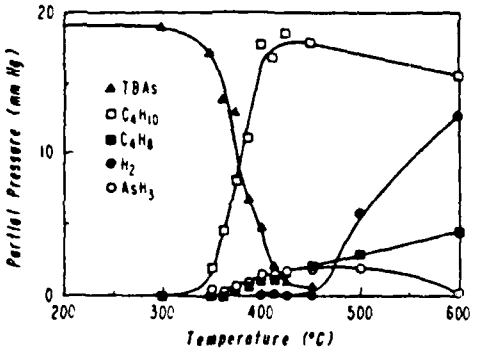

Fig. 2. Decomposition products of 3% TBAs in D_2; surface is 50 cm^2 SiO_2.

which have homogeneous and heterogeneous contributions. The major reaction in all cases is an intramolecular coupling step, analogous to reductive coupling observed in several transition metal compounds [7]. The reaction is shown below:

$$TBAs \rightarrow C_4H_{10} + AsH. \quad (1)$$

The tertiarybutyl group bonds with one of the H atoms attached to the central As atom to form the C_4H_{10}. The remaining AsH unit is unreactive to D_2 and in fact does not decompose until the temperature is high enough to also decompose AsH_3.

The other pathway for decomposition is a β-elimination, well known for transition metal [7] as well as main group compounds [8]:

$$TBAs \rightarrow C_4H_8 + AsH_3 \quad (2)$$

In this step the C_4H_9 ligand donates one of its H atoms to the As atom upon leaving. Thus the C_4H_8 and AsH_3 partial pressures are initially the same, until the reactor is hot enough to decompose the AsH_3. Studies of the decomposition as a function of residence time show that TBAs pyrolysis is first order overall. The C_4H_{10} and C_4H_8 concentrations were both found to vary linearly with initial TBAs concentration. Thus both steps are first order, and the product ratio equals the branching ratio. The extent of the surface reactions may be deduced from the data at high and low GaAs surface areas, yielding the following rate constants:

$$\log_{10}k_{1,hom} = 13.08 - 41.48(kcal/mol)/2.303RT,$$

$$\log_{10}k_{1,het} = 8.82 - 29.18(kcal/mol)2.303RT,$$

$$\log_{10}k_{2,hom} = 14.24 - 48.49(kcal/mol)/2.303RT,$$

$$\log_{10}k_{2,het} = 9.99 - 36.37(kcal/mol)/2.303RT,$$

where the subscripts refer to the homogeneous and heterogeneous components of reactions (1) and (2), respectively.

3.2. TBAs with TMGa

Fig. 3 compares the decomposition of TBAs with and without TMGa. The addition of TMGa has little effect on the pyrolysis temperature of TBAs. This is to be expected, since TBAs decomposes at lower temperatures than TMGa. Conversely, TBAs greatly lowers the temperature at which TMGa decomposes, as seen in fig. 4. The decomposition products of a TBAs-TMGa mixture with a V/III ratio of 3:1 over a high surface area of GaAs are given in figs. 5a and 5b. Comparison with fig. 2 shows that the major products are nearly the same as for the case without TMGa. The main exceptions are the notable lack of H_2 and AsH_3. A large amount of CH_4 is produced. Fig. 5b shows that minor products include methyl-

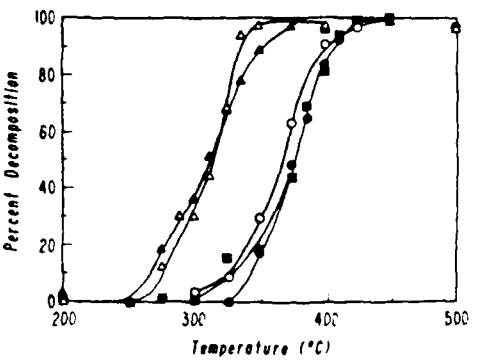

Fig. 3. Decomposition of TBAs in D_2 with added TMGa versus temperature: (○) 3% TBAs, 50 cm^2 GaAs (no TMGA; data from fig. 1); (■) 3% TBAs, 0.3% TMGa, 50 cm^2 GaAs; (●) 0.9% TBAs, 0.3% TMGa, 50 cm^2 GaAs; (▲) 3% TBAs, 1200 cm^2 GaAs (no TMGa, data from fig. 1); (△) 0.9% TBAs, 0.3% TMGa, 1200 cm^2 GaAs

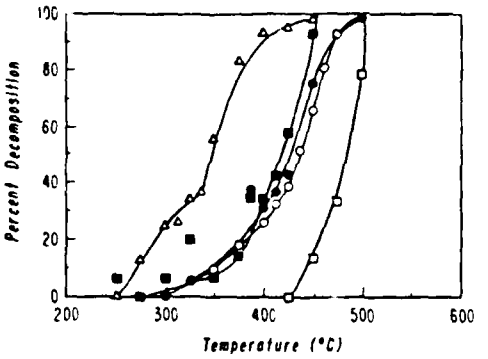

Fig. 4. Decomposition of TMGa in D_2 versus temperature: (□) 3% TMGa, 50 cm² GaAs; (○) 0.3% TMGa, 0.3% AsH_3, 50 cm² GaAs (data from ref. [10]); (■) 3% TBAs, 0.3% TMGa, 50 cm² GaAs; (●) 0.9% TBAs, 0.3% TMGa, 50 cm² GaAs; (▲) 0.9% TBAs, 0.3% TMGa, 1200 cm² GaAs.

arsine (CH_3AsH_2) and neopentane (C_5H_{12}). The pressure of C_5H_{12} was found to be linear with V/III ratio but independent of surface area. Thus its formation is via a gas phase reaction. The C_5H_{12} is evidence of formation of a homogeneous adduct between TBAs and TMGa which subsequently eliminates the alkane [9]. This is similar to earlier studies on the TMGa–AsH_3 system [10], which yielded mainly CH_4 with no deuterated species in spite of a large excess of D_2. In that case it was concluded that all decomposition was through an adduct route, with elimination of a methyl group and H atom to give CH_4. If the TBAs–TMGa system decomposed entirely analogously, the ratio of C_5H_{12} to CH_4 would be 1 : 2. This clearly is not the case, and decomposition occurs mainly by other routes. Nevertheless, there is clear evidence of some adduct pyrolysis. As with TBAs alone, no deuterated species were detected. Thus there is no independent decomposition of TMGa, which yields CH_3D and C_2H_6 [10].

The reaction mechanism between TBAs and TMGa is quite complex. The TBAs is seen to decompose principally by the same four reactions described above, namely homogeneous and heterogeneous coupling and β-elimination, with a small contribution from a TBAs–TMGa reaction. This reaction cannot account for the dramatic lowering of the TMGa pyrolysis temperature when TBAs is present. Some further reaction or reactions must be involved to decompose the remaining TMGa. In order to elucidate the complicated reaction scheme, a numerical modeling approach was used. Rate constants for the unimolecular TBAs decomposition were those given above. First, the rate parameters for the TMGa–TBAs reaction were found by adjusting to give the best fit of the TBAs pyrolysis curves of fig. 3. Next reactions between TMGa and the AsH_3 (from the β-elimination step) were added. This is reasonable in light of the disappearance of AsH_3 when TMGa is introduced. The parameters for these reactions were obtained from data of ref. [10], and include homogeneous and heterogeneous parts. Inclusion of these two reactions still failed to account for the majority of the TMGa decomposition, so a third reaction was proposed between the TMGa and the AsH. This was done to account for the lack of H_2 in fig. 5b:

$$\mathrm{TMGa + AsH \rightarrow CH_4 + products.} \qquad (3)$$

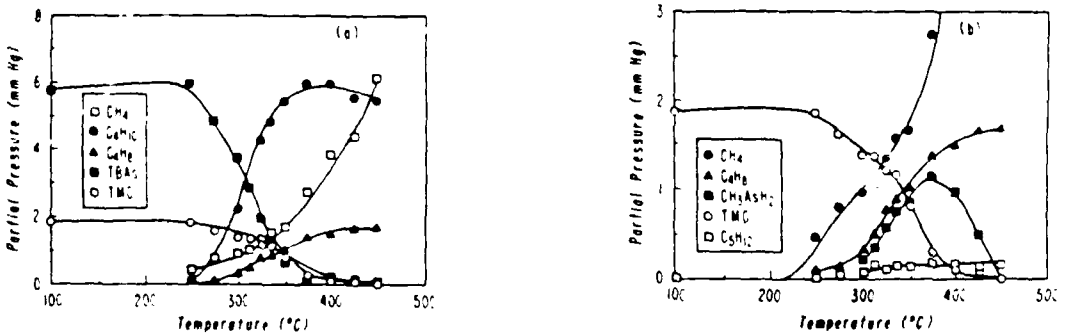

Fig. 5. Major (a) and minor (b) decomposition products of 0.9% TBAs, 0.3% TMGa mixture in D_2; surface is 1200 cm² GaAs

The AsH is the by-product of the unimolecular coupling step of TBAs. The identify of the "products" was not determined in our study. With proper choices of the activation energy and pre-exponential factor for this step, the model was able to fit the experimental data over the entire range of TMGa decomposition. The model predicts that the anomalous plateau in the high surface area curve of fig. 4 corresponds to saturation of the TMGa–AsH_3 and TMGa–TBAs reactions followed by onset of the TMGa–AsH reaction. Thus the model predicts that reaction (3) is the predominant route for the disappearance of TMGa.

It is now possible to account for the low carbon content of TBAs-grown GaAs. The independent decomposition of the TBAs provides a ready supply of the AsH groups, which diffuse to the wafer surface. In our study TMGa decomposed solely by reaction with TBAs or its decomposition products. At the high temperatures used for OMVPE growth TMGa decomposes independently to some extent, producing free methyl radicals which are the source of the carbon contamination. It is known that carbon is incorporated into As vacancies in the growing crystal [11]. The AsH effectively completes with the methyl groups to prevent their inclusion, and probably rapidly donates its remaining H atom to give CH_4 which then desorbs. When AsH_3 is used, on the other hand, it is the TMGa which decomposes first. Then there is little AsH to compete for the As sites and the level of carbon impurities is increased.

5. Summary

TBAs seems to be an ideal material to replace AsH_3 as the As source in OMVPE due to its low toxicity and the high quality of GaAs layers grown with TBAs. It has been shown that TBAs decomposes by two routes. The dominant one is a unimolecular coupling reaction with yields C_4H_{10} and AsH. The other pathway which becomes important at higher temperatures is a β-elimination step to give C_4H_8 and AsH_3. When TMGa is added there is little perturbation of TBAs decomposition, but the pyrolysis of TMGa is enhanced. Numerical modeling demonstrates that TMGa reacts with TBAs and AsH_3, but the majority of the TMGa reacts with the AsH groups. In OMVPE reactors TMGa probably decomposes independently, but the large concentration of AsH on the surface prevents inclusion of CH_3 into the growing crystal. It is hoped that these studies will lead to further improvements in designing source materials.

Ackowledgements

This work was supported by a grant from the US Air Force, Contract No. AFSOR-87-0233. The authors wish to thank American Cyanamid Company for supplying the tertiarybutylarsine.

References

[1] Private communication, American Cyanamid Company.
[2] CRC Handbook of Laboratory Safety, Ed. N.V. Steere (Chemical Rubber Co., Cleveland, OH, 1967).
[3] C.H. Chen, C.A. Larsen and G.B. Stringfellow, Appl. Phys. Letters 50 (1987) 218.
[4] M.J. Cherng, H.R. Jen, C.A. Larsen, G.B. Stringfellow, H. Lundt and P.C. Taylor, J. Crystal Growth 77 (1986) 408.
[5] I.A. Frolov, E.M. Kitaev, B.L. Druz' and E.B. Sokolov, Zh. Fiz. Khim. 51 (1977) 1106.
[6] C.A. Larsen and G.B. Stringfellow, J. Crystal Growth 75 (1986) 247.
[7] J. Kochi, Organometallic Mechanisms and Catalysis (Academic Press, New York, 1978).
[8] M.E. O'niell and K. Wade, in: Comprehensive Organometallic Chemistry: The Synthesis, Reactions and Structures of Organometallic Compounds, Vol. 1, Eds. G. Wilkinson, F.G.A. Stone and E.W. Abel (Pergamon, Oxford, 1982) p. 7.
[9] D.G. Tuck, in: Comprehensive Organometallic Chemistry: The Synthesis, Reactions and Structures of Organometallic Compounds, Vol. 1, Eds G. Wilkinson, F.G.A. Stone and E.W. Abel (Pergamon, Oxford, 19820 p. 711.
[10] C.A. Larsen, N.I. Buchan and G.B. Stringfellow, Appl Phys. Letters 52 (1988) 480
[11] B.J. Skromme, T.S. Low, T.J Roth, G.E Stillman, J.K. Kennedy and J. K. Abrokwah, J. Electron Mater. 12 (1983) 433.

Reaction Mechanisms in OMVPE Growth of GaAs Determined Using D_2

Labelling Experiments

G.B. Stringfellow
Departments of Materials Science and Engineering
and Electrical Engineering
University of Utah
Salt Lake City, Utah 84112

INTRODUCTION

The emergence of organometallic vapor phase epitaxy (OMVPE) as a viable commercial growth technique for III/V semiconductors has prompted renewed interest in understanding the basic growth chemistry. To date, the reactions occurring during the OMVPE growth of GaAs using TMGa and AsH_3 are not fully understood. Efforts to improve the technique, including the search for new and better source materials, are dependent on obtaining a more detailed understanding of the growth kinetics.

This paper will focus initially on the growth of GaAs using trimethylgallium (TMGa) and arsine (AsH_3). These results will be contrasted with the reaction mechanisms occurring during the OMVPE growth of GaAs using the newly developed organometallic As source, tertbutylarsine (TBAs), which is more attractive than AsH_3 for practical systems since it is much less hazardous, pyrolyzes at lower temperatures, and apparently results in no additional carbon contamination of the epitaxial layer.

EXPERIMENTAL

Studies of the pyrolysis of TMGa, AsH_3, and TBAs were performed in a simple flow tube apparatus with a tube diameter of 4 mm and a length of 41.5 cm. The pyrolysis experiments were performed in D_2, H_2, and He ambients, with a mass spectrometer used to monitor the volatile products. The product partial pressures, corrected for the appropriate sensitivity factors, were determined versus temperature, surface area and type, and gas

phase composition to elucidate the reaction mechanisms. Deuterium was used to allow identification of the reaction mechanisms via isotopic labelling.

EXPERIMENTAL RESULTS AND DISCUSSION

Trimethylgallium

The pyrolysis of TMGa was first studied in a toluene flow system [1]. The first methyl group came off in a homogeneous reaction above 500°C, but the second radical was liberated only above 550°C. The activation energies for removal of the first two methyl radicals were 59.5 and 35.4 kcal/mole, respectively. The third gallium-methyl bond did not break but instead a solid $(GaCH_3)_n$ polymer was formed.

The reaction in an atmospheric pressure OMVPE apparatus was reported to be faster in H_2 than in N_2, as found by mass spectrometry [2], although this was later tentatively ascribed to the longer entrance length in N_2 than in H_2 by Lee et al[3], who found little effect of ambient (either H_2 or He, which are hydrodynamically similar) on pyrolysis rate for a low pressure OMVPE system with sampling through an orifice in the graphite susceptor. However, an alternate explanation is that less ambient effect is expected at low pressures where gas phase interactions are reduced. This represents a significant difference, in general, between low pressure and atmospheric pressure approaches to OMVPE.

The results of Larsen *et al*[4] are given in Fig. 1, which shows the percent pyrolysis versus temperature in various ambients. The results for an inert He ambient, which is hydrodynamically similar to H_2, are similar to those of Jacko and Price[1], with a similar activation energy, indicating the pyrolysis mechanism is simple homolysis. D_2 accelerates the reaction, and H_2 lowers the pyrolysis temperature even more. The difference between H_2 and D_2 indicates that the carrier gas is involved in the rate determining steps. Increasing the surface area had a minimal effect on the rate, so the decomposition is predominantly homogeneous.

A number of papers have reported the main pyrolysis product in H_2 to be methane, with small amounts of ethane and higher hydrocarbons[2,3,5,6]. Yoshida et al[2] concluded that the reaction in N_2 was via homolytic fission, but that in H_2 the mechanism was hydrogenolysis, in which an H_2 molecule bonds simultaneously with the central atom and one of the ligands. Lee et al[3] interpreted their results in terms of a simple homolytic fusion process. *In situ* infrared (IR) absorption studies of the reaction in H_2 at 7.6 Torr [7] gave clear evidence of free gas phase methyl radicals.

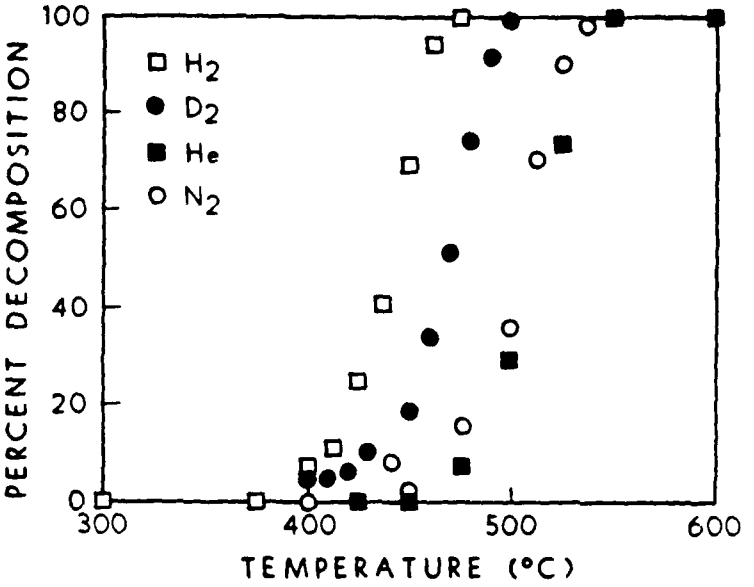

Figure 1: Temperature dependence of TMGa pyrolysis in H_2, D_2, and He ambients. (After Larsen et al, Ref. 4).

The major product of the decomposition measured by Larsen et al[8] in D_2 is CH_3D, with C_2H_6, CH_4, and HD also being produced. The other studies also reported CH_4 as the main product in H_2, but the D_2 studies elucidate the source of the methanes: they come mainly from reactions between the methyl radicals and the ambient. The most likely route for CH_3D formation is a metathesis between gas phase methyl radicals and D_2 molecules as given in step 2 below. This also produces D atoms which can further participate in the process. It is probable, based on the pyrolysis of TMIn in D_2[9], that these D atoms attack TMGa molecules as one of the decomposition steps. The following mechanism for TMGa decomposition is consistent with the experimental results:

$$(CH_3)_3Ga \rightarrow 2\,CH_3 + CH_3Ga \qquad (1)$$

$$CH_3 + D_2 \rightarrow CH_3D + D \qquad (2)$$

$$D + (CH_3)_3Ga \rightarrow CH_3D + (CH_3)_2Ga \qquad (3)$$

$$2\,CH_3 \rightarrow C_2H_6. \qquad (4)$$

Step 1 is an initiation step of homolytic fission of methyl groups from TMGa molecules. Steps 2 and 3 are the propagation steps of a chain reaction between the D atoms, the unreacted TMGa molecules and the methyl groups. The chain cannot propagate in an N_2 or He

carrier. Under low pressure conditions or in cases where the residence time is short the propagation steps may also not be favorable, perhaps explaining the lack of an ambient effect for the data of Lee et al. When the D_2 is replaced with H_2, the lower dimer bond strength results in faster reactions. The chain is terminated by the recombination step 4 to give C_2H_6.

Arsine

The decomposition of AsH_3 on As surfaces in a static system was found to be a first order reaction with an activation energy of 23.2 kcal/mole [10], considerably less than the average bond strength of approximately 59 kcal/mole[11]. Decomposition of a mixture of AsH_3 and AsD_3 yielded primarily HD, while a mixture of AsH_3 and D_2 gave no HD. Frolov et al [12] studied AsH_3 pyrolysis in a flow system on glass, As, and GaAs surfaces. Their results confirmed the decomposition to occur by a first order, heterogeneous process. Changing the ambient from H_2 to He had no effect on the pyrolysis rate. The pyrolysis was found to be strongly catalyzed by the presence of a GaAs surface.

Larsen et al [8] found the temperature at which pyrolysis is 50% complete, T_{50}, to be approximately 600°C for SiO_2 surfaces in both D_2 and N_2 ambients. On GaAs surfaces, the value of T_{50} was reduced by more than 100°C to 476°C. For both surfaces, AsH_3 pyrolysis in D_2 produced only H_2 with no HD detected in excess of the background concentration. Any H atom liberated in the gas phase would react with the D_2 ambient producing HD. Thus, the reaction occurs on the surface where adsorbed H atoms recombine to form the H_2 detected. The dependence of reaction rate on partial pressure indicated the process to be first order. Thus, the rate limiting step appears to be release of the first H atom. In addition, the surface is not saturated with adsorbed AsH_3.

Tertbutylarsine

TBAs is found to pyrolyze at temperatures well below those of AsH_3 and the CH_3 and C_2H_5 substituted alkyls due to the weaker As-C bond strength of the t-butyl radical. This is seen in Fig. 2 where the percent decomposition in one atmosphere of D_2 is plotted vs. temperature for: i) 3% TBAs, unpacked silica tube, ii) 3% TBAs, packed silica tube, iii) 0.3% TBAs, unpacked silica tube, iv) 3% TBAs, unpacked GaAs coated tube, and v) 3 % TBAs, packed GaAs coated tube[13]. The difference in pyrolysis temperatures for the unpacked and packed silica tube is slight. The GaAs surface in the unpacked tube lowers the decomposition temperature by only 10°C, but the high GaAs surface decreases the pyrolysis temperature markedly.

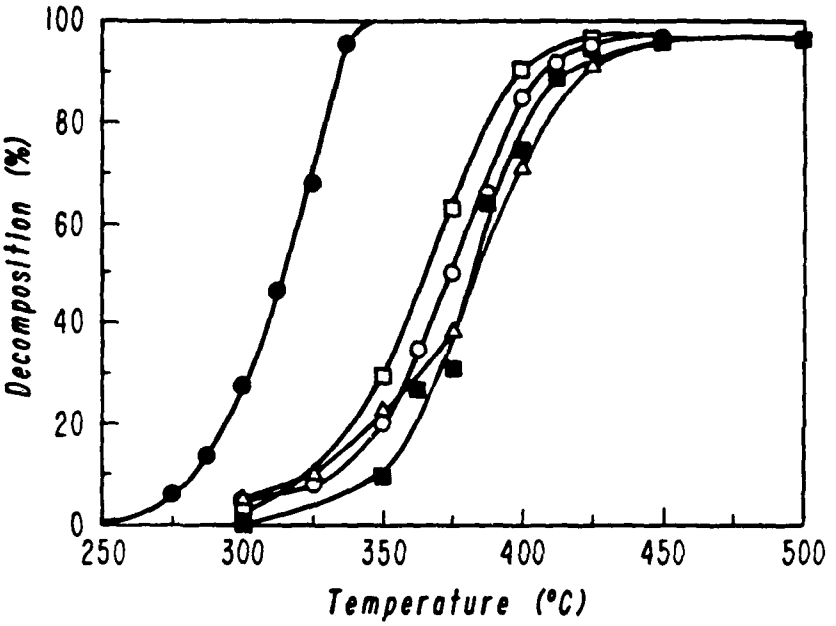

Figure 2: Temperature dependence of TBAs pyrolysis in D_2 for concentrations of 0.3 and 3% on various surfaces: ■, 3% TBAs, 50 cm^2 SiO_2; ○, 3% TBAs, 1200 cm^2 SiO_2; △, 0.3% TBAs, 50 cm^2 SiO_2; □, 3% TBAs, 50 cm^2 GaAs; ●, 3% TBAs, 1200 cm^2 GaAs. (After Larsen et al, Ref. 13).

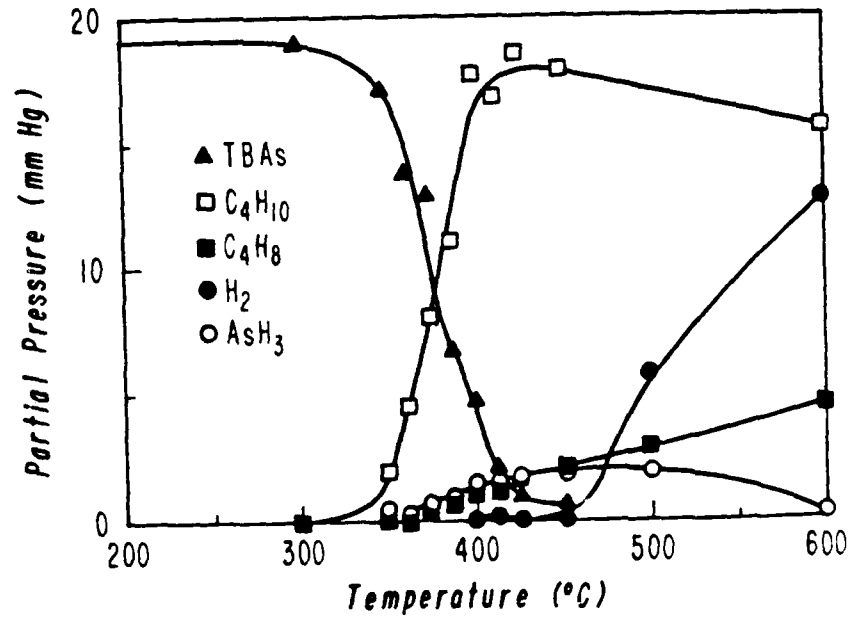

Figure 3: Temperature dependence of decomposition products of 3% TBAs in D_2; surface is 50 cm^2 SiO_2. (After Larsen et al, Ref. 13).

Thus the decomposition is almost completely homogeneous except at very high GaAs surface areas. This is in marked contrast to AsH_3 which is strongly catalyzed by both silica and III/V surfaces.

The temperature dependence of the product partial pressures for the decomposition of a 3 % TBAs mixture determined by Larsen et al[13] is shown in Fig. 3 for the unpacked silica tube. The major products are found to be isobutane (C_4H_{10}) and H_2. The C_4H_{10} appears at the same temperature at which the TBAs begins to decompose, i.e. around 300°C. The other products are isobutene (C_4H_8) and AsH_3. The ratios of C_4H_8 to AsH_3 are approximately 1:1 up to 450°C, at which temperature AsH_3 begins to decompose, suggesting a β-proton elimination reaction occurs. AsH_3 decomposition coincides with H_2 production. A significant feature is that the decomposition temperature and product ratios are essentially independent of the initial TBAs partial pressure. Superficially, both observations are suggestive of simple, unimolecular pyrolysis reactions.

Increasing the surface area gives rise to nearly identical products. For a high surface area of GaAs the AsH_3 and C_4H_8 signals are significantly attenuated. This would be consistent with expectations for the β-proton elimination reaction, since the lone electron pair on the As would be occupied by the suface Ga atom, preventing interactions with the H atoms on the t-butyl ligand. There was no evidence in any of the experiments that deuterated species were formed. It is clear that TBAs does not react with the D_2 ambient as part of the decompsition mechanism.

The data are insufficient to give an unambiguous determination of the pyrolysis mechanism(s). Several of the results can be interpreted in terms of a reaction pathway not involving free radicals. Production of both C_4H_{10} and C_4H_8 can be postulated to be due to homogeneous unimolecular proceses:

$$C_4H_9AsH_2 \rightarrow C_4H_{10} + AsH \quad (5)$$

$$C_4H_9AsH_2 \rightarrow C_4H_8 + AsH_3. \quad (6)$$

Reaction (5) is a reductive coupling step. The transition state is a three centered complex between the central As atom, the central carbon atom on the *tert*-butyl ligand, and one of the H atoms bonded to the As. The leaving group is a complete isobutane molecule. The last step, reaction (6) yielding isobutene and AsH_3, is a ß-elimination process. In ß–elimination, a four-center transition state is formed with one of the H atoms on the *tert*-butyl ligand forming a bond to the central As atom. The radical subsequently leaves as isobutene.

Thus the C_4H_8 and AsH_3 partial pressures track each other in all cases until temperatures are reached at which AsH_3 decomposes.

These mechanisms explain the experimental results presented in this paper. However, very recent additional results appear to indicate the involvement of *t*-butyl radicals[14]. Radicals intentionally added to the system using the *t*-butylazo compound, $(C_4H_9)_2N_2$, with *t*-butyl radicals attached to either end of a double bonded N_2 pair, are found to attack TBAs, forming ditertbutylarsine, $(C_4H_9)_2AsH$, and $(C_4H_9)_2As_2H_2$. The absence of observable C_4H_9D, expected from the reaction of the C_4H_9 radicals with the D_2 ambient during TBAs pyrolysis, may be due to more rapid reaction with the precursor itself or reaction products such as AsH_2.

TMGa and AsH_3

Several studies of the pyrolysis of mixtures of TMGa and AsH_3 have shown the enhanced pyrolysis of AsH_3 due to the presence of TMGa[5,7,15-17].

Butler and co-workers[7,18] have clearly shown, using IR absorption spectroscopy to monitor CH_3 concentrations, that methyl radicals attack AsH_3. By measuring the decay of the CH_3 signal, they have determined the rate constant for the process.

Another model is that formation of an adduct leads to increased pyrolysis rates for AsH_3 in the presence of TMGa[8]. A new absorption band appearing in the IR spectrum of the TMGa + AsH_3 system was reported by Nishizawa and Kurabayashi[17] may be a direct indication of adduct formation. At very low temperatures of <259°C, Schlyer and Ring [16] studied the pyrolysis of neat mixtures of TMGa and AsH_3. They proposed that the first step in the reaction was independent adsorption of the two reactants, followed by formation on a surface adduct.

The detailed pyrolysis studies in a D_2 carrier gas, indicate clearly that interaction between TMGa and AsH_3 plays an integral role in the combined pyrolysis reactions. Comparing the data reproduced in Fig. 4 with the earlier data for the independent pyrolysis of TMGa, clearly shows a significant reduction in the pyrolysis temperature for both reactants. An additional important feature of the data in Fig. 4 is that the amounts of As and Ga removed from the vapor by pyrolysis are equal. The products are CH_4 and H_2. No CH_3D is detected.

The broad features of this data can be interpreted using either of the models mentioned above. If TMGa pyrolysis produces a single CH_3 and DMGa, which adsorbs on the surface. We would expect a 1:1

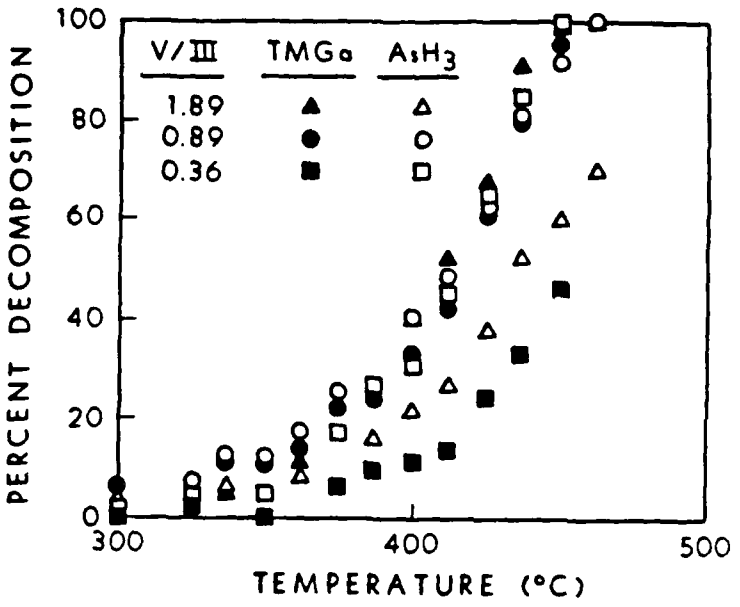

Figure 4: Pyrolysis of TMGa-AsH_3 mixtures at various V/III ratios. (After Larsen et al, Ref. 4).

ratio of TMGa and AsH_3 pyrolyzed. Since the rate constant for reaction of CH_3 with AsH_3 is much larger than for reaction with D_2, little CH_3D would be formed. However, the entire pyrolysis process would be expected to proceed at a rate equal to the pyrolysis rate for TMGa alone, which is clearly not the case.

The adduct model seems to give a more natural explanation of the data. The 1:1 adduct would automatically give a 1:1 ratio of TMGa to AsH_3 molecules pyrolyzed. Adduct formation would weaken both the Ga-CH_3 and As-H bonds, resulting in a lower pyrolysis temperature than for either TMGa or AsH_3 alone. As a consequence, only CH_4 would be formed.

TMGa and TBAs

The temperature dependence of the decomposition of TBAs for various conditions is shown in Fig. 5. Included are data for the pyrolysis of TBAs with no TMGa in the presence of GaAs surfaces for both low (50 cm^2) and high (1200 cm^2) surface areas. This data of Larsen et al[19] show that addition of a small amount of TMGa, to give a V/III ratio of 10:1, has very little effect on the reaction rate. When the TBAs concentration is decreased by a factor of three the results are still nearly identical to the no-TMGa case. At high surface areas there is a small shift in the slope of the curve due to the TMGa. In all cases the decomposition of TBAs is only slightly affected by

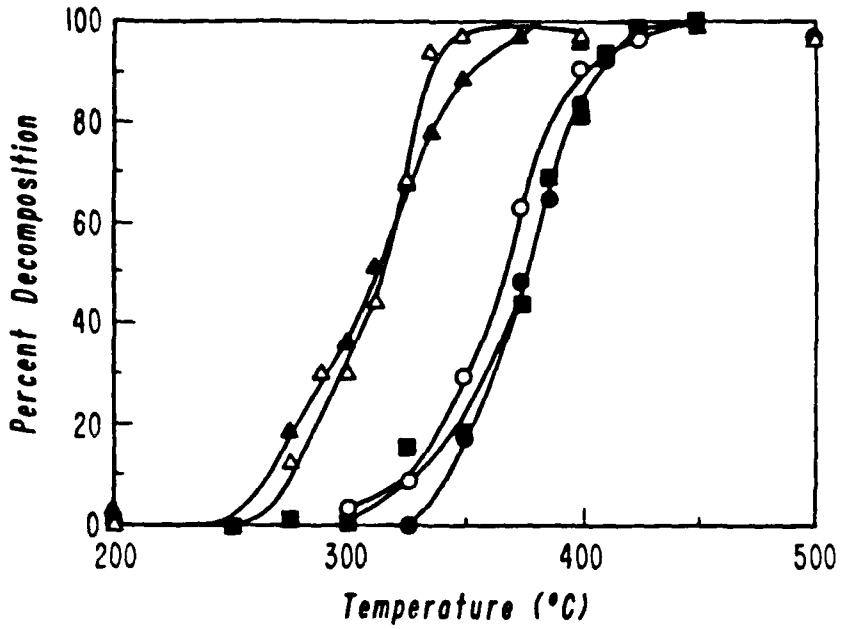

Figure 5: Decomposition of TBAs in D_2 vs. temperature.○, 3% TBAs, 50 cm^2 GaAs (no TMGa; data from Fig. 2); ■, 3% TBAs, 0.3% TMGa 50 cm^2 GaAs; ●, 0.9% TBAs, 0.3% TMGa, 50 cm^2 GaAs; ▲, 3% TBAs, 1200 cm^2 GaAs (no TMGa; data from Fig. 2); △, 0.9% TBAs, 0.3% TMGa, 1200 cm^2 GaAs. (After Larsen et al, Ref. 19).

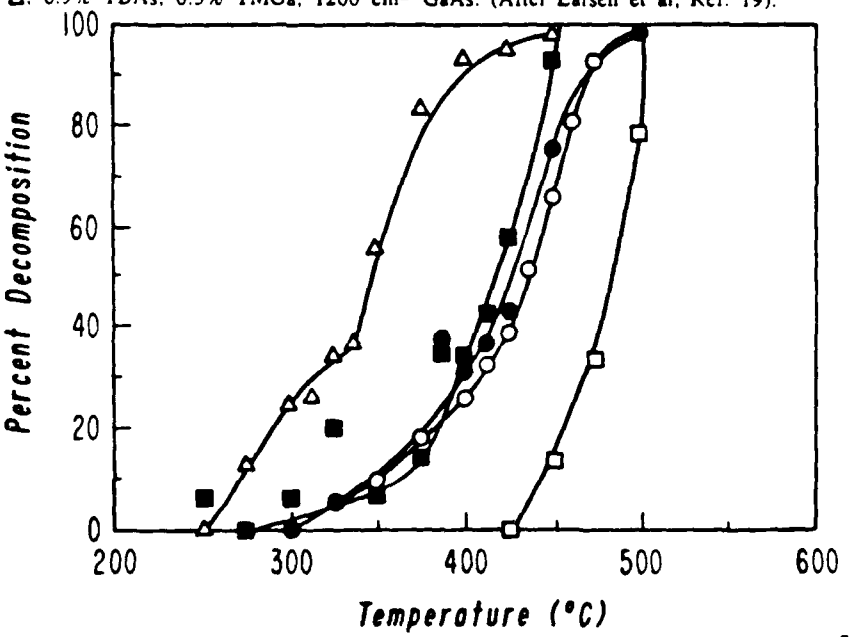

Figure 6: Decomposition of TMGa in D_2 vs. temperature. □, 3% TMGa, 50 cm^2 Ga.○, 0.3% TMGa + 0.3% AsH_3, 50 cm^2 GaAs; ■, 3% TBAs + 0.3% TMGa, 50 cm^2 GaAs, ●, 0.9% TBAs + 0.3% TMGa, 50 cm^2 GaAs; △, 0.9% TBAs + 0.3% TMGa, 1200 cm^2 GaAs. (After Larsen et al, Ref. 19)

TMGa. This contrasts markedly with the TMGa-AsH_3 system in which TMGa significantly lowers the AsH_3 pyrolysis temperature for both high and low GaAs surface areas. Thus TBAs decomposes by the same primary mechanisms with and without TMGa.

The corresponding plot describing the behavior of TMGa, again from Larsen et al[19] is given in Fig. 6. Data for TMGa alone and TMGa with AsH_3 are also shown. The data show that TMGa decomposition is enhanced somewhat by adding TBAs, but the pyrolysis temperature is nearly independent of the TBAs/TMGa ratio. Increasing the surface area results in a marked lowering of the temperature for the pyrolysis.

The temperature dependence of the product partial pressures obtained by Larsen et al[19] in a D_2 ambient is much the same as with no TMGa. That is, the major product is isobutane (C_4H_{10}), with isobutene (C_4H_8) produced at higher temperatres. CH_4 is also one of the major products, but no CH_3D was found. The minor products include CH_3AsH_2 (methylarsine), C_5H_{12} (neopentane), and AsH_3. In the case of TBAs alone the AsH_3 and C_4H_8 were produced in nearly one-to one ratios at low temperatures. With added TMGa the AsH_3 is attenuated by GaAs-catalyzed decomposition as well as reaction with TMGa directly. H_2 is created by the decomposition of AsH_3 and other reaction products such as AsH and AsH_2. No deuterated species were detected in the product gases. When the V/III ratio was reduced to 3/1 the AsH_3 was found to be severly attenuated. No H_2 was detected, from which it may be concluded that the AsH_3 and the other As-containing products react with TMGa to yield CH_4 before they decompose independently. Increasing the surface area by a factor of 24 (for the 3:1 ratio) yields the same products, C_4H_{10}, C_4H_8, and CH_4. There is no detectable AsH_3 in this case. It is important to emphasize that there is no CH_3D or C_2H_6 in any of the cases studied. This indicates that there is no independent decomposition of TMGa. Again, no H_2 was detected.

TMGa-TBAs reactions differ from those between TMGa and AsH_3. The preferred model for TMGa and AsH_3 involves formation of adducts, which subsequently eliminate CH_4 molecules. If the TMGa-TBAs interactions were strictly analogous, C_5H_{12} and CH_4 would be produced in a 1:2 ratio. This is not the case. Some C_5H_{12} is formed, with pressures proportional to the V/III ratio, indicating that adduct reactions do occur. However, adducts are plainly not the major pathway for TMGa decomposition in the presence of TBAs.

An examination of the rate constants for C_4H_{10} production with and without TMGa indicates that the dominant route for C_4H_{10}

production on the surface is the same with and without added TMGa. Comparing the heterogeneous rate constant for production of C_4H_8 with that of heterogeneous C_4H_8 production with TBAs alone, however, shows a large discrepancy. The data strongly suggest a surface reaction between TBAs and TMGa which yields C_4H_8, in addition to that produced by the unimolecular β-elimination reactions of TBAs.

The TMGa + TBAs growth reactions in H_2 yield GaAs with properties similar to those produced using TMGa and AsH_3[20,21]. The abundance of AsH, AsH_2, and AsH_3 on the surface apparently prevents excess carbon incorporation. The high growth efficiency demonstrates the absence of parasitic reactions.

SUMMARY

In conclusion, the pyrolysis reactions for TMGa, AsH_3, and TBAs in various ambient indicate that TMGa pyrolyzes by a complex chain reaction mechanism and AsH_3 pyrolyzes by a simple heterogeneous H elimination reaction. The TBAs pyrolysis mechanism has not been completely determined. Some results are explained by a pair of homogeneous, unimolecular reactions. Other results are indicative of C_4H_9 radical reactions. TMGa and AsH_3 together pyrolyze by a process not seen for the individual reactants alone. The most likely model is the formation of an adduct, which results in a higher pyrolysis rate than for either component alone, gives a 1:1 ratio of pyrolyzed As and Ga, and yields CH_4 as the major product, even in a D_2 ambient. The pyrolysis of TBAs is not affected by the presence of TMGa; however, it results in a strong increase in the TMGa pyrolysis rate. This is attributed to heterogeneous attack of TMGa by TBAs, as well as other As-species produced by TBAs pyrolysis.

ACKNOWLEDGEMENTS

The author wishes to thank his students, N.I. Buchan, S.H. Li, and C.A. Larsen for allowing the use of experimental results prior to publication and for enlightening discussions. This work was supported by the Air Force Office of Scientific Research.

FIGURE CAPTIONS:

Fig. 1: Temperature dependence of TMGa pyrolysis in H_2, D_2, and He ambients. (After Larsen et al, Ref. 4).

Fig. 2: Temperature dependence of TBAs pyrolysis in D_2 for concentrations of 0.3 and 3% on various surfaces: ■, 3% TBAs, 50 cm^2 SiO_2; ○, 3% TBAs, 1200 cm^2 SiO_2; △, 0.3% TBAs, 50 cm^2 SiO_2; □, 3%

TBAs, 50 cm^2 GaAs; ●, 3% TBAs, 1200 cm^2 GaAs. (After Larsen et al, Ref. 13).

Fig. 3: Temperature dependence of decomposition products of 3% TBAs in D_2; surface is 50 cm^2 SiO_2. (After Larsen et al, Ref. 13).

Fig. 4: Pyrolysis of TMGa-AsH_3 mixtures at various V/III ratios. (After Larsen et al, Ref. 4).

Fig. 5: Decomposition of TBAs in D_2 vs. temperature.○, 3% TBAs, 50 cm^2 GaAs (no TMGa; data from Fig. 2); ■, 3% TBAs, 0.3% TMGa 50 cm^2 GaAs;●, 0.9% TBAs, 0.3% TMGa, 50 cm^2 GaAs;▲, 3% TBAs, 1200 cm^2 GaAs (no TMGa; data from Fig. 2);△, 0.9% TBAs, 0.3% TMGa, 1200 cm^2 GaAs. (After Larsen et al, Ref. 19)

Fig. 6: Decomposition of TMGa in D_2 vs. temperature. □, 3% TMGa, 50 cm^2 Ga;○, 0.3% TMGa + 0.3% AsH_3, 50 cm^2 GaAs; ■, 3% TBAs + 0.3% TMGa, 50 cm^2 GaAs; ●, 0.9% TBAs + 0.3% TMGa, 50 cm^2 GaAs; △, 0.9% TBAs + 0.3% TMGa, 1200 cm^2 GaAs. (After Larsen et al, Ref. 19).

REFERENCES

1) M.G. Jacko and S.J.W. Price, Can. J. Chem. **41** 1560 (1963).
2) M. Yoshida, H. Watanabe, and F. Uesugi, J. Electrochem. Soc. **132** 677 (1985).
3) P.W. Lee, T.R. Omstead, D.R. McKenna, and K.F. Jensen, J. Crystal Growth **85** 165 (1987).
4) C.A. Larsen, S.H. Li, N.I. Buchan, and G.B. Stringfellow, (unpublished results).
5) S.P. DenBaars, B.Y. Maa, P.D. Dapkus, A.D. Danner, and H.C. Lee, J. Crystal Growth **77** 188 (1986).
6) M.R. Leys and H. Veenvliet, J. Crystal Growth **55** 145 (1981).
7) J.E. Butler, N. Bottka, R.S. Sillmon, and D.K. Gaskill, J. Crystal Growth **77** 163 (1986).
8) C.A. Larsen, N.I. Buchan, and G.B. Stringfellow, Appl. Phys. Lett. **52** 480 (1988).
9) N.I. Buchan, C.A. Larsen, and G.B. Stringfellow, J. Crystal Growth (to be published).
10) K. Tamaru, J. Phys. Chem. **59** 777 (1955).
11) T.J. Cottrell *The Strength of Chemical Bonds*, (Butterworth, London, 1954).
12) I.A. Frolov, E.M. Kitaev, B.L. Druz, and E.B. Solokov, Russ. J. Phys. Chem. **51** 651 (1977).
13) C.A.Larsen, N.I. Buchan, S.H. Li, and G.B. Stringfellow, J. Crystal Growth (to be published).
14) N.I. Buchan, S.H. Li, C.A. Larsen, and G.B. Stringfellow (unpublished results).

15) T.F. Kuech, E. Veuhoff, T.S. Kuan, V. Deline, and R. Potemski, J. Crystal Growth 77 257 (1986).
16) D. J. Schlyer and M.A. Ring, J. Organometallic Chem. 114 9 (1976).
17) J. Nishizawa and T. Kurabayashi, J. Electrochem. Soc. 130 413 (1983).
18) D.K. Gaskill, V. Kolubayev, N. Bottka, R.S. Sillmon, and J.E. Butler, J. Crystal Growth (Proceedings of ICMOVPE #4, to be published).
19) C.A. Larsen, S.H. Li, N.I. Buchan, and G.B. Stringfellow, J. Crystal Growth (to be published).
20) C.H. Chen, C.A. Larsen, and G.B. Stringfellow, Appl. Phys. Lett. 50 218 (1987).
21) R.K. Lum, J.K. Klingert, and M.G. Lamont, Appl. Phys. Lett. 50 284 (1987).